Aus dem Centrum für Muskuloskeletale Chirurgie
der Medizinischen Fakultät der Charité – Universitätsmedizin Berlin

DISSERTATION

On the Influence of Mechanical Conditions on Osteochondral Healing

Zur Erlangung des akademischen Grades
Doctor rerum medicarum (Dr. rer. medic.)

vorgelegt der Medizinischen Fakultät der Charité –
Universitätsmedizin Berlin

von

Zully M. Ritter (geb. Maldonado Mora)

aus Cúcuta/Kolumbien

Gutachter: 1. Prof. Dr.-Ing. Georg N. Duda

2. Prof. Dr. habil. Michael M. Morlock

3. Prof. Dr. Thomas Mittelmeier

Datum der Promotion: 24 März 2006

Zusammenfassung

Osteochondrale Defektheilung nach Traumata oder degenerativen Krankheiten bleibt weiterhin ein häufiges, klinisches Problem. Es ist bekannt, daß die mechanischen Eigenschaften der neudifferenzierten Gewebe, welche osteochondrale Defekte ausfüllen, minderwertig sind im Vergleich zu den hochspezialisierten hyalinen Knorpeln. Unter bestimmten Bedingungen (z.B. sich widerholende, stoßende oder torsionale Belastungen) können in Gelenkgeweben Fibrillation und Spalten auftreten und es bilden sich schließlich osteochondrale Defekte. Ohne Behandlung tritt Osteoarthrose auf (posttraumatische Osteoarthrose). Gelenkdegeneration kann zum totalen Gelenkersatz führen. Das Verständnis von Veränderungen, Heilung und Behandlung von osteochondralen Defekten erfordert die Kenntnis des mechanischen Umfeldes des intakten und frakturierten Knochens. Der Einfluß der Knochenqualität auf seine Mechanik muß verstanden werden, um eine detaillierte Analyse des Gelenkbereiches, in welcher der osteochondrale Defekt lokalisiert ist, durchzuführen.

Ziele dieses Projektes waren zum Einen, das mechanische Verhalten des Knochens eines intakten Gelenkes unter physiologischen Belastungen unter besonderer Berücksichtigung der Knochenqualität zu analysieren und zum Anderen den Einfluß der mechanischen Bedingungen auf die osteochondrale Defektheilung zu bestimmen.

Um diese Ziele zu erreichen, wurde eine Studie des mechanischen Verhaltens des Knochen-Gelenkbereiches durchgeführt. Dies geschah am Beispiel proximaler Humeri. Kompressive Dehnungen in intakten und frakturierten Knochen unter physiologischen Belastungen wurden bestimmt. Die Armpositionen 90° Abduktion, 90° Vorwärtsflexion und 0°, die neutrale Position, wurden dafür simuliert. Der Einfluß der Knochenqualität auf seine Heilung wurde durch die Analyse der kompressiven Dehnungen von osteoporotischen Knochen mit verschiedenen Dichteverteilungen (DEXA = 0,26gm/cm^2 und DEXA = 0,49gm/cm^2) berücksichtigt. Anschließend wurde osteochondrale Defektheilung in einem lokalen Modell des Gelenkbereiches studiert.

Der Einfluß mechanischer Rahmenbedingungen auf die osteochondrale Heilung wurde durch ein eigens entwickeltes biphasisches Modell für die Gewebedifferenzierung untersucht. Diese Gewebedifferenzierung wurde durch iterative Veränderungen des Elastizitätsmodules simuliert. Dabei wurde eine Kombination von berechnetem mechanischen Stimulus und gewebespezifischen Faktoren für Wachstum und Resorption benutzt. Diese Faktoren basieren auf *in vivo* Daten und konnten im Rahmen dieses Projektes erstmalig mittels numerischer Methoden berechnet werden. Mit der Benutzung des Gewebedifferenzierungsmodelles wurden die Steifigkeiten der verschiedenen, neudifferenzierten Gewebe während der osteochondralen Heilung quantifiziert und mit den histologischen und histomorphometrischen Untersuchungen aus einem komplett dokumentierten Tierversuch verglichen. Zum Schluß wurden die mechanischen Aspekte der osteochondralen Heilung anhand spezifischer, geometrischer Konstellationen von osteochondralen Defekten untersucht. Dazu wurde der Einfluß der lokalen Geometrie des Defektes auf die Heilung analysiert. Modelle mit Defekten von verschiedenen

Breiten und Tiefen wurden erzeugt. Der Einfluß der Knorpeldicke auf die Qualität des neugebildeten Knorpels wurde bestimmt. Osteochondrale Defekte sind in konvexen Gelenkoberflächen öfter zu beobachten als in konkaven. Trotzdem ist die Rolle biomechanischer Bedingungen auf die Heilung bislang noch nicht untersucht worden. Deswegen wurden nach Änderungen der Gelenkgeometrie die jeweils resultierenden lokalen mechanischen Bedingungen und deren Einfluß auf die Heilung untersucht. Zusätzlich wurden die entstehenden mechanischen Bedingungen von verschiedenen, vorgefertigten Defektausfülllungen evaluiert: Heilung unter Verwendung von Grafts mit 100% und 50% der ursprünglichen Kochensteifigkeit wurde vergleichen.

Nach Analyse der Knochenheilung des proximalen Humerus wurden maximale Dehnungen in intakten und frakturierten Knochen bei 90° Abduktion gefunden. Die Ergebnisse zeigten höhere kompressive Dehnungen (bis zu 30%) in Knochen mit niedrigerer Dichteverteilung (geringere durchschnittliche DEXA Werte). Der Einfluß der Knochenqualität auf seine Heilung erwies sich als wichtiger als die Art der physiologischen Belastung; daher sollten neue Konzepte der chirurgischen Behandlung komplexer Frakturen im proximalen Humerus die individuelle Verteilung der Knochendichte explizit berücksichtigen. Dadurch wird eine effektive Stabilisierung der Frakturen in osteoporotischen Patienten oder in Patienten mit osteopenischer Knochendichte ermöglicht.

In der Histologie zeigten osteochondrale Defekte Resorption an der Basis und Ausfüllung an dem Rand des Defektes. Der Defekt wurde hauptsächlich mit fibrösem (70%) statt mit hyalinem Knorpel ausgefüllt. Die Quantität der neugebildeten Gewebe während der Heilung stimmten in dem Finite-Elemente-Modell gut mit der histomorphometrischen Analyse (nach 4, 6 und 12 Wochen) überein; gleiches gilt auch qualitativ für die simulierte osteochondrale Defektheilung mit der in den histologischen Präparaten beobachteten.

Hyaliner Knorpel wurde nur in der ursprünglichen Defektsituation und der mit erhöhter Defektbreite (+33%) gebildet (ca. 35% und 20%). Zirka 5% und 3% von hyalinem Knorpel wurde für die Modelle mit erhöhter Tiefe (+50%) und erhöhter Knorpeldicke (+15%) bestimmt.

Das Modell mit einer konkaven Krümmung (R= 15mm) zeigte einen höheren prozentualen Anteil an hyalinem Knorpel (bessere mechanische Qualität) im Vergleich zu einem Modell mit entsprechender konvexen Krümmung (ebenfalls R= 15mm). Wiederherstellende Defektausfüllung mit der gleichen Knochenqualität erlaubte ebenfalls die Bildung von Knorpelgewebe mit einem höheren Anteil an hyalinem Knorpel im Vergleich zu der Defektausfüllung mit reduzierter Steifigkeit. Auch wurde nur im Graft der ursprünglichen Knochensteifigkeit kalzifizierender Knorpel neu aufgebaut. Eine verminderte mechanischen Qualität der umliegenden Gewebe wurde in beiden Modellen beobachtet im Vergleich zu den intakten Gewebesteifigkeiten.

Insgesamt erlaubte der Algorithmus das Finden mechanischer Erklärungen für ganz unterschiedliche Fälle der osteochondralen Defektheilung. Beispielsweise ergibt sich dadurch der Grund, weswegen der Heilungsprozeß in konvexen Gelenkflächen ungünstiger verläuft.

Die Benutzung eines vorhersagenden Gewebedifferenzierungsmodelles zur Analyse des Heilungsprozesses mag zukünftig in der klinischen Praxis ein Werkzeug zur individuellen Behandlung werden, um die Heilungsbedingungen durch Wahl von Graftsteifigkeit und Belastungen für jede individuelle Knochen-Knorpel Geometrie und Defektsituation zu optimieren.

Summary

Osteochondral healing after trauma or degenerative diseases remains a clinical challenge. It is known that the mechanical properties of the newly differentiated tissue filling osteochondral defects are inferior to the highly specialized native hyaline cartilage. Under specific loads (repetitive, impact or torsional loads) joint tissues could develop fibrillation, fissures and finally osteochondral defects are formed. Without treatment, osteoarthrosis (posttraumatic osteoarthrosis), the most common of the joint injuries, is then expected. Joint degeneration leads to total joint replacement affecting a considerable percentage of the population, which implies a significant social and economic burden. Understanding changes, healing and treatment of osteochondral defects requires studying the mechanical environment of the bone-joint system under physiological loads. The influence of the bone quality on the bone mechanics must be understood to perform a detailed analysis of the joint region where the defect is localized.

The aims of this project were, therefore, first to analyze the mechanical behavior of a bone with an intact joint under physiological loads taking into account the influence of the bone quality and second, to analyze the influence of the mechanical conditions on osteochondral healing.

In order to achieve these goals a study of the bone-joint mechanics was realized. Proximal humeri were used. The strain fields of intact and fractured bones under physiological-like loading were determined. Arm positions of 90° abduction, 90° forward flexion and 0°, the neutral position, were considered. To quantify the influence of the bone quality, the bone tissue straining of osteoporotic bones (DEXA = 0.26 gm/cm^2, and DEXA = 0.49 gm/cm^2) was analyzed. Finally osteochondral defect healing was studied with a local model of the joint region.

To study the influence of mechanical conditions on osteochondral healing, a predictive biphasic model for tissue differentiation was developed. Tissue differentiation was simulated through iterative changes of the elastic modulus of Young. A combination of a mechanical stimulus with a factor for differentiation defined for each tissue was used to regulate tissue differentiation. These factors, which are based on *in vivo* data, were calculated for the first time during the development of this project using numerical methods.

Applying the tissue differentiation model, the stiffness of each differentiated tissue during osteochondral healing was quantified and compared with histological and histomorphometric healing outcome of a well-documented experiment with animals. Finally, mechanical aspects of healing in specific geometric constellations of osteochondral defects were evaluated. The influence of the local defect geometry that allows healing was analyzed. Defects with different width and depth were modeled. The influence of the cartilage thickness on the mechanical quality of the differentiated cartilage was evaluated. In clinical practice osteochondral defects appear to occur more frequently in convex joints than in concave joints. The mechanical environment generated after changes in the joint curvature and how it affects the process of healings was determined. Finally, the mechanical conditions arising from different predesigned

defect fillings were evaluated: Healing using grafts with 100% and 50% of the native subchondral bone stiffness was compared.

Analyzing bone healing in proximal humerus, maximal strain values were found for the intact and fractured bone at a 90° abduction. This study demonstrates that in a fractured bone of poor quality considerably higher bone strains (up to +30%) are found than in a more healthy bone. New concepts for the surgical treatment of complex fractures of the proximal humerus should take the specific bone density distribution of osteoporotic or osteopenic bones into account and thereby allow an effective stabilization of fractures in osteoporotic patients.

Histologically, the osteochondral defects showed bone resorption at the base and bone formation from the circumference. The defect was principally filled with a fibrous cartilage (70%) and only a minor percentage of hyaline cartilage formed (30%). The amount of cancellous, cartilaginous, and fibrous tissue and the size of the unfilled defect as measured in histomorphometric analysis for three time points (4, 6 and 12 weeks) were comparable in magnitude to that predicted by finite element analysis. Qualitatively, simulated healing agreed with the histological findings.

Only in the initial defect and the larger defect situation (defect width +33%) did the adaptive finite element analysis predict cartilage formation (app. 35% and 20%). Minor hyaline cartilage formation (<5% and <3%) was predicted in the models with increased depth (+50%) and increased cartilage thickness (+15%) respectively. The concave model (R= 15mm) showed a more appropriate filling of the defect with tissues of higher quality than those obtained with a convex model of the same radius of curvature. Defect filling restoring subchondral bone quality allowed a larger amount of hyaline cartilage formation than a less rigid filling. In both models the mechanical quality of the remaining cartilage appeared to be reduced compared to the intact tissue stiffnesses.

In general, the algorithm allowed a mechanical explanation to be formulated for the healing response of the different evaluated cases, since, for example, a mechanical reason for the less favorable clinical outcome of convex surfaces was found. The usage of a predictive tissue differentiation model to analyze osteochondral healing might even be extended in conjunction with patient specific data to predict the outcome of osteochondral repair. It will allow an optimization of boundary conditions required for osteochondral healing through selection of appropriated loads and/or stiffness of defect fillings.

1 Introduction

Approximately 50% of the elderly population, and even young patients normally after traumatic events, suffer joint disorders. In fact, the World Health Organization (WHO) declared the years 2000-2010 to be the bone joint decade. Cartilage damage, osteochondral defects (defects going from cartilage through bone) and cartilage degeneration is thus an important topic requiring deeper understanding. Mechanical conditions influencing osteochondral healing is the theme of the present work. The mechanical quality of the repaired tissues after the healing process is essential to preserve joint functionality. Tissue repair means restoration of the initial mechanical quality of affected tissues (after injury or trauma) and the consideration of biological aspects related with their healing process. Successful healing is characterized not only by reestablishing full functionality but also by avoiding long-term acceleration of degenerative damage. The tissues that actually are most frequently treated for repair are skin (replacement), cartilage (induced repair, replacement), bone (replacement), liver (artificial transplants) and heart (cardiac prostheses) (Lysaght and Hazlehurst, 2004). To be able to repair cartilage tissue, the study of its biomechanical aspects is required.

Biomechanics can be defined as the application of principles derived from engineering sciences (mechanics) to understand and to explain biological events (gait analysis, musculoskeletal movement) and processes (fracture healing, osteochondral healing, damage, cell differentiation). Classical concepts of physics, chemistry, mathematics and biology are also used. From this topic, tissue engineering was developed as a research discipline in the 1970s and matured into preclinical application during 1990s (Lysaght and Reyes, 2001). It has been defined as devices or processes that: 1. Combine living cells and biomaterials. 2. Utilize living cells as therapeutic or diagnostic reagents 3. Generate tissues or organs *in vitro* for subsequent implantation and/or 4. Provide materials or technology to enable such approaches (Griffith and Naughton, 2002; Lysaght and Hazlehurst, 2004; Lysaght and Reyes, 2001).

A vigorous development of tissue engineering has been focused on repairing osteochondral defects. The mechanobiological study of osteochondral defect healing requires the knowledge of physiology and pathology of cartilage. Articular cartilage acts mainly by transmitting physiological loads between joints to the underlying subchondral bone. In an intact situation, articular cartilage shows a white, smooth and almost frictionless surface. When damage occurs, the first changes appear in the surface: micro-cracking, fibrillation, loss of the superficial layer, osteophytes formation, which implies an increase of the friction coefficient and diminution of the range of motion. Moreover, a reduction of the water content can be observed. Finally, the tissue could fail, thereby creating osteochondral defects (Buckwalter and Mankin, 1998; Buckwalter and Mankin, 1998; Buckwalter and Mankin, 1998; Carter, et al., 2004; CHEN and BROOM, 1998; Eckstein, et al., 2001). As a result, understanding biological (Benjamin and Ralphs, 2004; Revell and Heatley, 1988; Zhurakovskii, et al., 2002), genetic (Fortier, et al., 2001; Grande, et al., 2003; Hidaka, et al., 2003; Pascher, et al., 2004), mechanical (Boschetti, et al., 2004; D'Lima, et al., 2001; Frost and Jee, 1994; Heiner and Martin, 2004; Kääb, et al.,

1998; Li, et al., 2005; Smith, et al., 2004) and mechanobiological aspects (Beaupré, et al., 2000; Carter, et al., 2004; Carter and Wong, 2003; Frederick H. Silver and Bradica, 2002; Loboa, et al., 2003; Raimondi, et al., 2001; Sarin and Carter, 2000; Silver and Bradica, 2002; van der Meulen and Huiskes, 2002) of cartilage and osteochondral healing becomes important. Specifically, research has been directed to find a practicable clinical solution to restore joint mechanics in order to avoid or to delay the employment of prostheses for total joint replacement. Interdisciplinary cooperation is necessary to develop tools that can be employed to diagnose joint damage, to repair it and to maintain the optimal long-term mechanical properties of the repaired tissues (Buckwalter and Brown, 2004; Buckwalter, et al., 2003; Butler, et al., 2004; Guilak, et al., 2001; Hattori, et al., 2004; Poole, 2003; van den Berg, et al., 2001; Wang and Yu, 2004). Actual studies (animal models, numerical approaches, etc.) investigate the role of mechanical conditions on osteochondral healing. The loads acting on the joint should then be evaluated as well as the mechanics of the bone to facilitate a more precise local study of the joint region.

The aims of this project were to understand the biomechanical behavior of an intact and injured joint under physiological loads while taking into account the influence of the bone quality, and subsequently to study the mechanical aspects of osteochondral healing.

This work is subdivided into five chapters. In Chapter 1, the **introduction**, four sections are found: The clinical problem, related to osteochondral healing is described. Cartilage analysis and function follows in which the physiology of the articular cartilage, the pathology of synovial joints and its treatments, as well as the techniques used to measure the cartilage material properties are presented. Additionally, this section describes several tissue differentiation models. The third section, preliminary work summarizes the previous two projects by Lill, related to bone – joint mechanics and Bail, related to osteochondral healing, whose results were used to validate the models developed in the present work. Hypotheses and aims of the present project are then stated. Subsequently, the remaining chapters, **material and methods**, **results**, **discussion** and **conclusions** are presented.

1.1 A brief introduction to osteochondral healing

1.1.1 The clinical problem

Trauma, degenerative diseases or repetitive and sudden loads, through sports activities for example, can produce articular damage, which could result in osteochondral defects (Arokoski, et al., 2000; Brittberg and Winalski, 2003; Petersen, et al., 2003; Sgaglione, 2003). Approximately 60% of these defects occur after trauma in teenagers (Buckwalter, 1999) (Fig. 1.1). In older patients, articular damage is attributable to degenerative diseases (50% in individuals > 60 years old) (Buckwalter and Mankin, 1998; Hjelle, et al., 2002).

Independently of the causes (trauma or disease), osteochondral defects commonly do not heal or are filled with a fibrous instead of hyaline cartilage, which is characterized by reduced mechanical properties compared with the highly specialized compressive capabilities of the

native tissue. As a result, fragmentation and degradation of the fibrous tissue may occur, thus exposing the subchondral bone to further damage (Buckwalter, 1999). Without treatment, osteoarthrosis and potentially joint replacement could be expected (Petersen, et al., 2003). The treatment of chondral and osteochondral defects remains one of the most ambitious challenges in the field of traumatology and orthopedics.

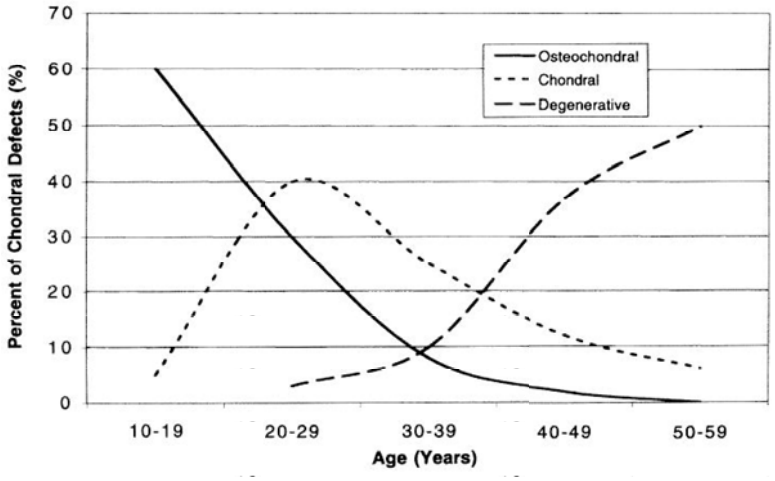

Fig. 1.1: Schematic representation of the relationship between age and types of chondral defects. Osteochondral defects included osteochondritis dissecans and low energy osteochondral fractures occur most frequently in skeletally immature individuals and individuals who recently have completed skeletal growth. Chondral defects, localized tears or disruptions of articular cartilage that do not extend into subchondral bone occur most frequently in young adults. With increasing age the frequency of degenerative lesions of the articular surface increases (Buckwalter, 1999) (figure with corresponding text).

1.1.2 Searching for a solution

Some experimental studies with animals have demonstrated the influence of mechanical conditions on osteochondral repair (Buckwalter, et al., 2003; Case, et al., 2003; Salter, et al., 1980). In an *in vivo* experiment with 120 rabbits, 480 osteochondral defects were surgically created and stimulated to induce repair through passive motions (Salter, et al., 1980). The results demonstrated that healing was not only faster than in the control group (without stimulation) but also that after histological analysis the restored tissues showed a better mechanical quality.

More recently, tissue differentiation models have been developed to analyze the influence of specific mechanical boundary conditions on healing. The usage of these models allows the determination of the strain environment for differentiation that enables healing, which is indeterminable *in vivo* (Duda, et al., 2005; Kelly and Prendergast, 2004). Improved understanding of the influence of mechanical conditions on osteochondral repair may contribute to elucidate its relation with the biological healing process in order to prevent osteoarthrosis and thus, limit loss of joint functionality (Buckwalter and Brown, 2004). Apparently, clinical

reports indicate that convex joints are more frequently affected by osteochondral defects compared to concave ones (Hjelle, et al., 2002). However, no study has so far been published to explain this occurrence. Healing of osteochondral defects could be influenced by the local mechanical environment generated after changes in the mechanical boundary conditions of the defect.

Considering the restricted capacity of the cartilage to repair itself, techniques have been developed to reestablish joint functionality (Cancedda, et al., 2003; Chu, et al., 1995; Wang, et al., 2004). One of these treatments employs the usage of autografts. Since only a limited quantity of unloaded cartilage regions are available, the implantation of predesigned plugs made out of biomaterials becomes an important alternative (Buckwalter, 2003; Evans, et al., 2004; Giannini, et al., 2002; Gole, et al., 2004). The mechanical properties of the used fillings and the subchondral bone possibly need to be similar in order to reduce stress concentration at the interface graft-host tissue. This could avoid the frequently reported loss of anchorage between the host tissue and the defect filling (Akens, et al., 2001; Hangody and Fules, 2003; Kuroki, et al., 2004; Nam, et al., 2004; Tibesku, et al., 2004).

1.2 Cartilage analysis and function

From a study of 1000 arthroscopies, 61% of the revised patients revealed any type of chondral or osteochondral defects of which 19% were focal osteochondral defects (Hjelle, et al., 2002). In the USA, the annual costs for the treatment of joint degeneration amounts to more than $60 billion, thus affecting the quality of life of more than 20 million of Americans, implying an immense social and economic burden[1] (Buckwalter, et al., 2004).

As a result, a high percentage of clinical and basic research has aimed to analyze the nature of the cartilage and the surrounding tissues of the joint. After interdisciplinary studies of the joint region, it has been possible to elucidate its mechanical behavior, its structure characterization, its material properties and its diseases. The knowledge of cartilage nature and properties can be used to prevent cartilage damage or to promote its repair. Even at a cellular level, the mechanical properties of chondrocytes have been analyzed. The most frequent techniques used are high-resolution sonography (Keogh, et al., 2004), atomic force microscopy (AFM) (Park, et al.), nuclear magnetic resonance (NMR) (Perez and Santos, 2004), magnetic resonance imaging (MRI) (Burstein and Gray, 2003; Chen CT, et al., 2003; Graichen, et al., 2004; Kornaat, et al., 2004) and Doppler effect (Strunk, et al., 2004). Some of these techniques have been implemented in innovative devices (ultrasound arthroscopic indenters (Laasanen, et al., 2003; Toyras, et al., 2001), creep cytoindentation apparatus (CCA) (Koay, et al., 2003), handheld dynamic indenters (Appleyard, et al., 2001), arthroscopic dynamic and static

[1] *Burden of disease:* refers to the combination of the incidence/prevalence, impact (in terms of quality of life and disability) and cost of musculoskeletal conditions. Defined by the Bone and Joint Decade 2000-2010 Council.

indenters (Lyyra-Laitinen, et al., 1999; Toyras, et al., 2001)) to measure *in vivo* and *in vitro* mechanical parameters (elastic modulus of Young, permeability, Poisson's ratio, etc.) from cartilage specimens or chondrocytes. These mechanical parameters show how cartilage changes its material properties as a response under specific physiological and pathological conditions. Additionally, new concepts such as pathways signaling and regulating chondrocyte activity have been used to explain the complex mechanobiological behavior of this zone. In this work a model for tissue differentiation is proposed as a potential tool to understand the mechanical aspects of this region. Using the finite element method (FEM), changes in the mechanical properties of the tissues during healing could be predicted in dependence of the acting mechanical conditions. For the development of a tissue differentiation model, some concepts involving bone remodeling, tissue differentiation and cartilage repair were linked and the corresponding models studied.

A synovial joint consists of hyaline cartilage, subchondral bone plate (calcified cartilage), subchondral bone and cancellous bone. Hyaline cartilage is an avascular, aneural and alympathic tissue, which lives from diffusion. The synovium, a fine membrane at the articular interfaces, secretes synovial fluid and provides the nutrients required by the tissues within the joint. Articular cartilage is a multiphasic material with a fluid and a solid phase. The fluid phase is composed of water and electrolytes and the solid phase consists of chondrocytes, collagen, proteoglycans and other proteins. Each phase contributes to the mechanical and physicochemical properties of the articular cartilage. Physical models should thus describe cartilage as a biphasic material, whose mechanical behavior is given by the concepts and laws used in soil mechanics (rule of mixtures). Mow and his group have made several contributions to illustrate this and justify the usage of this assumption (Mow, et al., 1989; Mow and Ratcliffe, 1997).

Structurally, cartilage components (chondrocytes and extracellular matrix) are arranged in distinct zones each with a different and specific structure and function: a superficial or tangential zone, a middle zone or transitional zone, a deep zone and a zone of calcified cartilage (Fig. 1.2) (Buckwalter, 1983; Horký, 1993; Hunziker, et al., 2002). These zones are characterized by a distinct microstructure associated with a specific capacity to support and to transmit acting external loads. Hence a relation between each structure zone of the cartilage and its function has been established. The superficial tangential zone (10 to 20% of the total cartilage thickness) is limited by a superficial layer or *lamina splendes*, which serves as a skin or barrier protecting the cartilage from the synovial environment. This zone has a high water content and shows ellipsoidal chondrocytes parallel to the synovial surface. This structure contributes principally to the dissipation and transmission of load, principally tensile and shear, allowing large compressive strains. The middle zone represents approximately 40% to 60% of the total cartilage thickness with low fluid flow and shows redounded chondrocytes forming a quadratic array similar to vertical "arcades" (Benninghoff model). Such structural arrengements are appropriate for the support and transmission of compressive loads allowing moderate compressive strains (Mow and Ratcliffe, 1997).

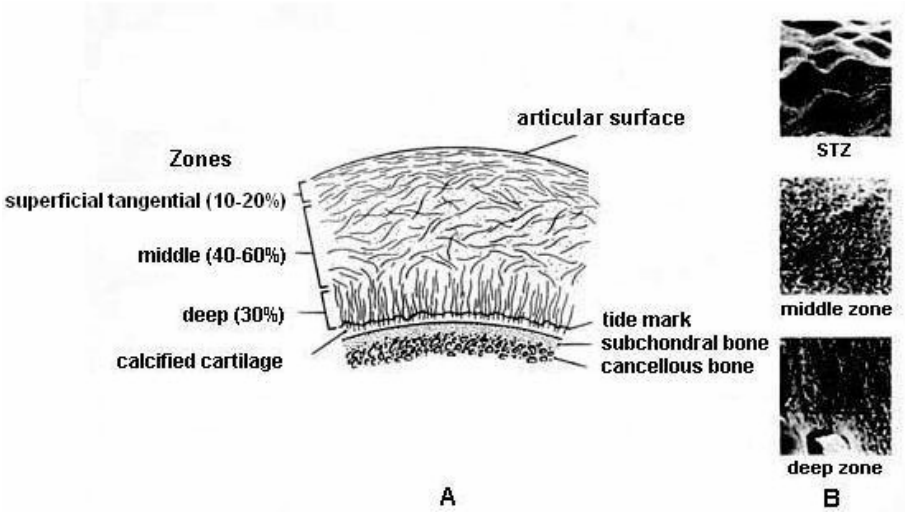

Fig. 1.2: Schematic representation of the cartilage zones. The mechanical properties of cartilage are changing in a functional – structure relation. The elastic modulus of Young is reduced from the upper zone (tangential) to the deeper regions (Mow and Ratcliffe, 1997).

The deep zone (about 30% of the total articular thickness) shows a minor quantity of chondrocytes, which are aligned, perpendicular to the subchondral bone traversing the "tidemark" or *lamina limitants* with anchorage in the calcified cartilage. The structural conformation of all these zones has been associated with the cartilage's capacity to support compressive loads. However, according to latest publications minor differences have been encountered, when these zones have been included or excluded in the simulation of the mechanical behavior of the joint. In this project, cartilage was simulated as biphasic, isotropic, linear elastic without consideration of the above described structural cartilage zones (tangential, middle, and deep zone). Only insufficient information exists to describe all mechanical parameters of each cartilage zone necessary to model it as a non-homogeneous biphasic material (e.g. permeability and porosity defined in dependence of the cartilage deep). Therefore, cartilage was modeled as an isotropic biphasic material - that is, stiffness, Poisson's ratio and permeability were defined to be the same in each material direction. However, the differentiation model created in this project is able to predict inhomogeneous cartilage stiffness. That is, the stiffness distribution of the cartilage after healing was different in different locations of the cartilage (non-homogeneous). In this form, although the tissue differentiation model started with a homogeneous material definition for the cartilage, a non-homogeneous stiffness distribution can be predicted.

1.2.1 Joint diseases and treatments

When an external load acts on a joint, the fluids inside the cartilage are activated and its movement known as fluid exudation is initiated. Fluid exudation implies the movement of the fluids in a parallel but opposite direction to the applied load. The principal tasks of these fluids are to attenuate the acting loads between the collagen matrix and the subchondral bone (Bader, et al., 1992; Broom and Poole, 1982; Buckwalter, 1983; Buckwalter and Mankin, 1998;

Ghivizzani, et al., 2000; Hunziker, et al., 2002; Hunziker, et al., 1996; Ikenoue, et al., 2003; Poole, et al., 2001). The collagen fibrils query the form and tensile strength properties to the cartilage tissue. The interaction between the aggrecans (a component of the cartilage) with the cartilage water is responsible for its compressive stiffness and its durability. When the loads are slowly applied, the cartilage is able to achieve a maximal deformation by fluid exudation and fluid redistribution, which reduces the effect of the acting load by generation of hydrostatic pressures. In contrast, when sudden loads act on the joint, a high percentage of the acting load is directly transmitted to the collagen matrix and could cause its collapse (fractures). Finally, cartilage cells are affected: overstrains could cause structural changes producing cellular damage including cell death. Consequently, joint mechanics are altered, thus loosening their ability to attenuate and to transmit the acting loads. In normal conditions sudden and quick external forces are absorbed by muscle contractions as well. However, in some situations the loads act so rapidly that neither are the muscles able to respond nor are the fluids inside the cartilage able to attenuate the acting forces. Damage at the articular surface occurs. A study of the response of human's articular cartilage from humans to blunt trauma showed that it could resist impact loads of as much as 25N/mm^2 (25MPa) without apparent damage. However, repetitive loading can propagate along vertical cartilage fissures from the joint surface to the calcified cartilage, extending oblique fissures into areas of intact cartilage. Thereby the affected areas increase, eventually generating cartilage flaps and free fragments (osteochondrosis dissecans). In general, three major cases exist in which damage of cartilage and joint degeneration may occur: trauma, disease or sports.

Three classes of chondral and osteochondral injuries can be identified based on the type of tissue damage and repair response: 1. Damage of the joint surface without visible mechanical disruption of the articular surface; however this does cause chondral damage and may cause damage of the subchondral bone. 2. Mechanical disruption of the articular surface limited to articular cartilage 3. Mechanical disruption of articular cartilage and subchondral bone simultaneously (Buckwalter, 2002). In this project, osteochondral defects corresponding to the third injury category were analyzed.

To classify articular defects, some systems and nomenclatures have been suggested: Outerbridge described four grades of cartilage damage in chondromalacia. Grade I describes softening of the surface, the grade II fissuring without reaching the subchondral bone, and grades III and IV describe defects going into or beyond the subchondral bone plate with exposition of the bare bone. Bauer and Jackson used a descriptive arthroscopic classification. Grades I to IV are used for defects on the articular cartilages with cracks, flaps and crater formation and grades V and VI for acute injuries and degrading cartilage with fissuring for older degenerative lesions (Nehrer and Minas, 2000). In order to standardize the system of articular defect classification, the International Cartilage Repair Society (ICRS) proposed a nomenclature to describe the grade of damage of the cartilage (Fig. 1.3). This classification is based on a combination of the defect depth (quantitatively) and a qualitative description of each joint region. Four different grades of the defect have been defined: the first three involve

different depths of defects inside the cartilage and the last grade describes a defect which moves to the subchondral bone. In all computer models developed in this project, cartilage defects grade 4B (Outerbridge IV) were simulated. However, some cases following a detailed histomorphometric analysis of cartilage defects revealed that damage of the matrix can occur without disruption of the surface. Subsequently, rupture of the collagen fibrils, depletion of proteoglycans and increase in the hydraulic permeability leading to insufficient mechanical function of the joint is expected with consequential joint degeneration.

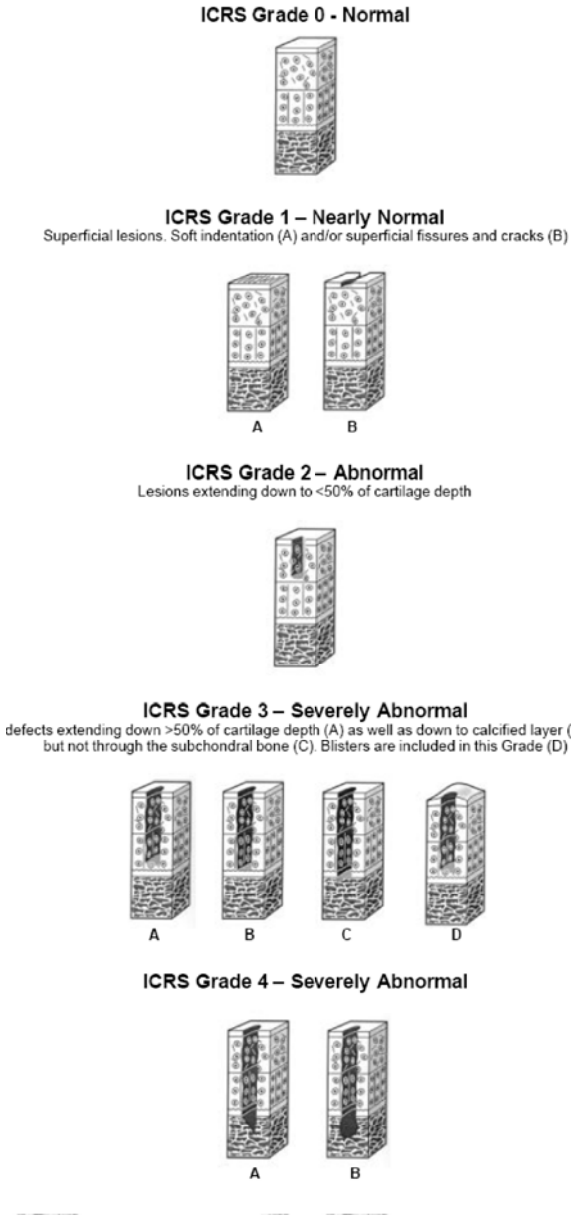

Fig. 1.3: ICRS classification of osteochondral defects. In this project osteochondral defects grade 4B (severely abnormal) were modeled.

Conservative treatments such as the use of drugs could help to avoid severe pain and to reduce the inflammatory response of the cartilage damage. Physiotherapy is used to reduce the symptoms of the cartilage damage. Joint mobility and range of motion should be thereby

maintained. When cartilage suffers severe damage surgical treatment is required. Although treatment of symptomatic full thickness defects remains a challenge, the objectives are to restore joint function, providing a pain-free weight-bearing joint with full range of motion. Additionally, the rebuilt tissue should demonstrate mechanical properties that prevent any articular degeneration. In general, two different treatments exist: one that simulates or initiates a repair process and another that uses replacement or transplantation of tissues. The first category includes debridement, lavage, blot clot techniques, osteotomy, joint distraction, soft tissue grafts, cell transplantation, growth factors and artificial matrices. In essence these techniques support chondrogenic cells to reach the injury site. Cells can generally migrate from the bone marrow, from a graft of periosteum or perichondrium, from cultured periosteal or perichondreal cells or from pure chondrocytes. The second category includes graft transplantations: autografts, allografts und xenografts.

1.2.1.1 Techniques to stimulate repair

1.2.1.1.1 Debridement and lavage

Jackson, a pioneer of arthroscopy, used the effect of joint lavage for the first time in North America. He found that during arthroscopy the usage of high flow water cleans the knee joint of debris from degenerated and inflammatory regulators in the joint. This fact produced pain relief without the necessity of any surgical intervention. Some patients showed improved joint functionality after 3 years of arthroscopic examination. The technique was combined with debridement of cartilage flaps, retrieval of loose bodies and partial synovectomy. Even better results were obtained as a result. The technique was later applied for treatment of young patients. However, after comparing the healing outcome for 14 years, only 50% of the patients showed joint degeneration. Thus this technique is unable to induce any repair and therefore cannot prevent joint degeneration. Surgical treatment of joint defects includes blot clot techniques (abrasion, drilling and microfracture), osteotomy, usage of soft tissue grafts and artificial matrices to stimulate the formation of a new articular surface.

1.2.1.1.2 Blot clot techniques

The depth of the defect is essential for cartilage repair. When the depth of the defect reaches the subchondral bone disruption of the blood vessels occur. Blood clots inundate the defect region. If overloading is avoided, undifferentiated mesenchymal cells migrate into the clot, proliferate and differentiate to cells with morphological features of chondrocytes. The differentiation process continues until a tissue with stiffer mechanical properties fills the defect. However, it is up to now unclear exactly how this process takes place. Mechanical, biological and chemical pathways have been proposed and analyzed. Even if the initial defect does not reach to the subchondral bone, a penetration into the subchondral bone layer is artificially created in order to promote a clot blood formation and the subsequent healing cascade. These surgical techniques belong to the most frequently used in clinical practice and include subchondral drilling, microfracturing and abrasion arthroplasty.

Drilling

In 1959 this technique was described first by Pridie and it is the oldest of these perforation techniques. The subchondral bone is drilled, bleeds and the healing process is started. Usually fibrous tissue is formed after the usage of this technique. Its main risks are damage to the subchondral bone by heat from the drill or causing subchondral bone haematoma. The obtained results are good, achieving an efficiency of 85% after 62 months of follow-up, principally when this technique is combined with a high tibial osteotomy.

Microfracture

Steadman employed this technique for the first time in 1999. After a meticulous debridement of the cartilage defect (including the calcified cartilage), the subchondral bone is penetrated using small awls approximately 3 mm deep and with perforations approximately 2 to 3 mm apart. From a study of 255 consecutive cases of subchondral defects grade IV (ICRS classification) performed by Steadman's group, 75% of the patients showed pain relief and good functional outcome, 20% demonstrated no benefit and 5% needed revision surgery after 5 years (Steadman, et al., 2001). The advantage of this technique in comparison with drilling is that the possible damage of the subchondral bone by heat of the drill is avoided. Studies conducted by Rodrigo et al., showed that this technique, accompanied with a rehabilitation therapy of passive motion, increases its efficiency even further.

Abrasion arthroplasty

Abrasion arthroplasty is performed arthroscopically with an automated burr by removing up to 2mm of the exposed sclerotic bone down to the vasculature of the subchondral bone plate and fibrillation at the border of the defect. When the tourniquet is relaxed a blood clot is formed in the defect. This technique achieves a 53% efficiency rate in elderly patients and 86% in short-term follow-up of younger patients (Johnson, 2001). Bone marrow stimulation techniques require an intensive rehabilitation program. However, passive motion and protected weight bearing during the first six weeks have shown better healing results than cases lacking this therapy.

Although the blot clot techniques allows pain relief and an acceptable grade of joint functionality, the repaired tissue always consists of fibrous tissue only. Additionally, it was found that after repetitive intentional penetrations of the subchondral bone, the formation of multiple calluses as a repair response could cause subchondral sclerosis generating a negative cascade of biological responses that finally deteriorates the newly differentiated cartilage.

1.2.1.1.3 Osteotomy

Osteotomy is a surgical technique to treat hip and knee joints with localized loss or degeneration of the articular surfaces. The surgery consists of a cut of the bone tissue in the proximal or distal region. The aim of the surgery is to perform changes in the slope or in the angle formed between the planes passing through the contact areas of the articular surfaces of

the bones involved. Such changes reduce, or even eliminate, contact pressures or overloaded regions that could cause damage of the articular surfaces. These changes induce variations in the rotation centers of the hip-knee-ankle joint system correcting its possible misalignment (Buckwalter and Mankin, 1998). Alignment is measured on an axis passing through the center of the femoral to the center of the ankle (up to 1.2° varus in healthy patients). A high tibial osteotomy refers to a cut below to the level of the articular surface of the proximal tibia, normally on the tibial tuberosity, parallel to the joint, which can be complete or partial (an intact bone region remains). Patella kinematics and patello-femoral contact areas have been studied in healthy patients and in patients with genus varus and mild osteoarthritis to determine the mechanical parameter that could be altered due to improper joint alignment and how it could be corrected (Hinterwimmer, et al., 2004). Osteotomy has been used to treat primary osteoarthrosis (developed without trauma) of the ankle. In general, osteotomies can be performed in the coronal plane (varus and valgus osteotomies) or in the sagittal plane (flexion and extension osteotomies). The effect of correction in the sagittal and frontal plane by high tibial osteotomy has been demonstrated (Marti, et al., 2004; Trumble and Verheyden, 2004).

Recent studies showed that the valgus high tibial osteotomy for unicompartmental varus osteoarthritis could reduce compressive pressure distribution in the posterior part of the tibial plateau. In this form the damaged zone could be unloaded avoiding its total degeneration (Agneskirchner, et al., 2004). Other authors combine high tibial osteotomy for varus knee correction with resurfacing techniques (subchondral bone penetration) to treat chondral defects (Sterett and Steadman, 2004). In this technique, external fixators are used to stabilize the osteotomy. The question is to decide when there is “enough” consolidation of the bone for safe removal of the external fixator. This technique has the principal advantages of decreasing symptoms and stimulating the formation of new cartilage. However, the patients suffer recurrent pain and demonstrate evidence of progressive osteoarthritis.

1.2.1.1.4 Soft tissue transplantation

This technique is used to treat chondral and osteochondral defects in which soft tissues (fascia, joint capsule, muscle, tendon, periosteum or perichondrium) are used to cover the defect region. Two theories underlie this clinical practice: 1. The defect should be covered mechanically and 2. In the case of periosteum or perichondrium a number of pluripotent stem cells in the perichondrium or in the cambium layer of the periosteum exist to differentiate into chondrocytes. The soft tissue grafts can be fixed into the defect using fibrin glue or sutures. Typical failures of this technique are calcification and ossification in the graft area. In this case collagen type X (bone) instead type II (cartilage) is detected indicating chondrocytes hypertrophy, which promotes enchondral ossification in the defect (Nehrer, et al., 1999; O'Driscoll, 1999).

In experimental studies with animals osteoperiosteal grafts were implanted to treat osteochondral defects. The potential of immobilization, intermittent active motion, and continuous passive motion to stimulate repair was evaluated (O'Driscoll and Salter, 1986). A

group of animals without stimulation was used for control. After five weeks, hyaline cartilage was predominantly found in 70% of the defects treated with continuous passive motion compared with 10% observed in the group treated with immobilization, intermittent passive motion, and the control group.

In a later study periosteum transplants were combined with the application of transforming growth factor-ß. Experimental studies with animals showed good results. Xeno-transplantation has been studied as an alternative. In an experiment with animals, cultured chondrocytes from pigs were injected under a periosteal flap to treat chondral defects in rabbits. The chondral defect was filled to 90% with good integration between the host cartilage and the neo-differentiated cartilage. The repair tissue showed a smooth surface with cells similar to chondrocytes and a hyaline-like extracellular matrix (Ramallal, et al., 2004). However, in clinical practice detachment of the graft can occur later (O'Driscoll, 2001; O'Driscoll and Fitzsimmons, 2001; O'Driscoll, et al., 1988).

1.2.1.1.5 Autologous chondrocyte implantation

This method is complementary to the soft tissue transplantation technique. Autologous chondrocytes are cultured *in vitro* and are injected under the soft tissue transplant, which is sutured to the defect. The reason for the selection of chondrocytes for implantation is obvious: chondrocytes form cartilage by synthesis and chondrocytes are responsible for the unique feature of articular cartilage. The goal of the orthopedic surgeon is to try to deliver an optimal number of the acquired cell types (autologous chondrocytes) into the cartilage region to best achieve repair. Peterson and co-workers performed the first investigations using this method in 1984. Autologous chondrocytes transplantation was used to treat defects in the rabbit patella and comparisons between healing after periosteum transplantation with and without application of a suspension of cultured autologous chondrocytes were carried out. Brittberg considerably improved the surgical technique and used the same rabbit model experimentally (Brittberg, 1999; Brittberg, et al., 1994; Brittberg, et al., 2001; Brittberg and Winalski, 2003). Subsequently, the technique was employed to treat chondral defects at the knee. Brittberg and co-workers have obtained good results with patients for several years. They are convinced that the future in the treatment of chondral and osteochondral defects should include the development of biodegradable grafts with implantation of cell suspensions containing a large number of autologous chondrocytes. They called this possible technique biomedical surgery (Brittberg, et al., 2001). The O'Driscoll group has investigated this technique and compared the usage of autologous chondrocytes to human mesenchymal stem cells. They demonstrated that the usage of stem cells showed better healing outcome than by injection of autologous chondrocytes (O'Driscoll, 1999). Autologous chondrocyte transplantation is actually a promising field of research in which the question has been directed to determine the optimal type of cell (should autologous chondrocytes be replaced by autologous stem cells?) as well as the number of required cells to guarantee cartilage repair.

1.2.1.2 Transplantation techniques

These techniques are frequently used to treat osteochondral defects of high diameter. They use transplantation of cartilage as a part of an osteochondral graft to replace focal regions of damaged articular cartilage. The plugs normally have a diameter of 5 to 15mm and can be used to fill defects of up to 9 cm^2 of superficial area. The graft technique is subdivided in autografts, when the graft is taken from an "unloaded" region of an articular surface of the same patient, allografts when the graft is taken from another patient (same specie), and xenografts, when the graft is taken from articular surfaces of another organic entity (animals). Each technique is selected in dependence of the bone quality, age of the patient and size of the defect. The principal advantages of using grafts are to provide a fully formed articular cartilage matrix and the potential for transplanting viable chondrocytes that can maintain the matrix.

Fibrous cartilage is appropriate to support and to transmit tensile loads, but in fact, in the majority of the cases, compressive loads act on synovial joints (e.g. at the knee), which could be optimally supported by hyaline cartilage. These joints are known as weight-bearing joints. For this reason cartilage transplantations from the same patient are currently used to fill the defect using autografts taken from "unloaded" regions at the joint. Since only a limited number of these regions are available, and such a transplantation in some cases represents a risk for the patient, allografts or predesigned biomaterials with a porous structure are frequently used to fill the defect (Evans, et al., 2004; Hunziker, 1999; Jackson, et al., 2001; Porter, et al., 2004). This practice is specially employed for the treatment of osteochondral defects in young patients (Buckwalter, 1995; Roughley, 2001) or in patients with defects with a diameter smaller or equal to 20 mm (Buckwalter, 1999; Ghadially and Ghadially, 1975; Hunziker, 2002; Kaar, et al., 1998; Newman, 1998; O'Driscoll, 1998; O'Driscoll and Fitzsimmons, 2001). In critical situations the usage of transplantations of stem cells from the bone marrow or from perichondrium are recommended (Barry and Murphy, 2004; Breinan, et al., 1997; Grande, et al., 2003; Meinel, et al., 2004; Oreffo and Triffitt, 1999; Rutherford, et al., 2003; Shapiro, et al., 1993; Wakitani, et al., 1994).

The first clinical reports about the usage of autografts showed a newly formed cartilage with 70-80% of hyaline consistence. However, the principal reason to use grafts in a long-term treatment is to conserve the original structure and the mechanical quality of the subchondral bone and within its capacity to transmit the acting external forces. In the present work, the effect of predesigned biomaterials on healing was evaluated using a tissue differentiation model to simulate osteochondral repair. Other treatments include the usage of hormones, medicaments or growth factors to promote or to improve osteochondral repair.

1.2.1.2.1 Autologous graft transplantation

Basically this technique involves cylinders of cartilage and subchondral bone taken from "unloaded" or minor weight-bearing areas of the patient and implanted into the prepared defect. Wagner used this technique for the first time in 1964. Hangody et al. and Bobic have been

performing further developments since 1996 (Bobic, 1999; Hangody, et al., 1997; Hangody, et al., 1998). Hangody et al. implanted an average of 7 grafts per defect in 113 patients with mainly femoral defects from 1 to 8 cm^2. After 3 years, the patients showed good joint functionality. Using the hospital for special surgery knee score system (HSSK) they determined scores from 91 (range 52 – 100), 91% of the patients showed pain relief and joint functionality after surgery. According to Hangody and co-authors in 10 years of clinical experience, this technique is ideally suited for osteochondral defects between 1 to 4 cm^2 in patients less than 50 years old and without signs of osteoarthroses in another articulation (Hangody and Fules, 2003). The non-weight bearing patello-lateral periphery is usually selected as the donor site which later can be filled with fibrous cartilage. The treatment of large size defects with autografts is possible but implies the risk of donor-site morbidity. The surgical technique has recently been updated and is well documented (Hangody, et al., 2004). This technique, combined with osteotomy of the anterior cruciate ligament, showed good results (Ueblacker, et al., 2004). Lane and co-workers reported histological, chemical and biomechanical follow-up in a 6 months study of osteochondral defects filled with autologous plugs. The results showed bone restoration in all cases and a newly fibrous tissue filling the cartilage region. However, a gap at the interface between newly formed hyaline-like cartilage and host tissue was observed. The authors concluded that autogenous transplantation of osteochondral plugs is possible with integration of subchondral bone and preservation of chondral viability[2] (85% at 6 months follow-up) although a cleft between the host cartilage and the differentiated cartilage was visible. An important observation in that study was that the stiffness of the graft from the donor site was not the same as that encountered in the recipient joint. They close the discussion by proposing the necessity to perform an experiment in which the stiffness of the donor site matches with the stiffness of the recipient site and to analyze its effect on osteochondral healing (Lane, et al., 2004).

1.2.1.2.2 Allografts

The same surgical procedure as used in the autograft techniques can be employed to implant fresh or frozen donor osteochondral grafts. This technique is used for large, posttraumatic defects of the joints. The main advantages are that there is no limit for the number of plugs that can be used and that it can be prepared in any size. Therefore, this technique is used more frequently than the autologous one. The defects can heal to the host tissue and restore an articular surface (Buckwalter and Mankin, 1998). Fresh allografts and autografts allow a transplantation of viable chondrocytes. However, the usage of fresh allografts signifies not only logistic difficulties but also a risk of infection. The principal disadvantage of frozen allografts is the poor viability of the cartilage during long-term storage (20-30%). Some studies have been

[2] Viability: Refers to the capacity of cells/tissues to live, to develop or to germinate under favorable conditions. Capable of living outside of the uterus. Used for a fetus of a newborn: quality or state of being viable. That is, the ability to live, grow and develop.

performed to increase this cell survival percentage by determining optimal banking conditions (temperature, cryopreservative substances and techniques, etc.) (Csönge, et al., 2002). In a recent experimental study, the viability of press-fit preserved allografts to fresh autografts implanted into load-bearing and non load-bearing sites in mature sheep stifle joints was compared. The study showed in a 1-year follow-up that in all cases a better healing outcome was observed in the grafts implanted in load bearing regions. Histologically in all cases the line of demarcation between the graft and the host cartilage was indistinguishable. In a comparison of the viability (%viable/total cells) in the grafts implanted in the load bearing regions, the differences were not significant but they were slightly higher in the autografts compared with allografts (77.24% vs. 76.5%). In the non load-bearing regions 70% of viability was obtained for the autographs and 25% for the allografts (Gole, et al., 2004). After a comparison of all allografts versus all autografts implants, a viability of 55% vs. 77.5% was determined. By analyzing the results published by Gole et al. it can be concluded that the influence of the mechanical aspects on healing is higher as than the influence produced by biological conditions.

1.2.1.2.3 Xenografts

This technique refers to the usage of osteochondral grafts with tissues from donors of different specie than the receptor. In the majority of cases xenografts from pigs are cultivated *in vitro* and subsequently implanted in human patients. This technique has been developed as an alternative when there is a high risk for the patient (infection, morbidity of the donor site) to use autografts from non-load bearing regions of the patient or when a matching graft is not available due to the limited number of donors. Two possibilities have been investigated the usage of xeno-chondrocytes, which can be cultivated *in vitro* in an artificial matrix for the human cartilage or xeno-tissues, which are implanted into human defects. The usage of xeno-tissues has been studied experimentally using different animal models. The aim is commonly to reduce the inflammatory response and the delayed rejection of xeno-implants from donors to receptors. As part of the study of the xeno-implants, the process of xenogeneic graft rejection using pig chondrocytes implanted in mice was performed. The study identified a specific antigen and concluded that both native and *in vitro* transgenic cartilage from pigs could be used to treat cartilage defects in humans. The usage of xeno-transplantation and xeno-chondrocytes could be possible by controlling or eliminating such antigen (Costa, et al., 2003).

In a similar study, Stone and co-workers implanted pig cartilage in cynomolgus monkeys. They reduced the immune rejection of the xenografts by eliminating a specific pig antigen. Simultaneously they found that due to the elevated number of cells encountered in the synovial tissue, it showed a strong inflammatory response and concluded that the synovial tissue should be completely removed from cartilage xenografts (Stone, et al., 1998).

In an *in vitro* model, xeno-transplantation of pig chondrocytes to repair chondral defects in human cartilage was investigated. Here cultured cartilage implants were employed to treat defects of 2mm diameter and 2mm depth surgically created in femoral cartilage explants from

donors. Histological analyses after 4, 8 and 12 weeks were performed. At the 12th week a hypercellular hyaline-like region rich in proteoglycans was observed, which showed very good bounding with the host cartilage. Formation of collagen type 1 and 2 in the newly differentiated tissue was detected. It was concluded that chondrocytes xenotransplantation could be used to repair defects in humans (Fuentes-Boquete, et al., 2004).

Some authors have reported that grafts improve their mechanical properties after a chemical process known as photooxidization. Additionally this process reduces the antigenetic response of the host tissues. The grafts are oxidized by immersion in an alkaline substance as methylene blue solution and are subsequently exposited to light with high frequency. In 1991 Nadler et al. presented results of a comparative *in vivo* study of osteochondral defects treated with different grafts in sheep. In their study a comparison between the healing outcome of autografts with and without photooxidation and xenografts after 12 and 18 months was performed. Histologically, fusion between host cartilage and the photooxidized grafts was found both times but it was not observed in non-photooxidized autografts and xenografts. Viability of the cartilage matrix was only detected in the oxidized grafts. In a similar study a comparison between the healing process between xenografts and autografts in sheep was performed and evaluated histologically after 6, 12 and 18 months. Parts of the xenografts were pre-treated with photo-oxidation. Although the xenografts were taken from bovine shoulder joint and transplanted into femoral joint defects no congruency[3] problems were found. However, differences in the cartilage thickness were difficult to avoid. Such an experiment demonstrated fusion between photooxidized grafts and host cartilage. After 18 months, the hyaline cartilage structure was newly established and preserved at the interface photooxidized graft-host cartilage. Cartilage degradation and/or major gaps were observed in the control group as well as the autografts and xenografts without previous oxidization. Therefore the authors concluded that xenografts treated with photooxidization represent a good transplant possibility to treat osteochondral defects (Akens, et al., 2001).

In general, the usage of different resurfacing types of techniques such as autologous chondrocytes transplantation, in combination with treatment of axial malpositioning and ligament instabilities has showed to be an alternative for young patients with large defects (Steinwachs and Kreuz, 2003; von Rechenberg, et al., 2003).

The shape of the grafts appears to determine the success of healing. After long-term observation cylindrical grafts frequently show failures in the anchorage at the interface graft-host tissues. Therefore some investigators suggest that changes in the geometry of the graft could improve the healing outcome of osteochondral defects by altering mechanical conditions at the graft's edges. In a comparative study, Rechenberg et al. analyzed the healing outcome of

[3] Congruency problems refers to negative biological process (necrosis of the tissues in contact) derived from inefficient assembly, after geometrical differences, between the donor and the receptor site of the graft.

cylindrical and mushroom-structured osteochondral grafts. They found that the mushroom structured grafts differentiated into a less fibrous tissue, leading to an increased number of cells in the basal remodeling zones, a better restored subchondral bone and a minimal matrix degradation of the adjacent host cartilage after 6 months. The authors emphasize the importance of the subchondral bone for osteochondral bone survival and demonstrate the influence of the graft structure on the architecture of the subchondral bone and thereby the quality of the formed cartilage (von Rechenberg, et al., 2004).

In clinical practice combinations between techniques to stimulate repair and for transplantation are frequently found. One of the most frequently used is the implantation of cells in soft grafts and artificial matrix grafts. Autologous cultured chondrocytes and xeno-cultured chondrocytes are thereby employed. An alternative is the usage of differentiated chondrocytes from human stem cells, adult circulating blood cells, umbilical cord blood cells and more recently fetal circulating blood cells from rats (Naruse, et al., 2004). *In vitro* experiments have clearly established the necessary conditions to differentiate stem cells to chondrocytes (Barry, 2003; Barry and Murphy, 2004; Grande, et al., 2003; Hiraki, et al., 2001; Johnstone and Yoo, 1999; Luyten, 2004; Oreffo and Triffitt, 1999). The development of techniques and products to treat articular defects as part of the topics considered by tissue engineering has obtained a remarkable importance during the last decades. However, a comparative study of diverse industrial tissue-engineered products in the world showed that after an initial boom economy declined drastically since 1995 (Lysaght and Hazlehurst, 2004). The study showed that this industrial sector could be on the borderline of a collapse. The authors compare data on all active firms in the field of tissue engineering in 1995, 1998, 2000 and 2002. The analyzed data include number of full time employees (FTEs), investment, number of firms created per year, annual spending and capital and the number of approved tissue-engineered (TE) products by the American Food and Drug Administration (FDA). The results show for example that the capital valuation of publicly traded firms was reducing from $ 1.9 billion in 1998 to $0.3 billion in 2002. At the end of the same year, twenty products had entered the FDA clinical trial. Four were approved but none of these are yet commercially successful.

An important conclusion from the literature, especially from the studies considering animal models, is that mechanical conditions appear to have a stronger influence on healing than biological or genetic ones. Therefore, although in this work spontaneous healing and the usage of defect fillings was evaluated without consideration of biological aspects, the predicted healing outcome after evaluation of the mechanical conditions on the repair process of osteochondral defects should be sufficient to evaluate a better treatment for a specific, individual situation. Each technique has strengths and weaknesses. Independently of the technique used, the newly formed tissue usually consists of a fibrous or hyaline-like structure because although the new tissue shows morphological and biochemical similarities to the original hyaline cartilage, it does not possess a structure comparable with the host cartilage tissue. Hence, every surgical technique should be selected in accordance with specific conditions such as age and bone quality of the patient, and/or size of the defect to improve the

mechanical properties of the tissues to be repaired. Perhaps the usage of a simulation tool, which is easy to handle and to implement, could help to determine more precisely how each of the involved parameters affects the final tissue quality. In this form, the determined mechanical conditions for an individual situation should be reproducible *in vivo* in order to obtain tissues capable to resist bearing loads without damage. This work mainly describes how such a simulation tool has been developed, evaluated and how it was applied to investigate the influence of mechanical conditions on healing.

1.2.2 Cartilage characterization

Usually *in vitro* mechanical tests are used to determine mechanical properties of the cartilage. Due to the consideration of a biphasic behavior of the cartilage, it is necessary to determine the mechanical properties related with its fluid (permeability, aggregate modulus, etc.) as well as its solid phase (elastic modulus of Young's, Poisson's ratio, shear modulus, etc).

Before describing the more frequent tests used to determine mechanical material properties and the devices employed in these measurements, some basic engineering concepts shall be given as background information.

1.2.2.1 Mechanical parameters of cartilage and bone

1.2.2.1.1 Young's module (E)

Uniaxial tensile or compressive loads are employed to calculate mechanical material properties. Uniaxial implies that stresses and strains are calculated in only one direction. After application of a tensile load (P) acting in an area (A) a deformation (ε) is expected. The deformation (ε) is calculated by relating the original length of the test specimen with the final deformed length. The tensile modulus of Young (E) is a measurement of the mechanical behavior of the specimen after load application.

$$E = \sigma / \varepsilon = \sigma / \left[(L - L_0) / L_0 \right]$$ Tensile Young's module

1.2.2.1.2 Poisson's ratio (ν)

Tensile loads produce not only an elongation in the axial direction (ε) but also a lateral contraction (ε_d) by forming a neck around of its neutral axis. Compressive loads would cause a shortening in the axial direction and a lateral expansion. Poisson's ratio is a physical measurement that correlates the lateral strain (ε_d) with the axial strain (ε) by:

$$\nu = -\varepsilon_d / \varepsilon = - \left[(d - d_0) \right] / d_0 \Big/ \left[(L - L_0) \right] / L_0$$ Poisson's ratio

Where d_0 is the original lateral dimension and d the deformed lateral dimension. Similarly L_0

and L are the original and the deformed longitudinal dimension of the specimen, respectively. Poisson's ratio magnitudes are usually tabulated for different materials in technical reports of public access. The Poisson's ratio for isotropic materials varies between 0 and 0.5. A Poisson's ratio of 0 corresponds to a material that is maximally compressible, and a Poisson's ratio of 0.5 corresponds to an absolutely incompressible material. However, the determination of the Poisson's ratio for biological tissues is still in permanent study. Cartilage, for example, has a Poisson's ratio of 0.167 and bone has a Poisson's ratio of 0.3.

1.2.2.1.3 Permeability (*k*)

Cartilage shall be considered as linear biphasic. The elastic compressive modulus (E), the Poisson's ratio (ν), and the permeability (k) are the parameters that describe the mechanical behavior of the solid phase (extracellular matrix) in relation to the fluid phase (water). Permeability can be determined experimentally using Darcy's law. Darcy's experiment consisted of a fluid (water) going through a mechanism that allowed measuring the quantity of water absorbed by the solid content (sand). He established a relation between the volume of water, the size of the soil and the velocity by means of which the water flowed through the soil. The permeability (or perviousness) of rock (initially defined only for soils) is its capacity for transmitting a fluid. Degree of permeability depends on size and shape of the pores, size and shape of their interconnections, and the extent of the latter. It is measured by the rate at which a fluid of standard viscosity can move a given distance at a given interval of time. The unit of permeability is the Darcy[4] (L^2). The determination of the permeability in tissues such as cartilage is recent. A tissue with a high permeability has a low percentage of solids and vice versa. Cartilage e.g. has a higher permeability than the cancellous bone. Permeability is therefore normally closely related to the above mentioned material properties.

1.2.2.1.4 Material orientation

Materials are normally anisotropic. Yet in simplified representations a material can be modeled as orthotropic, transversally orthotropic or isotropic. An anisotropic material is characterised by possesses different material properties in all directions (E_n). An orthotropic material has different material properties in the principal three-dimensional directions E_1, E_2, and E_3. A transversally orthotropic material has different material properties in a principal direction (E_1) and in a transversal plane perpendicular to the direction of the load application ($E_2 = E_3$). An isotropic material has the same material properties in all directions ($E_1 = E_2 = E_3$). In dependence of the material orientation assumed to represent a model with its material properties, several equations correlate mechanical parameters with each other.

---

[4] Named after H. Darcy (1803-1858), one Darcy corresponds to the volume of a liquid with a dynamic viscosity of 1 centipoise flowing through a porous material with a cross section of 1 cm^2 in 1 second when undergoing a pressure drop of 1 atm/cm. This unit was used in hydrology and civil engineering to measure the permeability of porous materials.

1.2.2.2 Test description

In order to calculate these parameters (elastic deformation, elastic modulus of Young, etc.) cartilage samples were tested under compressive loads (Appleyard, et al., 2003; Boschetti, et al., 2004; Franz, et al., 2001; Wei and Messner, 1998). With the use of mechanical tests, it is intended to reproduce the mechanical boundary conditions activated during joint movements (axial, bending and torsional loads). Three different methods are frequently used to estimate the cartilage material properties: confined compression, unconfined compression and indentation, whose differences are based on the boundary conditions assumed during testing (Bae, et al., 2004; Goldsmith, et al., 1996; Korhonen, et al., 2002; Korhonen, et al., 2002; Lyyra, et al., 1999; Ming, et al., 1997). In correspondence to these boundary constraints, changes in the fluid direction and thereby in the material properties are expected. When a joint is in contact with any another joint, e.g. at the knee joint, and the fluids do not have perpendicular restrictions relative to the direction of the compressive active load, these boundary conditions are referred to as confined compression. In contrast, when the fluids inside the cartilage do not have movement restrictions in the radial direction and the fluids could move only in a perpendicular direction of the acting load, an unconfined compression constraint is defined. An indentation test measures the deformation at the cartilage surface after compressive load application using an appropriated device (indenter; see below).

1.2.2.2.1 Indentation

Indentation is a mechanical test in which a device (indenter) applies a compressive load to the articular surface to be characterized. The indenter has strain gauges coupled to the indenter surface, which is able to measure deformations of the cartilage surface. The force (P), applied with the indenter and the contact area indenter-cartilage (A) are known parameters. The compressive stress during the test is calculated as the linear relation between these two parameters (P/A). Compressive stress versus deformation during the test can be plotted. The slope relating these two parameters represents the compressive elastic modulus of Young (E). The following equation correlates the different mechanical parameters involved during an indentation test through (*k*).

$$k = P\left(1-\nu^2\right) \Big/ 2aE\omega$$

Where P is the force applied to the indenter

ν the Poisson's ratio of the test tissue

E the Young's modulus of the test tissue

ω the indentation depth

a the radius of the indenter

Using this equation and assuming different values for (ν) the parameter (*k*) can be calculated.

The principal advantages of this mechanical test are that it does not require special specimen preparation, it is made *in situ* - thereby the boundary conditions are near to the ones encountered in the physiological situation - and it does not cause specimen damage. Stress controlled indentation testing of simple chondrocytes has been performed using a novel creep cytoindentation apparatus (CCA) (Koay, et al., 2003).

1.2.2.2.2 Unconfined compression (E, ν)

This mechanical test consists of the application of a compressive load on the specimen, in this case cartilage, which is fixed between two plates (Fig. 1.4a). The cartilage is then deformed in a direction parallel to the applied force (lateral). During load application the displacement of the deformed surface is then measured. The elastic modulus of Young (E) can be determined as the slope of the linear region in a plot of the history of load application versus the corresponding history of displacements. Using optical techniques it is possible to measure the lateral cartilage deformation. Knowing the lateral and the longitudinal deformation, the Poisson's ratio can be determined. An unconfined compression test has been performed directly in chondrocyte cells using a novel system (a combination between a cell cultured nuclear microscopy and a laser indenter) (Leipzig and Athanasiou, 2005). An elastic modulus of 2.55 $\pm$ 0.85 KPa was measured using a linear elastic model. Similar values were found using a viscoelastic (2.47 $\pm$ 0.85 KPa) and a biphasic model (2.58 $\pm$ 0.57 KPa) to characterize the cartilage's mechanical behavior.

1.2.2.2.3 Confined compression (H_A, *k*)

This mechanical test is similar to the unconfined compression (Fig. 1.4b). But in this case the specimen is additionally constrained in the radial direction to the applied load. The specimen is placed in a chamber and a constant compressive load is applied to it. The lateral constrain avoids free lateral cartilage deformation developing a lateral pressure. The fluids inside the cartilage are then pressurized.

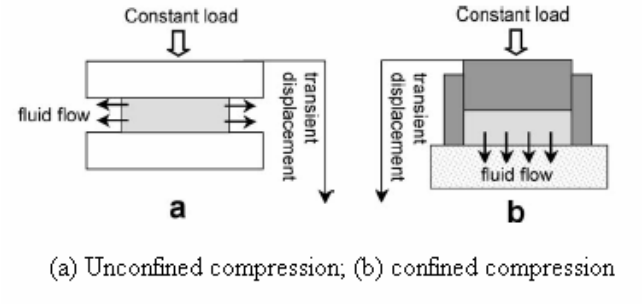

(a) Unconfined compression; (b) confined compression

Fig. 1.4: Schematic illustration of unconfined (a) and confined (b) compression test for cartilage samples (Boschetti, et al., 2004).

Creep deformation occurs as the fluid is forced to flow from the tissue. Plotting a graph of the compressive stress versus the corresponding measured displacements, the slope shows the effect of the fluid pressurization, this parameter is known as aggregate modulus (H_A). The

aggregate modulus is calculated at creep equilibrium. The following equations correlate the aggregate modulus (H_A) with the compressive modulus of Young (E) and shear modulus (μ) for an isotropic material.

$$H_A = \frac{1-\nu}{(1+\nu)(1-2\nu)}E$$ Aggregate modulus

$$\mu = \frac{E}{2(1+\nu)}$$ Shear modulus

Taking into account the pressurization of the fluid phase of the cartilage implies the consideration of another mechanical parameter of fluids: the permeability. Athanasiou and co-workers reported values of the aggregate modulus (H_A) of 0.47 $\pm$ 0.15 MPa and *k* 1.4 $\pm$ 0.60 e-15 $m^4N^{-1}S^{-1}$. The permeability is a parameter that relates the fluid velocity to the capacity of a material to absorb water.

1.2.2.2.4 Porosity (ϕ)

Porosity is a mechanical parameter that relates the percentage of the solid phase and the fluid phase present in a biphasic material. This parameter can be evaluated from the water content, determined by the difference between the weights of hydrated and dried samples. Cartilage for example has a porosity of 0.8. That means that cartilage consist of 80% water and 20% solids (aggrecans and extracellular matrix).

1.2.2.3 Recently developed devices and techniques for measuring mechanical cartilage properties in vivo and in vitro.

1. In 1995 Lyyra and co-workers presented a static indenter that was arthroscopically controlled (Lyyra, et al., 1995). The accuracy of the device was tested by comparison between arthroscopic measurements of the cartilage deformation and measurements realized with a conventional indenter from stress-relaxation tests in cadaveric knee joints. A good agreement between both indentation methods was thereby achieved. The authors conclude that such a device can be used in clinical practice.
2. A handheld dynamic indentation system was introduced by (Appleyard, et al., 2001). This novel device was developed to determine the dynamical mechanical properties of the articular cartilage *in vitro*. The manipulability of the device allows measuring the mechanical properties of all zones of an articular surface eliminating the accuracy problem of measurements in a joint with strong local differences in curvature. A map of forces acting on the articular surfaces can in this way be determined. With this device the dynamic shear modulus was calculated using the Hayes model.
3. Ultrasound elastomicroscopy imaging of soft tissues. This method consists of a compressive device to apply loads on a soft tissue specimen *in vitro*. During the test elastic radio frequencies are acquired from a scan, which produces formatted images

of tissue response during load application. The compressive strain could then be calculated from the shape of the deformed specimens measured in the scanned images (Zheng, et al., 2004).

4. Using a high-frequency pulse echo ultrasound device, a Japanese research group (Kuroki, et al., 2004) determined the mechanical tissue quality during healing of osteochondral defects treated with autologous graft transplantation in rabbits. Kuroki et al. demonstrated that such a device indeed was not able to show any differences between the joint with the implant and the contra-lateral control joint at 0 days, as expected. The differences in the ultrasound signal intensity were detectable after 2, 4, 8, 12 and 24 weeks. Histological and microscopic analyses were additionally performed in which degradation, from 2 week, and detachment of the implant, between 12 and 24 postoperatively, were observed. A proper evaluation confirmed a close relation between the mechanical properties of the tissues (ultrasound signal intensity) and the degradation process. The intensity was reduced when damage was increased. Between week 2 and week 12, postoperatively, the intensity in the grafted joint was slower than that for the intact contra-lateral joint. Ultrasound can be applied in both *in vivo* and *in vitro*.
5. Articular damage as produced by rheumatoid arthritis (RA) could be detected by alterations in the fluid flow patterns inside the cartilage or by changes in the synovium. Synovial vascularization and fluid velocities can be detected by the Doppler technique. Ozgocmen and co-workers used the Doppler effect to determine flow patterns in joints with RA. Flow patterns have a strong correlation to intra articular bone and cartilage degeneration (Ozgocmen, et al., 2004). Power Doppler ultrasonography (PDUS) appears to be appropriate for determination of intraarticular vascularization and flow patterns of normal and osteoarthritic cartilage. Strunk et al. employed the Doppler technique for the first time (Strunk, et al., 2004).
6. Saarakkala and his group used an ultrasound indentation instrument to determine mechano-acoustic properties of the cartilage *in vivo*. After measurements of the speed of sound in the cartilage and its reflection coefficient, they succeeded in obtaining the elastic and dynamic modulus of the cartilage. These ultrasonic and mechanical parameters were compared for intact and degenerated cartilage specimens. A correlation between the ultrasonic responses with the grade of articular damage (estimated from the elastic modulus of Young) was found. The sound speed and the reflection coefficient increase for tissues with high values of dynamic and Young's modulus. The authors developed a method to diagnose osteoarthroses *in situ* (Saarakkala, et al., 2004; Saarakkala, et al., 2004).
7. The mechanical environment of chondrocytes has been studied. Using different experimental techniques in combination with numerical methods the mechanical properties of chondrocytes were determined. Athanasiou and his group have developed a novel system that allows for the first time to realize creep indentation

(Koay, et al., 2003) and unconfined compression tests (Leipzig and Athanasiou, 2005) on simple chondrocyte cells. The system configuration consisting of a force transducer cantilever, a sensor (laser micrometer), a motor and a PC running with LabView (software package to control load application) was able to apply constant compressive stress to individual adherent cells. After determination of the elastic modulus of Young numerical models were used to determine the other mechanical parameters (Poisson's ratio, Aggregate modulus, permeability and viscosity). Previous approaches of measurements on cells have already been reported. Elastic modulus of Young on chondrocytes from normal and osteoarthritic cartilage samples were determined by applying pressure via cell aspersion (Jones, et al., 1999). Similarly, Poisson's ratio of chondrocytes from normal and osteoarthritic cartilage were estimated applying pressure to the chondrocyte surface by micropipete aspiration (Trickey, et al.). Using theoretical models, fluid pressure and shear strain state in chondrocytes have been calculated (Wu, et al., 1999). Employing finite element simulations, biphasic material properties of chondrocytes have been determined (Guilak and Mow, 2000). Other approaches use a combination of 3D confocal microscopy to determine volumetric changes *in situ* (deformation) during load application, and computer simulations to calculate additional mechanical properties (elastic modulus of Young, Poisson's ratio, etc.) (Guilak, 2000). Another new optical technique is video microscopy, which has been used to measure radial deformations of human cartilage during classical tests of confined and unconfined compression. As a result, Poisson's ratio, aggregate modulus and elastic modulus of Young can be determined. After evaluation of cartilage porosity, numerical approaches allow subsequent calculation of the related fluid parameters (permeability) (Boschetti, et al., 2004).

Generally ultrasonography appears to be a technique frequently used over the last years to estimate joint degeneration or to measure mechanical properties, and it has been employed to determine normal physiological values of diverse musculoskeletal regions. By determining physiological values in healthy tissues, the attempt was made to standardize musculoskeletal ultrasound measurements and to avoid erroneous interpretation of normal echoes as pathological values. Ultrasonography values from muscles, cartilage and tendons were measured and averaged in healthy individuals and presented by Schmidt (Schmidt, et al., 2004). Damage of articular surfaces can be determined with ultrasonography as well (Nieminen, et al., 2004).

Low-intensity ultrasound has been employed to stimulate differentiation of bone tissues (Korstjens, et al., 2004; Sakurakichi, et al., 2004; Tis, et al., 2002), of human mesenchymal stem cell into chondrocytes (Ebisawa, et al., 2004) or to analyze its viability proliferation and matrix production (Zhang, et al., 2003). Other authors have demonstrated that low-intensity ultrasound can even influence cartilage repair (Cook, et al., 2001; Zhang, et al., 2002) and cultured chondrocytes in 3D arrays (Nishikori, et al., 2002). Ultrasound has been employed to

analyze the state of repair after graft transplantation (Hjertquist and Lemperg, 1971) or to predict histological findings in regenerated cartilage (Hattori, et al., 2004).

1.2.2.4 Determination of the magnitudes of the mechanical parameters

In order to attenuate and to distribute uniformly the acting external loads, during joint functionality the fluids are moving physiologically with a slow and continuous velocity through the cartilage (Buckwalter and Mankin, 1998; Buckwalter and Mankin, 1998). Fluid velocity is directly related with the mechanical material properties of the cartilage by the magnitude of its permeability. Permeability was initially calculated experimentally for soils using the Darcy's law (Equation 1.1, Equation 1.2). With the Darcy's experiment the hydraulic conductivity (K) of a material can be calculated. Permeability is a parameter that depends on hydraulic conductivity (Equation 1.2). Since the Darcy experiment implies some technical complications to measure this cartilage parameter, it is frequently calculated in an indirect way using the finite element method. As input data the elastic modulus of Young, Poisson's ratio, compressive strains, and/or aggregate modulus of the cartilage are required.

$$q = K * A * \frac{h_2 - h_1}{L} \qquad \text{Flow rate} \qquad \text{(Equation 1.1)}$$

Where q = $\Delta V_0/\Delta t$ flow rate (Rate of volume V in a time t)

K = Coefficient of permeability or hydraulic conductivity

A = gross cross sectional area of flow

h = total head (L)

L = length of flow path

With the equation 1.1 K (Darcy's hydraulic conductivity) can be calculated.

$$k = \frac{K * n}{\rho * g} \qquad \text{Permeability} \qquad \text{(Equation 1.2)}$$

Knowing K the permeability can be determined by equation 1.2

Where n = fluid viscosity

ρ = fluid density

g = gravitational acceleration

According to Forchheimer's law, high flow velocities could reduce the effective permeability and consequently "chocking" pore fluid flow. As the fluid flow reduces, Forchheimer's law approximates Darcy's law (β = 0).

$$f(1+\beta\sqrt{v_w \cdot v_w}) = -\frac{k_s}{\gamma_w} k(\frac{\partial u_w}{\partial x} - \rho_w g)$$ Forchheimer's law (permeability)

(Equation 1.3)

$$f = s * n * v_w$$ Permeability depending of porosity (*n*)

(Equation 1.4)

$$e = n/(1-n)$$ Void ratio (*e*) dependent on the porosity (*n*)

(Equation 1.5)

$$n = n_0 + (1-n_0) * \varepsilon$$ Porosity (*n*) depends on the strain (ε). Where n_0 is the initial porosity (Equation 1.6)

Where, f = is the volumetric flow rate of wetting liquid per unit area of the porous medium (the effective velocity of the wetting liquid).

s = is the fluid saturation. s = 1 for a fully saturated medium, *s* = 0 for a completely dry medium. $s = dV_w / dV_u$

n = is the porosity of the porous medium. $n = dV_u / dV$

v_w = is the fluid velocity

e = $dV_u / (dV_g + dV_t)$ is the void ratio

dV_w is the wetting fluid volume in the medium

dV_u is the void volume in the medium

dV_g is the volume of grains of solid material in the medium

dV_t is the volume of trapped wetting liquid in the medium

β (e) is a "velocity coefficient", which generally depends on the void ratio of the material

$k_s(s)$ is the dependence of permeability on saturation of the wetting liquid such that k_s = 1.0 at s = 1.0

$\rho_w = \gamma_w / g$ is the density of the fluid

γ_w is the specific weight of the wetting liquid

k(e,θ) is the permeability of the fully saturated medium, which can dependent on the void ratio (e) and/or temperature θ

u_w is the wetting liquid pore pressure

x is the position

In Abaqus, a finite element solver, the permeability is defined as:

$$\bar{k} = \frac{k_s}{(1+\beta\sqrt{v_w.v_w}}k \qquad \text{(Equation 1.7)}$$

where k is the fully saturated permeability,

so that the Forchheimer's law can be written as:

$$f = -\frac{\bar{k}}{\gamma_w}(\frac{\partial u_w}{\partial x} - \rho_w g) \qquad \text{(Equation 1.8)}$$

Remark: $\bar{k}$ then have units of LT^{-1}. However, some authors use the hydraulic conductivity, which has units of L^2 (or Darcy). To use the saturated permeability in Abaqus, it needs to be multiplied by ν / g. Where ν is the kinematic viscosity of the wetting liquid (the ratio of the liquid's viscosity to its mass density).

$$K = \frac{v}{g}\frac{k_s}{(1+\beta\sqrt{v_w v_w})}k = \frac{v}{g}\bar{k} \qquad \text{(Equation 1.9)}$$

Permeability (*k*) can be determined by numerical approximations using the finite element method. With the equations 1.4, 1.5 and 1.6 the problem is completely defined. Experimentally the elastic modulus of Young (E), the Poisson's ratio (ν) and the compressive strains (ε) are determined from an unconfined test. Assuming porosity, void ratio is calculated from the equation 1.5 (Abaqus uses void ratio as input data). By inserting *n* from the equation 1.6 in the equation 1.4 an expression of permeability depending on strains can be determined.

The permeability is selected such that the strains measured in the unconfined test experiment are reproduced. When the equation is satisfied, the permeability of the tissue has been found. Once *k* is known, with the values obtained for fluid velocity (v_w) and pore pressure (u_w), the fluid mechanical parameters of the tissue are fully determined (Equations 1.7 and 1.8).

1.2.3 Osteochondral repair

A theory for osteochondral repair and its computer simulation should take two concepts into account: bone remodeling and tissue differentiation. These principles and concepts describe the mechanical and biological conditions, which are active in an osteochondral repair process

(Bagge, 2000; Scully, et al., 2001; Wang and Dumas, 2002).

The main aim of this project was the development and implementation of a tissue differentiation model, consistent with the histological findings, to evaluate the influence of mechanical conditions on osteochondral healing. Using linear monophasic material properties, the effect of the defect size, and cartilage thickness on healing was analyzed (Duda, et al., 2005). Subsequently, poroelastic non-linear biphasic materials were used to analyze the effect of joint curvature and the use of different defect filling stiffnesses in osteochondral repair.

The predictive tissue differentiation model was developed based on a theory for differentiation, which includes the bone remodeling concept and the acquired knowledge of tissue differentiation taken from osteochondral healing of animal experimentation. Prior to the development of a theory supporting the tissue differentiation model (see discussion), current models to simulate bone remodeling and tissue differentiation were investigated.

1.2.4 Current models used to simulate bone remodeling and tissue differentiation

The bone-remodeling concept dates back to 1638 when Galileo Galilei established a relation between the bone geometry and the acting external forces. He understood that without an intelligent internal structure bones should possess an extraordinary size in order to transmit external forces in an optimal way (Nigg and Herzog, 1994). Subsequently, other authors who studied this internal structure currently named cancellous bone and its characteristics; mechanical behavior and remodeling capacity were explained.

The bone remodeling concept clarifies how cells in a tissue (bone or cartilage), in dependence of acting external loads and boundary conditions active during this process, are able to absorb or to produce another new tissue (Aro and Chao, 1993; Bagge, 2000; Kerner, et al., 1999; Tsili, 2000; Wang and Dumas, 2002). Some research groups have proposed tissue differentiation models with material properties (e.g. stiffness, permeability), taken from literature. These models have principally been used to study bone remodeling (Kerner, et al., 1999; Mikic and Carter, 1995) and fracture repair (Ament and Hofer, 2000; Claes and Heigele, 1999; Lacroix and Prendergast, 2002). Before this project, no differentiation model existed to simulate or to study osteochondral repair.

In 1884 Wolff found a similarity between the cancellous bone structure and orthogonal curves known from analytical representations of strains and stresses in a loaded beam (Fung, 1993). Bones were then represented by an internal configuration whose trajectories and form evidenced the existence of an implicit dependence of the applied external loads. In 1895 Roux discovered that such trajectories were the consequence of a dynamic functional adaptation of the internal bone structure reacting on externally applied loads. Bone tissue was able to change and to adapt its mechanical properties in dependence of current load situations (Fung, 1993; Huiskes, 2000; Huiskes, et al., 2000; Nigg and Herzog, 1994; van der Meulen and Huiskes, 2002). Thus, bone degrades its density distribution when external loads are reduced (zero gravity or immobility) or as consequence of a disease which destroys its internal original

structure (e.g. osteoporosis) (Aloia, et al., 1987; Buckwalter and Mankin, 1998; Buckwalter, et al., 1994; Buckwalter and Brown, 2004). In this last case, a total destruction of cartilage has to be expected.

The determination of the mechanical cartilage properties is another topic of actual research. These are directly related to their remodeling capacity in the sense that the elastic modulus of Young is commonly selected to quantify the grade of remodeling or degradation of a tissue. To know the mechanical properties of the tissues is therefore fundamental.

In the following models this fundamental knowledge is used to explain how cells respond to changes in their mechanical environment stimulating biological processes such as growth or resorption. Histological analysis, *in vivo* and *in vitro* experimentation were and still are necessary to illustrate them. These models shall be introduced briefly.

1.2.4.1 Bone remodeling model based on a mechanical stimulus to stimulate bone adaptation (Huiskes's model).

Bones are able to adapt their internal structure in presence of mechanical stimuli generated after load application (Roux's law). Different pathways for cell mechanotransduction have been identified to explain how this process could take place. The interpretation of these signals allows the development of tissue differentiation models, in which the mechanical cell environment is simulated and analyzed. For interpretation of this remodeling process Huiskes used the existence of an equilibrium state, originally proposed by Frost, in which cellular activity does not occur. An intact situation stays in the equilibrium state. Hence, equilibrium could be defined as a state in which the groups of cells responsible for growth or resorption are inactive and the balance between the acting external loads and the generated mechanical response causes the equilibrium. Remodeling is a complete cycle of cell activity in which after perturbations (prostheses, defects at bone, new boundary conditions) the equilibrium is newly reestablished. In this process different types of cells (osteoclasts and osteoblasts) are involved. This group of cells is called a basic multicellular unit (BMU). A BMU consists of about 10 osteoclasts and some hundreds osteoblasts. These groups of cells can be considered to be a mechanism of bone repair. Some authors believe that biochemical reactions are involved in the activation of these cells. Huiskes and his group propose that the BMU have some mechanosensors, which respond in the presence of external loads. Hence, deformations (a direct measurable consequence of the applied load) could be used as the mechanical stimulus to initiate a remodeling process. In other words, when an elastic, axial compressive load is applied to a tissue (for example bone), the derived compressive deformations act as mechanical stimuli to initiate remodeling.

Huiskes used this idea to develop a numerical model in which the knowledge of the equilibrium state of each bone region calculated in an intact bone situation was necessary. A stimulus for differentiation is activated as a reaction to the equilibrium alteration. The remodeling process stops when a tissue with the same mechanical properties as defined for an intact situation is

completely reestablished in each affected region. The mandatory model of an intact bone must be calculated in order to know the strain magnitudes of the equilibrium state. After comparison of the straining of an affected and an intact situation, the necessary stimuli are calculated as a difference of these values. Huiskes schematized this process as a trilinear curve where maximal and minimal values of strains were used to define the range of change for each bone region. In this curve three points are defined to delimit the zones for growth, resorption, or equilibrium (dead zone) of each tissue as a function of a related stimulus (Huiskes, 1997; Huiskes, et al., 2000; Huiskes, et al., 1987) (Fig. 1.5). When the current strain falls below the value limiting the equilibrium zone, resorption sets in. In contrast, when the magnitude of the current strain is higher than the limits defined in the equilibrium zone, growth will occur. Following this schema, the elastic modulus of Young is continuously changed in an iterative process. With this model Huiskes calculated changes in the bone density (directly related to the elastic modulus of Young's) that occur after implantation of a hip prostheses (Huiskes, 1990; Huiskes, 1997; Huiskes, et al., 1987; Kerner, et al., 1999; Mullender and Huiskes, 1995; Prendergast and Huiskes, 1995; Prendergast, et al., 1997; Vena, et al., 2000). This model was also applied to analyze the effect of stress shielding and how bone remodeling occurs after total hip replacement. In that study a special emphasis of the interface bone-implant was made.

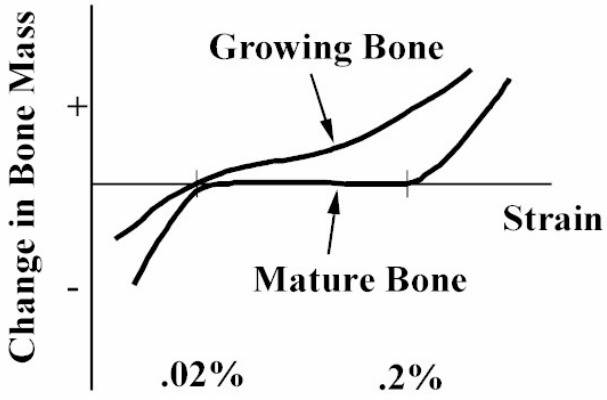

Fig. 1.5: Huiskes's model. Cell activity is represented by a tri-linear curve. High values of strain energy density conduce to growth activity, low values of strain energy density conduce to resorption activity. The dead zone represents cellular inactivity (Huiskes, et al., 1987).

1.2.4.2 Strain fields of each tissue type regulating the fracture healing process (Claes's model).

Although Huiskes's model showed a good correlation to the biological processes observed during and after a total hip implantation, this formulation was inappropriate to simulate fracture repair. Claes focused his work on the description of the mechanobiological process involved during fracture healing. After animal experimentation the total process from callus formation to cortical regeneration, the last state in a fracture repair, was documented and reconstructed through histological analysis at fixed points in time. In the Claes's theory cells response to local

strains and stresses, whose magnitude, position, and type could be determined. Claes modeled the geometry of the histological sections at the previously defined fixed points in time from his animal experimentation. Viscoelastic material properties taken from literature were used in these models. The finite element method was employed to determine mechanical strains and hydrostatic pressures for each tissue type (Fig. 1.6a).

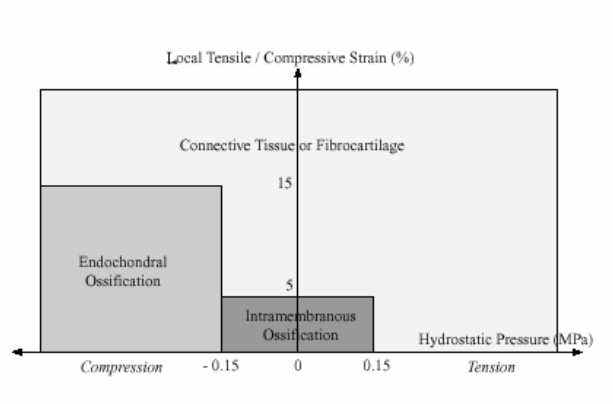

Fig. 1.6a: Claes's model. Characteristic limit values of strain and stresses are defined for each tissue type to simulate diaphyseal fracture healing (cortical remodeling through enchondral ossification) (Claes and Heigele, 1999).

The histological section showed how bone tissue was newly formed from an existent bone or cartilage region in an intramembranous ossification process. Cell differentiation for each tissue occurred in dependence of the acting strains or stresses whose magnitudes were previously determined with the computer model. Claes found that connective or fibrous tissue could be formed when hydrostatic pressures are higher than 0.15MPa and when the compressive strains are higher than 5% (Claes, et al., 1998; Claes, et al., 2002; Claes and Heigele, 1999).

Recently Claes's group extended their model incorporating fuzzy logic[5] (Shefelbine, et al.). This method uses a combination of mechanical stimuli to simulate differentiation with series of fuzzy sets. Some rules (for unclear boundary conditions) need to be consecutively evaluated to describe a specific tissue type during healing (Fig. 1.6b). The rules are based on *in vivo* observations of the fracture healing process.

[5] Fuzzy logic: Is a superset of boolean logic dealing with the concept of partial truth. Whereas classical logic holds that everything can be expressed in binary terms (1:yes; 0:no), fuzzy logic replace these simple boolean truth values with degrees of truth. This allows for values between 0 and 1, the concept of "maybe". It allows partial membership in a set (i.e. elements can belong to different sets simultaneously). The method can use logical connectors to describe unclear events or events that cannot be represented with unique true values. A membership function is normally required to adjudicate the grade of certainty of the variable to be evaluated. In this form unclear events can be treated with IF/THEN rules for final association of a deterministic success.

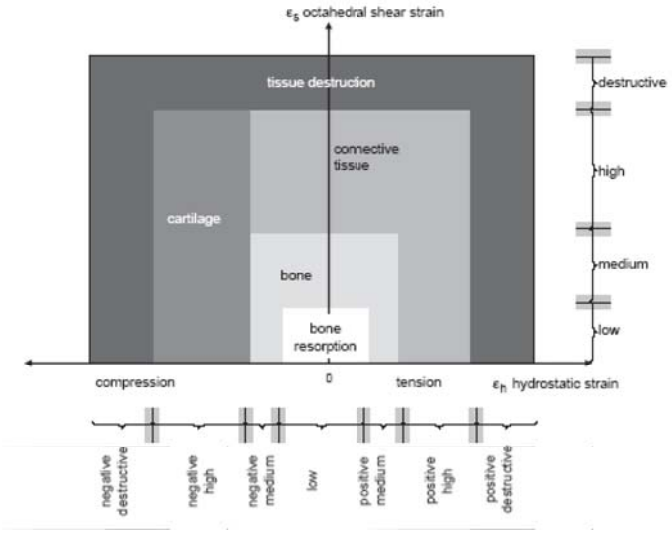

Fig. 1.6b: Fuzzy logic in combination with mechanical stimulus applied to simulate healing of trabecular fractures (intramembranous ossification). Fixed rules including biological factors regulate building or resorption of different tissue types (Shefelbine, et al.).

Claes's group demonstrated the possibility of using a general tissue differentiation model for fracture healing. In this form, the fuzzy logic model, which was initially employed to simulate diaphyseal fracture healing (Ament and Hofer, 2000), was further developed and applied to simulate metaphyseal fracture healing and bone remodeling. The first one refers to healing when the fracture occurs in the cortical bone. Cortical bone fractures heal by enchondral ossification: after a fracture, a callus replaces the formed haematoma. The callus is differentiated to fibrous and later to hyaline cartilage before it is replaced by cortical bone. The second one, metaphyseal fractures, compromises the trabecular bone. Trabecular bone fractures heal through intramembranous ossification: The bone is remodeled by activation of BMUs (basic multicellular units); osteoclasts and osteoblasts absorb and build new bone directly in dependence of biological and mechanical boundary conditions without cartilage formation. As a mechanical stimulus for differentiation they used octahedral strains in combination with hydrostatic strains.

Fuzzy logic is however a controversially discussed method because it anticipates the response of the healing process (or the system to be evaluated) showing logically a high dependency on the fixed rules. However, the major contribution of Claes's proposal is its intent to unify the fracture healing process for cortical and trabecular bone, allowing the analysis of fracture healing for different types of bones and different fracture localizations. Perhaps even more important is the point that his model allows the incorporation of biological factors observed during *in vivo* fracture healing such as different rates of vascularization and concentration of growth factors for the early and the late stages of healing.

1.2.4.3 Mechanoregulation of differentiated tissues during fracture repair (Prendergast's model).

Prendergast analyzed fracture repair under another perspective. Since following haematoma formation in the first stages of fracture repair only connective tissue is recognizable, which has a higher content of water, Prendergast proposed that cells react principally under the effect of this fluid phase. Fluid velocity and strains as a result of external loads should play an important role in the development of appropriate mechanical boundary conditions to initiate the repair process. Animal experimentation was used to define strain limits to start and to maintain cellular differentiation. During healing it was observed that micromovements at the bone surface stimulate bone repair. Using a biphasic, pore elastic model the mechanical shear strains and fluid velocities for each differentiated tissue during the repair process can be calculated. A mechanoregulation schema that combines these two mechanical parameters was then proposed to describe fracture healing (Fig. 1.7).

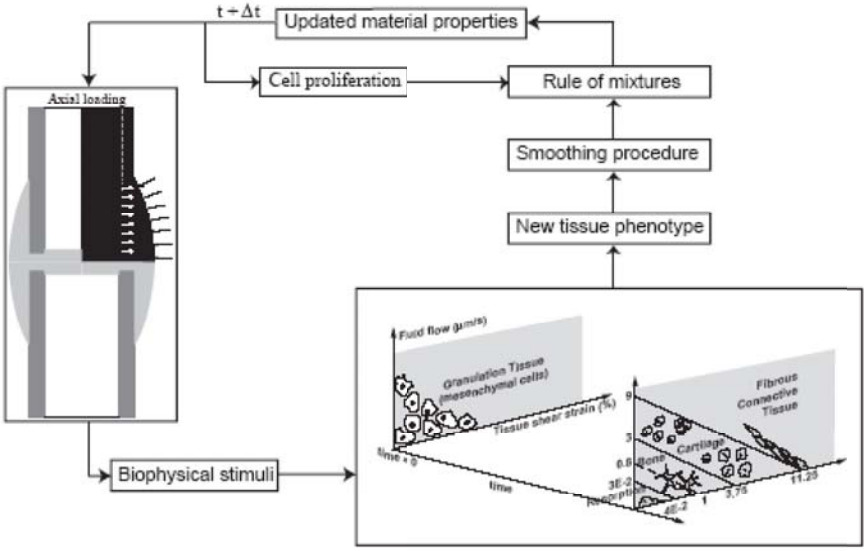

Fig. 1.7: Prendergast's model. Prendergast developed a mechanoregulation schema regulated by shear strains and fluid velocities defined for each tissue type (Lacroix and Prendergast, 2002).

It was determined for example that a combination of high values of shear strains and fluid velocities cause distortion in the mesenchymal stem cells acting as stimulus to differentiate these cells to connective tissue. In a similar way cartilage is formed after a combination of low values of shear strains and slow fluid velocities (Lacroix and Prendergast, 2002; Prendergast, 1997; Prendergast, et al., 1997; Prendergast, et al., 1996).

1.2.4.4 Influence of growth factors and mechanical stimulus during fracture repair (Bailon-Plaza's model)

Bailon-Plaza developed a predictive fracture healing hyperelastic model, in which growth factors were taken into account as an important parameter during repair. Plaza and co-workers proposed that growth factors are responsible for initiation and regulation of biological process of fracture healing. From *in vivo* studies the chondrogenic and osteogenic effect of two different growth factors were determined. The ability of these growth factors to regulate differentiation appears to be strongly related with the number of cells. A numerical implementation of this theory was used to simulate fracture repair. The model was able to predict and to demonstrate that the formation of osteogenic growth factors from osteoblastic cells and the duration of their production are necessary to obtain a full bone restoration after trauma. In her computer model dilatational and deviatory strains were used as stimuli to regulate the production of growth factors present principally in the first stages of fracture repair. The material properties used in her model were taken from literature (Bailon-Plaza, et al., 1999; Bailon-Plaza and van der Meulen, 2001).

1.3 Preliminary work

Since the study of bone-joint mechanics and osteochondral healing implies a very complex biological process, the knowledge of biological aspects related to bone healing, studied by Lill and his group (Hepp, et al., 2003; Lill, et al., 2002; Lill, et al., 2001; Lill, et al., 2003), and osteochondral healing, studied by Bail and co-workers (Bail, et al., 2003), were used.

The works conducted by Lill's group were basically employed to validate the model created in this project to analyze bone - joint mechanics (humerus project) and to perform a more realistic simulation of the bone specimens. In this project validation was made by comparing the measured stiffness in the mechanical test (compression and torsion) realized in human specimens to the mechanical stiffness calculated after simulation of these same tests in the same simulated bones. Following model validation, the influence of mechanical conditions on bone healing was evaluated through the analysis of straining of intact and fractured proximal humeri under physiological loads (in the rest of this project the corresponding sections are entitled bone-joint mechanics). The study in the proximal humerus realized by Lill's group was selected because it presents well documented data (e.g. bone stiffness, implant stiffness), compares mechanical parameters of standard with recently developed implants to stabilize proximal humerus fractures and their precise measurements of the bone density distribution allows the development of a more realistic bone model.

The work realized by Bail was employed to validate the tissue differentiation model created to analyze the influence of mechanical conditions on osteochondral healing. Geometry, boundary conditions, histological and histomorphometrical analysis from the animal experimentation were used. As explained in the material and methods section, this validation was performed by comparing the histological and histomorphometric analysis to the simulated healing qualitative

and quantitatively.

1.3.1 Bone joint mechanics: biomechanical analysis of proximal humerus

1.3.1.1 Previous work realized by Lill and his group

The work of Lill and co-workers is briefly introduced. In the biomechanics laboratory of the Musculoskeletal Research Center in Berlin, a previous study considering different bone qualities was realized (Lill, et al., 2002). Some parameters of humeral human bones were determined: stiffness, density distribution, trabecular bone orientation and volume bone fraction. Both intact and fractured human bones, stabilized with different medical devices, were mechanically tested and analyzed. The goal of Lill and his group was to determine favorable implant stiffness for fracture healing, taking into account the effect of the bone density distribution. Important implications for the treatment of fractures in osteoporotic patients were established.

Histomorphometrical, CT and MRI analysis were performed on 24 freshly harvested human cadaveric humeri. Histomorphometric analysis evaluated structural parameters (tissue volume to bone volume ratio, trabecular thickness), connectivity (number of nodes[6], node to node length), and trabecular orientation (mean bone length). Median ages of 46 (34 – 46 years) and 69 (46 – 90 years) were registered for the male and the female group independently. In four horizontal levels sliced from the humeral head, five regions of interest were defined in each cutting plane: anterior, posterior, lateral, medial and central (in accordance with the standard coordinate system used for human bodies). With the information obtained (structural bone parameters, connectivity and trabecular orientation), a complete description of the bone quality of each specimen was determined. Different grades of bone strength were identified in the analyzed specimens: peak values of histomorphometric parameters at the cranial section decreasing caudally were found. This information was translated to the simulated specimens in the present project: localized differences of the bone quality could then be modeled.

The center of the trabecular structure connects the center of the gleaned cavity. A correlation between the structural parameters of the trabecular network, its localization and the estimated bone quality was determined: higher bone stiffness was found in regions of high trabecular density and elevated number of nodes compared with regions of low trabecular density. The project of Lill and his group aimed to obtain knowledge of distribution, microstructure, and quality of bone in the humeral head, which allows the remaining bone stock to be used effectively, even in elderly patients, with a minimally invasive approach and maximum mechanical stability (Hepp, et al., 2003; Lill, et al., 2002; Lill, et al., 2001; Lill, et al., 2003). According to Lill's findings, bone quality appeared to be an important parameter to be evaluated. Therefore, the effect of the bone quality and its relation to the mechanical conditions

[6] Nodes: trabecular intersections at the cancellous bone.

(physiological loads) in intact and fractured bones during bone healing was then evaluated in this project.

In a subsequent study, 35 fresh human humeri were used to perform mechanical testing in order to determine *in vitro* characteristics such as stiffness of different conventional and new devices used to stabilize proximal humeri fractures. The implants tested under static and cycling loading included humerus T-Plate (HTP), the cross-screw osteosynthesis (CSO), the unreamed proximal humerus nail with spiral blade (UHN), the Synclaw Proximal Humerus Nail (Synclaw PHN) and the angle-stable Locking Compression Plate Proximal Humerus (LCP-PH). Three clinical load cases were evaluated: axial compression, torsion and varus bending. The results showed that the evaluated conventional devices (HPT, CSO, UHN, Synclaw PHN) presents a higher stiffness under static load than that encountered in the LCP-PH. Additionally, the torsional stiffness was strongly reduced with exception of the LCP-PH.

Lill and co-workers concluded that implants with low stiffness and corresponding elastic properties could minimize peak stresses, which could be related to the early loosening and failure of the interface implant-bone. Therefore low stiffness implants seem particularly suitable for fracture fixation in osteoporotic bones (Lill, et al., 2003).

1.3.2 *In vivo* analysis of an osteochondral defect

1.3.2.1 Description of an animal model of osteochondral defect healing

The animal experiment realized by Bail and co-workers is briefly summarized (Bail, et al., 2003). Osteochondral defects of 6 mm diameter and 1.5 mm depth from the subchondral bone plate were created at the left femoral condyle in 18 Yucatan minipigs.

1.3.2.2 Surgical Procedures

Under general anesthesia an osteochondral defect was created at the lateral surface of the trochelar groove of the left hind limb. The osteochondral defect was 6 mm in diameter and 1.5 mm in depth from the osteochondral junction (Fig. 2.2). To minimize soft tissue damage a sharp tube was pressed into the joint cartilage to the osteochondral border for guiding a 6 mm drill. A sleeve on the drill ensured the depth of the osteochondral defect. All wounds were sutured and covered with spray bandage. Animals received flunixin (Finadyne, Essex, Great Britain) as an analgesic for the first 7 days. Six animals were sacrificed after 4 weeks, nine after 6 weeks and the remainder after 12 weeks (Bail, et al., 2003).

1.3.2.3 Boundary conditions

In order to achieve a full load condition at the affected joint, an osteotomy at the contra lateral hind leg stabilized with a 8 to 10 hole DPC was created after surgery. To obtain a continuous load condition the animals were allowed to move freely after defect creation. The animals were on average 17.1 months old (10.5 to 30 months).

The following boundary conditions were reproduced in the model definition to perform osteochondral healing simulation: joint geometry and the defect size were modeled to resemble the mini-pig's knee joint, and the total load was continuously applied from the initial defect situation for the rest of the healing process miming the *in vivo* load situation.

1.3.2.4 Gait analysis

The animals walked on a compressive sensible platform. The measurements were made one day before surgery, three days after surgery and each week until the sacrifice of all animals. A complete gait cycle was defined as the enfolded step realized for a hind leg simultaneously with a foreleg. For each member 7 imprints were recorded (to minimize errors in the measurements). The weight of each animal was controlled during the realization of each gait analysis. After gait analyses an equivalent compressive load of 1.35 MPa was calculated from reaction forces of 1 body weight (BW) acting on an average area of 150 mm^2 at the femoral condyle.

1.3.2.5 Histological analysis

The histological sections were stained with Safranin-Orange van Kossa and Safranin-Light Green. This staining allows a clear identification of the formed tissue types. Safranin-Orange van Kossa stains the calcified tissues (e.g. subchondral bone) black and the non-calcified tissues (hyaline cartilage, fibrous cartilage and connective tissue) orange. Safranin-Light Green stains connective tissue and bone green, cartilage and cell nucleus are colored red. The mechanical tissue quality of the total group was slower than the corresponding of an intact situation.

1.3.2.6 Histomorphometrical analysis

The new formed tissues (hyaline and fibrous cartilage), the remodeled bone, and the remaining defect were quantified during healing by a histomorphometrical analysis (KS400 image analysis system, Zeiss, Germany). In three regions of interest (ROI), localized within the subchondral bone at the walls and at the basis of the defect, the structural orientation and the trabecular bone fraction were determined. For control purposes all histological and histomorphometrical analysis were made at the same regions of the contra lateral uninjured femur condyle. All statistical analyses ($p<0.05$) were carried out using a commercially available package (Statistical Package for Social Sciences, SPSS Inc., Chicago, USA) (Bail, et al., 2003). The trabecular bone fraction was increased indicating active remodeling regions.

Fraction of cancellous bone increased from 25% of the total area to 29.1 ± 10.6% at 4 weeks, subsequently to 33.0 ± 13.9 % at 6 weeks and to 33.2 ± 8.7 % at 12 weeks. Hyaline cartilage was increased from initially 0% to 8.1 ± 6.7 % at 4 weeks, 17.0 ± 12.5 % at 6 weeks, and 33.1 ± 25.4 % at 12 weeks. The fibrous tissue filling the defect decreased from 47.7 ± 14.2 % at 4 weeks to 35.2 ± 13.2 % at 6 weeks, and to 24.2 ± 18.7 % at 12 weeks. The defect region was

reduced from initially 75% of the total area to 15.2 ± 7.71 % at 4 weeks, to 14.8 ± 9.0 % at 6 weeks, and to 7.1 ± 2.9 % at 12 weeks. During healing it was found that the trabecular bone fraction increases indicating active remodeling regions (Bail, et al., 2003).

Additionally, Bail et al. reported a complete macroscopic and microscopic description of the repair process. New techniques such as a reproducible immunohistochemical color protocol for cartilage and bone repair analyses were developed.

1.3.3 Results used from the preliminary work

1.3.3.1 Results used from the humerus analysis (Lill et al.)

1. The implant LCP-PH was selected for analysis. After comparison between different implants to stabilize the proximal fractures, LCP–PH showed flexibility without compromising fracture fixation.
2. Two bones with known DEXA distribution, which were stabilized with a LCP-PH, were selected for reconstruction and analysis.

In this thesis the analysis, results and conclusions related to bone-joint mechanics, which was studied in humerus specimens under physiological loads, were identified as and reported under the name “humerus project”.

1.3.3.2 Results used from the animal model (Bail et al.)

From Bail’s animal experiment the following data was used:

1. The histological sections at 4, 6 and 12 weeks were employed. In this work his data was used first to reconstruct the geometry of the histological sections and to analyze these models numerically in order to determine straining of the tissues during healing and factors for growth and resorption for each tissue type. The stained tissues were used to identify each tissue (Fig. 3.5). Secondly, the spontaneous repair process observed in the histology was used to compare qualitatively the *in vivo* healing outcome to the simulated healing.
2. The histomorphometrical data at 4, 6 and 12 weeks was employed to validate the model quantitatively as explained in the material and methods section.
3. From the gait analysis the reaction forces were calculated. These measurements were employed to estimate the *in vivo* load condition on the joint and applied as mechanical boundary condition during the simulated healing.

The study of spontaneous repair of osteochondral defects using animals for experimentation were realized in line with a doctoral thesis in veterinary medicine entitled “Histologische, immunhistologische und histomorphometrische Untersuchungen der Wirkung von systemisch applizierten Wachtumshormon auf einen osteochondralen Knorpeldefekt am Yucatan-Minischwein” (histological, immunohistological and histomorphometrical analysis of the effect of systematical applied growth factors on an osteochondral defect in Yucatan minipigs) (Klein,

2001).

In this thesis all sections related to osteochondral defect healing have the title “Galileo project”. Historically, Galileo Galilei is considered to be a pioneer in the field of biomechanics. He not only used the term “mechanics” for the first time to relate acting forces, systems and its response, but also observed and applied such concepts to biological organisms. Galileo supposed for the first time a relation between bone and its mechanical boundary conditions. His contribution to biomechanics was the basis for further development of bone remodeling and tissue differentiation (a more general formulation). Such concepts have been refined, further developed and are recently called mechanobiology (van der Meulen and Huiskes, 2002). Therefore, the name “Galileo” was used to identify the study of the mechanical aspects of the biological process involved in osteochondral healing.

1.4 Hypotheses and aims

1.4.1 Hypotheses

1. Bone quality has a stronger influence on the mechanical behavior of intact and fractured bones than physiological loads. The resulting straining field on bone tissues can measure the influence of quality after load application. To test this hypothesis bone straining in intact and fractured proximal humeri with different density distributions under different arm positions were evaluated and compared.
2. Mechanical conditions influence the healing outcome of osteochondral defects. This can be proved using a validated differentiation model that allows performing changes in the mechanical boundary conditions and to compare the predicted healing outcomes to one another.
3. If the mechanical conditions affect osteochondral healing then local environment given by joint geometry is of concern. To corroborate this hypothesis osteochondral defects on concave and convex geometries were evaluated and the healing outcome was compared.
4. Since chondrocyte activity appears to be principally stimulated by compressive loads (Guilak and Mow, 2000; Heiner and Martin, 2004; Li and Herzog, 2004; Wong and Carter, 2003), compressive strains may be used as mechanical stimulus to simulate and to maintain differentiation.
5. If changes in the continuity of the subchondral bone hinder cartilage repair, then grafts with the same stiffness as the native subchondral bone could promote differentiation and maintenance of hyaline cartilage. To test this hypothesis, defect fillings with the same and different stiffness as the subchondral bone were simulated and the healing outcome qualitatively and quantitatively compared.

1.4.2 Aims

Before studying osteochondral healing the mechanical behavior of the bone-joint region was studied in a large model. The straining of the intact and fractured proximal humeri under physiological-like loading conditions was determined. The importance of tissue quality, for the straining of bone in intact and osteosynthetic stabilized proximal humeri, was demonstrated as a result. This project aimed to determine the influence of the mechanical conditions on osteochondral healing. To achieve this goal the development of a tissue differentiation model, which is able to predict healing with appropriate tissue quantification, was necessary. After validation by a comparison with the outcome from animal experimentation this model was used to answer some of the most frequently reported clinical questions, such as which is the maximum defect size that still produces tissues with a good mechanical quality, why osteochondral defects occur predominately on convex joint surfaces and, in the case of defect fillings, how stiff should a biomaterial be in order to guarantee a long-term joint functionality. The tissue differentiation model developed in this poroject demanded the proposal of a theory supporting its usage and implementation. Additionally, this project explored for the first time the usage of *in vivo* data to determine mechanical parameters (minimum principal strains, fluid velocity, pore pressure etc.) of the different tissue types during healing, some of which (e.g. fluid related material properties) are difficult to determine without the use of numerical tools.

2 Materials and methods

2.1 Bone-joint mechanics (humerus project)

To understand the mechanobiological behavior of a synovial joint the straining of the intact and fractured proximal humerus under physiological-like loading was determined. The model employed in this study was validated by comparison of the bone stiffness in the axial direction and in torsion calculated after numerical analysis to the results obtained from the *in vitro* analysis realized by Lill and co-workers.

For the analysis of the bone-joint mechanics (large model), the humerus bone was chosen for the following reasons: first, approximately six percent of all fractures occur in the proximal humerus, second: these fractures are critical in osteoporotic patients and remain a clinical challenge, third: new devices have been developed to achieve optimal healing, especially in weak bones, and need to be mechanically analyzed. Lill and co-workers conducted a research project involving all theses premises (Hepp, et al., 2003; Lill, et al., 2002; Lill, et al., 2001; Lill, et al., 2001; Lill, et al., 2003; Lill, et al., 2004). However, mechanical conditions affecting bone, measured in the straining pattern generated after implantation, are still unknown, and were studied in the first part of the present project.

2.1.1 Mechanical *in vitro* testing of proximal humerus defects

The procedure described by Lill et al. shall briefly be summarized. 24-paired fresh human humeri were obtained for histomorphometric analysis of the trabecular bone structure (Lill, et al., 2001). The selected specimens were comparable both in age and bone mineral density distribution (BMD) ($p>0.05$). Subsequently an *in vitro* test of intact and fractured human proximal humeri was performed. The fractured bones were stabilized with different osteosynthese types and tested under compressive and torsional loads (Lill, et al., 2003). Out of this group seven unpaired humeri were selected for biomechanical testing. The defect was stabilized by a new, internal fixator with locking screws (angular stability) using the standard instrumentation supplied by the producer (Locking Compression Plate for the proximal humerus LCP-PH, Mathys, Bettlach, Switzerland). In contrast to conventional plates the head of these screws is aligned to the body of the implant and provides the screw with angular stability with respect to the implant (Fig. 2.1, center).

Screw length and placement were chosen according to manufacturer's recommendations. Mechanical testing was performed using an electro-mechanical material testing machine (Type 1455, Zwick, Germany) in displacement control (Lill, et al., 2001). Relative movements of the proximal and distal fracture fragments were determined using an optical measurement system (PC Reflex, Qualysis, Sweden, accuracy < 0.1mm and $< 0.1°$) with reflective markers (Fig. 2.1, right). The technique and measurement accuracy of this procedure has previously been reported (Chu, et al., 2000). Implant stiffness was calculated from a 0.5 mm axial compressive displacement (5 mm/min) and 4° torsional rotation (50°/min) with an axial preload of 25 N. The specimens were kept moist during testing.

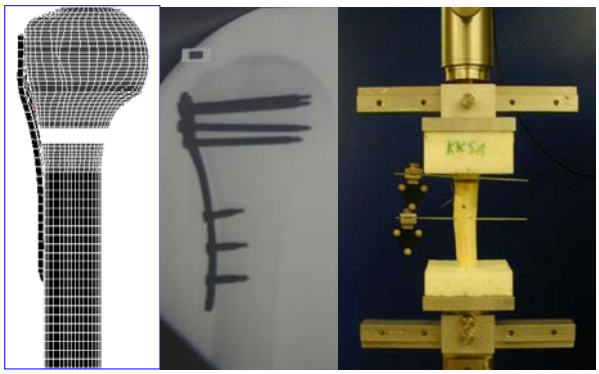

Fig. 2.1: Proximal humerus with defect localization and a LCP-PH implant under compressive loads. Left: Finite element model of the proximal humerus with implant, analyzed in this project. Middle: X-ray of a specimen with implant but prior to the osteotomy. Right: Specimen in material testing machine under pure compression. Reflective markers (distance between marker trees = 60 mm) are attached to each segment to allow determination of the interfragmentary movements. From these movements and loads, the stiffness of the bone implant construct was computed (Maldonado, et al., 2003).

2.1.2 Straining of intact and fractured proximal humerus under physiological loads

2.1.2.1 Simulation of the used human specimens and FEM validation

Out of the tested group, two representative humeri were selected for this study: one osteoporotic and one normal with reference quality, and scanned using both QCT and DEXA (average DEXA value = 0.26g/cm^2 and 0.49g/cm^2 respectively). Geometry and density distribution from QCT-scans for these two bones were determined and modeled.

The finite element models were created from the QCT data sets of these two specimens using an automated mesh-generation algorithm to define inhomogeneous material properties based on the CT density information (Seebeck, et al., 2001). A standard phantom (a reference calibrated pattern to estimate bone density in dependence on a gray scale from MRI images) provided a reference to determine apparent wet density. To assign the Young's modulus as a function of the apparent density, the relationship of Carter and Hayes was used (Carter and Hayes, 1976). According to a method described by Zannoni, a preliminary analysis was performed to define the minimum number of independent elastic modulus of Young's required to achieve a convergence of the analysis (Zannoni, et al., 1998). Based on this, the material properties of the matching voxel-based QCT data points were averaged for each element, leading to the definition of up to 127 material properties. In each finite element model the Young's modulus ranged between 22.3 MPa < E < 7837.9 MPa for the reference bone quality (RQ) and 22.3 MPa < E < 7422.5 MPa for the poor bone quality (PQ) specimens. The bones were modeled as isotropic, linear elastic and inhomogeneous material with a Poisson's ratio of ν = 0.3. The FEM meshes of the RQ and PQ specimens contained 58,048 and 56,682 eight-

noded brick elements (52,054 and 50,822 nodes) respectively.

Simulation of a 5mm osteotomy (shaft unimpacted in the Neer classification II (Neer, 1970) or proximal humeri A3 in the AO classification, (Müller, et al., 1989), at the level of the surgical neck was achieved by using low stiffness elements (E = 5 MPa, ν = 0.45) in both finite element models. The defect stabilization was simulated by modeling an angle-stable plate (LCP-PH, Mathys, Bettlach, Switzerland), consisting of 142 eight-noded brick elements and 108 thin 2-noded beam elements representing the screws. The screw length and placement was chosen according to the experimental model described before (Fig. 2.1). The implant materials, screws and the angle-stable plate, were modeled as isotropic, linear elastic and homogeneous with an elastic modulus of 110 GPa and a Poisson's ratio of ν = 0.3 (commercially used titanium, Mathys, Bettlach, Switzerland).

To verify the finite element models, the *in vitro* tests were simulated by applying nodal displacements to the most proximal (anatomical plane) node layer (0.5 mm axial compression and 4° angular rotation).

2.1.2.2 Simulation of physiological loads

To include the implant and muscle attachments the FE models were scaled to a total length of 345 mm by extruding the distal cross-sectional geometry and material properties. The attachments and orientations of 15 muscles that load the shoulder girdle for three different arm positions were taken from the literature and scaled to both humeral models (van der Helm, 1991; van der Helm and Veenbaas, 1991). A single vector represented each muscle. The loading scenarios included the neutral arm position (0°), 90° abduction and 90° forward flexion (Table 2.1). The contact force at the elbow joint was calculated from force vectors of those muscles crossing this joint and the corresponding resultant force vectors. Equilibrium was established by positioning the elbow contact force such that force and moment equilibrium for the whole humerus under physiological-like loading was achieved. The von Misses stress calculation is a common representation of results in continuum mechanics and applies to ductile materials (e.g. metals), which fail under shear loading. In contrast to metallic implants and since *in vivo* measurements are limited to strains principal strains were selected to represent the load state in the humerus sufficiently. All calculations were performed using the Marc/mentat package (Marc K72/Mentat 3.2; Marc Analysis Research Corp., Palo Alto, CA, USA) on a Unix workstation using linear elastic analyses (MIPS R 10000; Silicon Graphics Inc., Mountain View, CA, USA). The obtained results and clinical implications were reported by (Maldonado, et al., 2003).

2.2 Osteochondral healing (Galileo project)

Given the influence of mechanical conditions on bone healing, and the fact that the finite element method is able to simulate and analyze specific conditions (bone quality and physiological loads) during fracture stabilization, a similar approach should be applied for the study of osteochondral healing: A local model of the joint region necessarily needs to 1.

Determine which mechanical conditions have to be selected for analysis, 2. Determine the effect of local conditions such as contact with another joint surface and joint curvature, 3. Consider modeling of specific features such as joint structure (e.g. consideration of the subchondral bone plate) and fluid conditions (interchange of fluids between articular surfaces), 4. Develop a versatile tool that allows combining different mechanical conditions to analyze healing using the proved finite element method.

Force Vector	Fx (N)	Fy (N)	Fz (N)	Fr (N)
pectoralis major p. thorak	-29.5	-3.4	-12.4	32.2
pectoralis major p. clav.	-16.9	-0.2	-4.5	17.5
latissimus dorsi	0.0	0.0	0.0	0.0
deltoideus scapularis	-367.7	51.0	53.3	375.0
deltoideus clavicularis	-85.8	2.5	-9.6	86.4
supraspinatus	-25.4	-13.0	9.1	30.0
infraspinatus	-4.4	-5.0	2.0	6.9
subscapularis	-328.7	-140.9	40.3	360.0
teres major	0.0	0.0	0.0	0.0
teres minor	0.0	0.0	0.0	0.0
coracobraquialis	-8.5	1.1	-1.4	8.6
biceps breve	0.0	0.0	0.0	0.0
bicep caput longum p. cran	0.0	0.0	0.0	0.0
bicep caput longum p. cau	24.9	-0.7	1.9	25.0
brachioradialis	0.0	0.0	0.0	0.0
gleno-humeral contact force	346.6	79.9	-159.9	390.0
bone mass	0.0	-16.3	0.0	0.0
elbow contact force	495.4	45.6	81.1	504.1

Table 2.1: Weight, muscles and joint contact forces in Newton in 90° abduction

The first three points concern modeling and simulation and do not impose major planning; the fourth point required the development of a concept, a method to follow (numerical analysis of histological sections, development of an algorithm and its implementation) and, a very important point, the definition of boundary conditions that appropriately represent the observed and measured conditions during the animal experimentation. A detailed description of how this was performed is given in the following:

2.2.1 The tissue differentiation model

2.2.1.1 The concept

Based on acquired knowledge the new differentiation model should contain the following characteristics:

1. The model was considered to be poroelastic (biphasic), contrary to previous monophasic analysis, axisymmetric and with a non-linear mechanical behavior. The cartilage properties were defined by permeability, void ratio and elastic modulus of Young's. In this form cartilage was represented as an incompressible material with 80% water and elastic behavior. This approach then guarantees a more realistic simulation.
2. The strain limits, which were used as stimuli for differentiation, were determined for the first time from histological analysis (*in vivo* data).
3. The model to be developed should be so general that it does not depend on the mesh definition (localization or numeration of the elements).
4. The values used to define the trilinear curve for each tissue type should be implemented in the algorithms for differentiation to allow evolution from one tissue to another.
5. A theory describing this simulated healing process should explain how healing occurs and how the observations of histology can be reproduced.
6. After the validation of the simulated osteochondral repair, the model should be flexible, allowing an easy predictive evaluation of different clinical cases.

2.2.1.2 Numerical analysis of the histological sections

During animal experimentation, histological sections of a surgically created osteochondral defect in the Yucatan minipigs (Fig. 2.2) were stained with Safranin-Orange van Kossa and Safranin-Light Green, and then analyzed for 4, 6, and 12 weeks.

2D contours between different tissues were digitized and defined as B-Splines using Pro/Engineer, a commercial package for solid modeling. With the usage of a developed PYTHON subroutine the B-Splines were imported as composite curves in Marc/mentat, (Fig 2.3). A mesh was created according to the histological sections to determine strains and stresses. The models were loaded with a pressure of 1.35MPa (from gait analysis) acting at the upper boundary of the model. Tissue types during healing were identified from the stained regions of histology. The material properties were taken from literature (Guo, 2001; Lacroix and Prendergast, 2002; Smith and Mansour, 2000) and then assigned in correspondence with these regions.

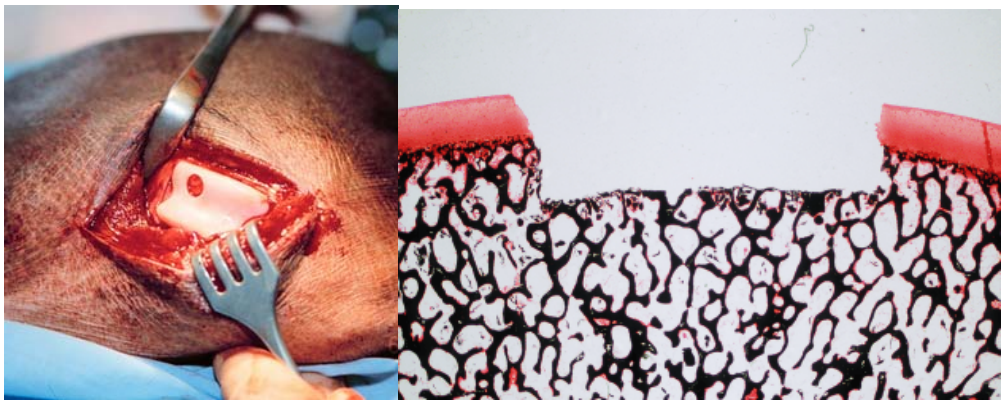

Fig. 2.2: Initial osteochondral defect created at the femoral condyle in Yucatan minipigs (∅ = 6mm, depth = 2mm). Left: from: (Bail, et al., 2003), right: from: (Duda, et al., 2005).

A maximal of 6757 quadrilaterals 4-noded elements and 6834 nodes were employed to analyze the histological sections. A convergence test was performed by duplication of the element number and by changing from quads 4 node elements to quads 8 node elements. Since the differences in the strain fields were less than 10%, the models with the minimal number of elements and nodes were considered to be sufficient to evaluate the state of straining during healing.

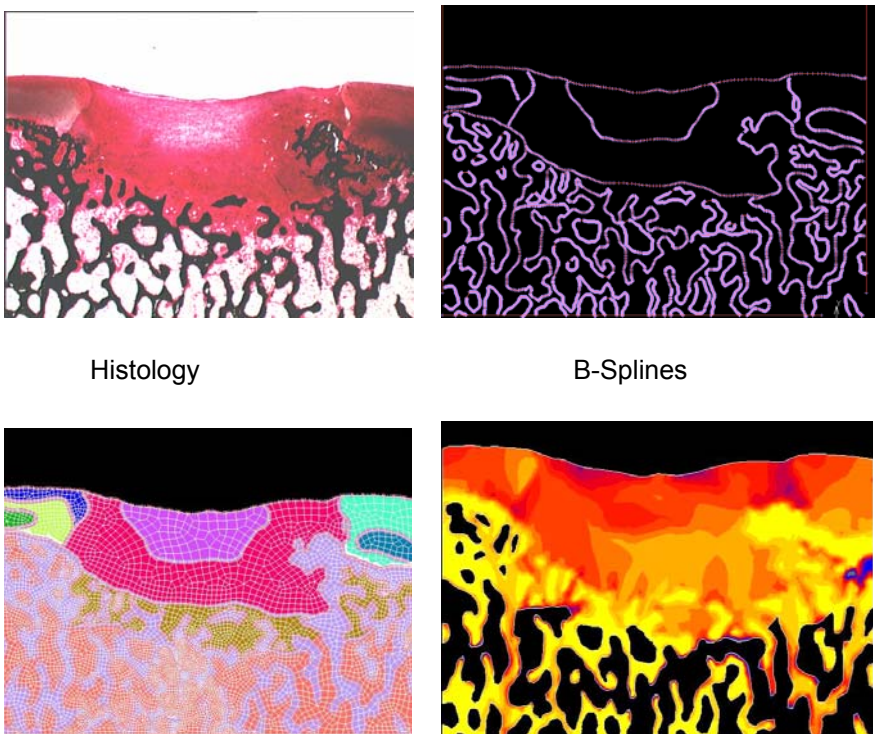

Fig. 2.3: Finite element analysis of histological sections to determine factor for growth and resorption. The contours of the different tissues in the histological sections are represented as B-Splines.

After FE analyses maximal and minimal values of the minimum principal strains were used to define the limits of the tri-linear curves given for each tissue type. A maximal strain value for a specific tissue represents in this case the limit for growth and the minimal strain value the limit for resorption. The rates of variation of these values were used to define factors for growth and resorption to simulate differentiation from one tissue type to another one. These new values were employed in the development of the tissue differentiation model described below.

This model is the first using *in vivo* data for the evaluation and calculation of parameters (limits of the trilinear curve and factors for growth and resorption) to simulate osteochondral healing. The current models generally use parameters to simulate growth and resorption obtained from sensitive parametric analysis using numerical models that is, the parameters are assumed - the model is numerically analyzed using such parameters and compared with histological observations. The parameters are then adjusted upwards to obtain a pattern similar to that observed in histology. To use parameters obtained from *in vivo* data represents the elimination of supposed parameters, and more importantly, the determination of how tissues respond mechanically under load application. Considering that the load is determined from the gait analysis, and the geometry is reconstructed from histological sections, its numerical analysis represents the *in vivo* straining of the tissues during healing, which are currently unknown.

2.2.1.3 Implementation of the tissue differentiation model

To develop this model, a previous study of the physiological loads in human bones allowed understanding of their mechanical behavior, taking into consideration specific characteristics such as geometry and bone quality (Maldonado, et al., 2003). Knowledge of bone strength is important for the understanding of the origin of fractures as well as for optimizing fracture fixations in weak bones (Lauritzen, et al., 1993; Miller, et al., 1996; Saitoh, et al., 1994). Radiological analyses of cadaveric proximal humeri have found an increasing dependency of the rate of bone tissue loss on age, especially in the region beneath the epiphyseal scar, the central zone, and in the greater tuberosity (Hall, 1963). A more recent study has described a strong correlation between radiological measurements, such as high values of bone mineral density (BMD) and mechanical strength of the trabecular bone in the proximal humerus (Lill, et al., 2001). In addition, age related differences in the female and region related differences in both genders were demonstrated for the proximal humerus. These findings provide an insight into the fracture patterns of the proximal humerus and form the basis for a re-design of implants for osteoporotic patients.

Additionally, the humerus project showed that some mechanical conditions influence bone healing stronger than others (bone quality has stronger effects on healing than physiological loads), and therefore the different impact of mechanical conditions in the case of osteochondral healing must be considered as well. Is defect width more critical than defect depth? Is the healing pattern different when the defect thickness is varied? Do the specific mechanical conditions, generated after changes in the joint curvature, have any influence on osteochondral healing? What happens when in the case of usage of grafts to fill the defect, the stiffness is

considered to be the same as the surrounding subchondral bone and what changes occur when the graft stiffness is reduced? To find answers to such questions the tissue differentiation model to simulate repair was developed and implemented.

To develop this type of model, some assumptions have been made and were considered: chondrocyte cells shall respond to mechanical signals especially under compressive loads. Due to the fluid phase of the cartilage, which amounts to approximately 80% of the cartilage composition, the effect of this second phase should be taken into account (biphasic material definition). Considering these two assumptions, the project was mainly aimed to develop a tissue differentiation model to analyze the influence of mechanical conditions on osteochondral healing to understand and even predict this healing process.

Differentiation was simulated by incremental changes in the elastic Young's modulus. Since chondrocyte activity appears to be principally stimulated by compressive loads (Heiner and Martin, 2004; Li and Herzog, 2004; Wong and Carter, 2003) compressive strains were used as mechanical stimulus to simulate and to maintain differentiation. Factors to simulate growth and resorption for each tissue type were defined after numerical analysis of histological sections. After load application, the stimulus was determined using the schema of a tri-linear curve conventionally used to simulate bone remodeling (Huiskes, 2000; Huiskes, et al., 2000; Ruimerman, et al., 2003; van Rietbergen, et al., 1993). For each tissue type a tri-linear curve was defined (Fig. 2.4; Table 2.2) in the following manner. At the initial state of the defect situation cartilage, cancellous bone, subchondral bone plate and defect (connective tissue) were simulated. In addition, the formation of fibrous tissue and calcified cartilage during healing was expected.

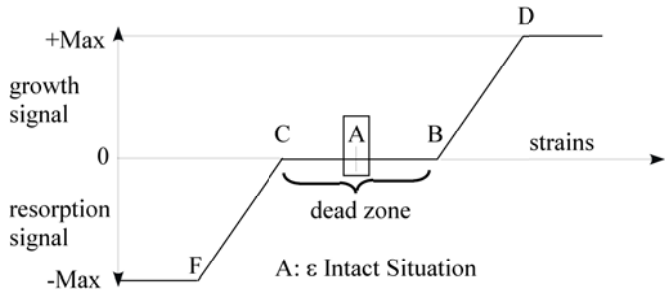

Fig. 2.4: Tri-linear curve used to simulate tissue differentiation. The center point corresponds to the strain value of an intact situation.

Using finite element models (FEM) selected histological sections at 4, 6 and 12 weeks were analyzed. From these numerical analyses two types of parameters to simulate healing were determined for each tissue type: the extreme points of the trilinear curves (F and D in Fig. 2.4) and parameters describing the rates of growth and resorption (Table 2.2). The extreme points were calculated from the average of the maximal and minimal values of the minimum principal strains (**mps**) measured at each time point (4, 6 and 12 weeks). The parameters describing the

rates of growth and resorption were determined from the average of the rate of change in the minimum principal strains between these FE models of histological sections at consecutive time points. The material properties were taken from literature (Guo, 2001; Lacroix and Prendergast, 2002; Smith and Mansour, 2000) (Table 2.3).

The mechanical stimulus was iteratively calculated as the difference between a current healing state and the state of strains in an intact situation. The new elastic Young's modulus for each material point (defined as the numerical grid point of the mesh in the model characterized by its momentary tissue type) was calculated following the scheme shown in Fig. 2.5 and using equation 2.1. Finally, the differentiated tissues during the simulated healing in an area (TA) including the defect region and the elements at its basis were quantified, as shown in Fig. 2.6. The percentage (i.e. number of elements) of each differentiated tissue type during healing (after each iteration) was then calculated. The simulated healing was compared qualitatively with histological (location) and quantitatively with histomorphometrical data.

$$E = E + stimulus * V \qquad \text{(Equation 2.1)}$$

Where, If $\varepsilon_F < \varepsilon_{current} < \varepsilon_C$ then $V = V_{growth}$,

$$stimulus = \left(\varepsilon_c - \varepsilon_{curr}\right) \Big/ \left(\varepsilon_c - \varepsilon_F\right)$$

If $\varepsilon_C < \varepsilon_{current} < \varepsilon_B$, then stimulus = 0

If $\varepsilon_B < \varepsilon_{current} < \varepsilon_D$, then $V = V_{resorp}$

$$stimulus = \left(\varepsilon_{curr} - \varepsilon_B\right) \Big/ \left(\varepsilon_{curr} - \varepsilon_B\right)$$

The index A, B, C, D and F refers to points in Fig. 2.4.

With, V_{growth}: Factor for growth defined for each tissue type (Table 2.2).

V_{resorp}: Factor for resorption defined for each tissue type (Table 2.2).

ε_A: Minimum principal strains in the intact model at each material point. Point A in Fig. 2.4.

ε_B: Minimal variation found in the mps after numerical analysis of histological sections during healing added to the mps in the intact model at each material point (ε_A). Point B in Fig. 2.4.

ε_C: Minimal variation found in the mps after numerical analysis of histological sections during healing subtracted to the mps in the intact model at each material point (ε_A). Point C in Fig. 2.4.

ε_{curr}: Minimum principal strains in the defect model during healing in the current step at each material point.

ε_D: Maximal value of the mps encountered in an intact situation added to the mps in the intact model (ε_A). Point D in Fig. 2.4.

ε_F: Maximal value of the mps encountered in an intact situation added to the mps in the intact model (ε_A). Point F in Fig. 2.4.

When the strain values exceeded the limits defined for each tissue (F and D in Fig. 2.4) the stimulus was set to the limiting value. Thus, a pentacurve was used.

	Defect connective tissue	Fibrous tissue	Cartilage	Calcified cartilage	Cancellous bone	Subchondral bone plate
E_{min} (MPa)	0.2	3.0	8.0	12.0	825	2300
E_{max} (MPa)	3.0	8.0	12.0	825	2300	22000
Width of the dead zone (CB)	0.1e-4	0.1e-3	0.1e-3	0.1e-3	0	0
Width of the differentiation region (FC; BD)	0.1295	0.1295	0.1295	1.536e-4	0.555e-3	0.555e-3
Factor for growth	1.2	1.15	1.0	1500	400	400
Factor for resorption	1.0	1.0	1.0	900	1500	1500

Table 2.2: Limits used in the tri-linear curves defining the differentiation process for each tissue type where $E_{min}^{\ tissue} < E_{elem} \leq E_{max}^{\ tissue}$.

The factors for growth and resorption, required to simulate differentiation, were defined such that: 1. They were able to reproduce the resorption zone at the basis, observed in histology. The factor for resorption “resorption velocity” in an early state of the healing process should be then significantly higher than the factor for growth at the lateral wall and at the center of the defect. 2. After resorption the increased defect filled with a non-structured, untidy, connective tissue should possess a slow factor for growth. Due to this effect the stiffness of the reabsorbed bone region and the defect should be similar. To simulate these changes each material point was able “to jump” freely from one to another tri-linear curve, in which the factors for growth and resorption, the stimulus and consequently the elastic Young modulus were updated.

In a similar way, pore pressure and fluid velocity were analyzed as possible stimuli to start and to maintain tissue differentiation as well. Pore pressure was set to zero in a perpendicular

direction to the model plane at the cartilage joint interface to allow fluid flow. The parameters for growth and resorption to simulate differentiation previously defined remained unchanged. The elastic modulus of Young at each material point was calculated and updated after each iteration. An iteration was defined as a simulating load maintained during 100 seconds. Each iteration was subdivided in 6 increments, in which the load was gradually applied. The material properties were iteratively changed at the last increment. The load was only applied after the change of all material points defined in the model. This whole cycle represents a load step. A maximum of 350 steps were required to achieve equilibrium.

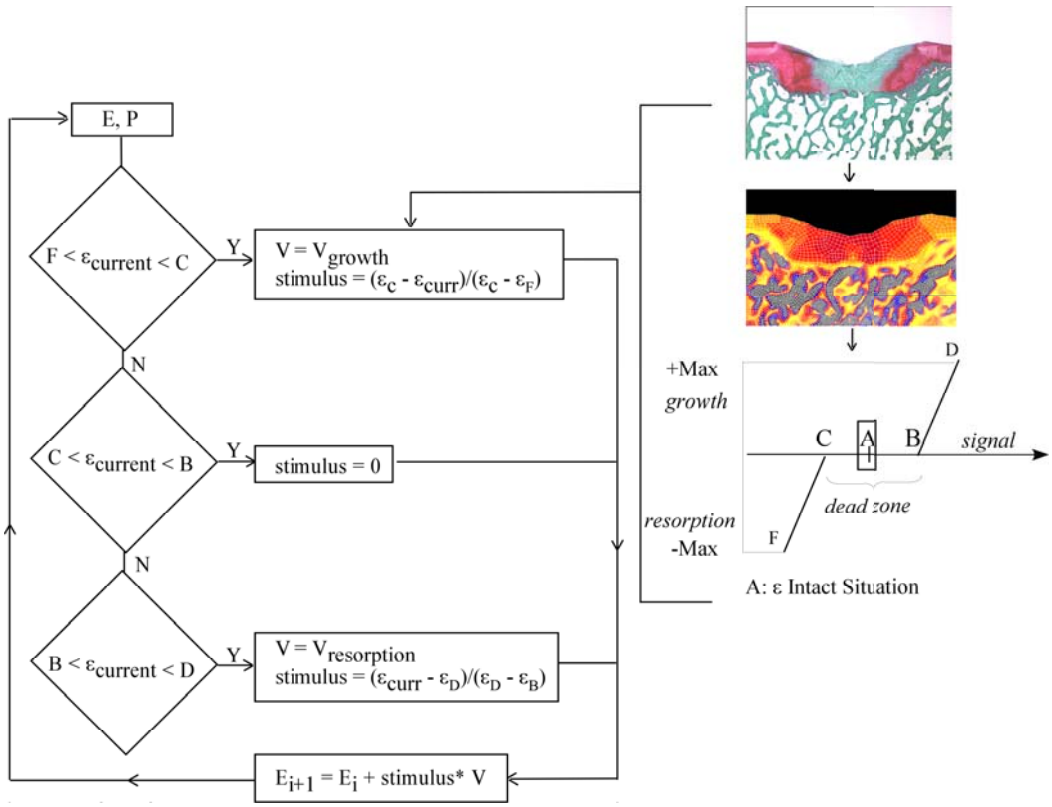

Fig. 2.5: Schematic representation of the tissue differentiation model. Differentiation was simulated by incremental changes in the elastic modulus of Young. Minimum principal strains were used as mechanical stimulus.

When in a load application step, the solution did not converge to the defined accuracy and the load step could, as a result, not be achieved in the initially defined number of increments (6); the increment of time was reduced using a predefined limiting value to assure convergence. The magnitude of this value was calculated using the corresponding equation specified in the ABAUS manual.

To control the numerical stability of the simulated healing, some elements were selected for graphical representation at the interfaces between the defect basis or defect wall with the surrounding tissues. Changes in the elastic Young's modulus in these previously selected elements during healing were plotted and evaluated until equilibrium was reached. Smooth profiles representing tissue differentiation is an indicator of a normal development of the

osteochondral ossification for cancellous bone and the formation of hyaline cartilage from connective tissue.

In the annex number 1 a brief report about the frequent errors occurring during the run of the present code and how they can be solved is given.

2.2.2 Boundary conditions

To set appropriate boundary conditions for osteochondral healing it is necessary to consider the main results of animal experimentation:

1. The defect localization influences the loads acting directly on the newly formed tissues. In the majority of the osteochondral healing studies, some authors selected the knee region to create osteochondral defects to analyze its repair process. Whereas at the patella and the lateral femur condyle low levels of compressive loads and high magnitudes of shear stresses are reported, high compressive loads have been measured in the medial femur condyle and the tibia plateau.
2. The healing process depends strongly on depth and width of the defect (geometrical parameters). Defects grade 1 (ICRS nomenclature) with a surface smaller than 2 cm^2 heal without the necessity of special treatments and in the majority of the cases the newly formed cartilage shows an acceptable mechanical stiffness. Defects grade 4, up to the subchondral bone, are able to heal only in a reduced number of cases, but are filled with fibrous cartilage with a low stiffness instead of the normal hyaline cartilage. When the superficial area is higher than 2 cm^2 the defect remains unfilled and alternative clinical treatments such as the use of allografts and autografts are more appropriate.
3. Another important point is the time after the surgery when loading of the affected joint is allowed. Some studies showed that after surgery immediate load application achieves a better healing than when the joint is totally unloaded or when an intermittent load is applied.
4. Finally the age of the patient is a factor to be considered. Young patients heal faster and the newly formed tissues show a better mechanical quality. The rule of thumb is the younger the patient is and the smaller the defect, the better are the healing chances and the long-term duration of the regenerated tissue.

All initial material properties used in the tissue differentiation model developed in this project were taken from literature (Guo, 2001; Lacroix and Prendergast, 2002; Smith and Mansour, 2000) Table 2.3. Taking into account that the geometrical limits of the joint were simulated, confined compression (see “cartilage characterization” from the introduction section) behavior was selected to reproduce the mechanical conditions acting at the knee joint. Their boundary conditions were modeled in the finite element model to simulate osteochondral repair. That means fluid exudation was allowed only between the articular surfaces and lateral cartilage deformation was avoided. Pore pressure at the joint curvature interface was set to zero in order

to allow the movement of the fluid phase between the cartilage regions in contact. No fluid movement was allowed between the other tissues.

All models were loaded with a displacement applied in an axial direction at the top of the cartilage layer calculated in an intact model under a compressive pressure of 1.35 MPa. This displacement was incrementally applied during the first 100 seconds and maintained constant during healing simulation. Load was applied via contact with an intact joint surface. The other boundary conditions are shown in Fig. 2.6.

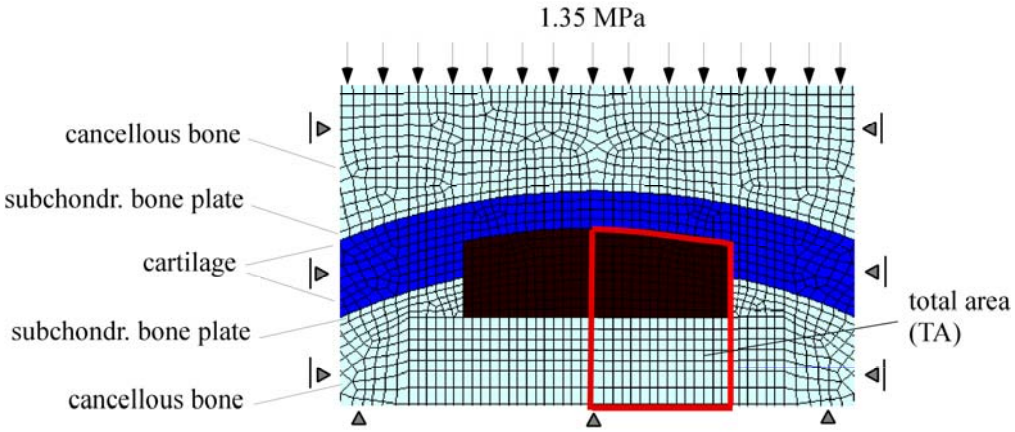

Fig. 2.6: Loads and boundary conditions used during healing simulation. TA represents the "total area" in which the percentages (number of elements) of the newly formed tissues were quantified during repair.

	Defect connective tissue	Cartilage	Cancellous bone	Subchondral bone plate
Young's module (MPa)	0.2	10	1750	20000
Poisson ratio	0.1627	0.1627	0.30	0.30
Permeability k(mm^4/N Sec)	1.0e-2	5.0e-3	2.019	1.0e-5
Porosity	0.8	0.8	0.8	0.04

Table 2.3: Initial material properties used in the finite element analysis (Guo, 2001; Lacroix and Prendergast, 2002; Smith and Mansour, 2000).

2.2.3 Parameter study

After the development of the tissue differentiation model to simulate healing some cases of defect in joints were modeled and analyzed: osteochondral defects with different defect geometries (variations in defect depth and defect width), cartilage with different thickness, osteochondral defects in flat, concave and convex joint surfaces and defect fillings with different

stiffness were evaluated. Using the method described above, the quantified tissues were calculated in an area (TA, Fig. 2.6) and compared during healing and when equilibrium was reached. This procedure was applied for all evaluated cases.

2.2.3.1 Analysis of the defect size

In a parameter study, the defect geometry was modified to reflect potential variations in the animal experimental configuration of the defect geometry. Three axisymmetric models were created. The total defect depth was increased from 1.6 to 2.4 mm, the defect diameter from 5.2 to 6.8 mm. Additionally the cartilage thickness was varied from 0.8 to 1.4 mm.

Convergence tests were performed by increasing the number of the elements and by changing from quads 4-noded finite elements to quads 8-noded finite elements. Differences under 10% in the strain fields indicated that models with 4-noded elements were sufficient to simulate healing.

2.2.3.2 Influence of the local joint curvature

To analyze the influence of the local joint curvature on healing, eight simplified axisymmetric geometries were developed: three models (flat, concave, convex) to represent the intact situation and five models to simulate the injured joint (flat, concave, convex, biomaterial with 100% native bone stiffness, and biomaterial with 50% native bone stiffness). To simulate the joint after the above-mentioned convergence, test models with a flat interface consisting of 1452 4-noded elements and 1564 nodes were created. Cartilage, subchondral bone plate, cancellous bone and an additional defect region (connective tissue) were modeled.

Biphasic behavior was simulated using the ABAQUS soils capabilities (element type CAX4P). The tissue differentiation model was validated qualitatively by comparison with the patterns described histologically. Quantitative validation was performed by comparison of the percentages of different tissue types predicted to form with the histomorphometric analysis at 4, 6 and 12 weeks.

To simulate osteochondral defects in concave and convex interfaces two models with a defect of the same dimension localized at each side of a curve interface were created. The concave situation was modeled with 1614 4-noded elements and 1721 nodes and a second model with 1603 4-noded elements and 1735 nodes was created to describe the defect on a convex interface. To resemble the tibio-femoral joint geometry of the animals, a radius of curvature of 15 mm was used (Fig. 2.6). The other parameters remained unchanged: material properties, tri-linear curves for each material, and factors for differentiation. Contact was modeled by a frictionless condition at the collinear nodes at the joint interface.

Pore pressure as stimulus for differentiation was analyzed in the convex interface, resembling the local geometry of the joint where the osteochondral defect was surgically created.

2.2.3.3 Analysis of the stiffness of defect fillings

To evaluate the effect of defect filling by means of different implant stiffness values, a cylindrical plug of 6mm diameter in a convex interface with a depth of 1.5mm from the bone plate and two different stiffness values of 100% and 50% of the elastic modulus of the cancellous bone were simulated.

Generally, all finite element analyses were performed using the Marc/mentat package (Marc Analysis Research Corp.) and ABAQUS (Hibbit, et al., 2003) package on a Unix workstation (Silicon Graphics Inc., MIPS R 10000).

2.2.4 The developed algorithm

The tissue differentiation model was written in FORTRAN. In general the algorithm follows the scheme shown in the Fig. 2.5. The code employs the commercial package ABAQUS as a visualization interface. In this tool the osteochondral defect model is shown as a continuous representation from the initial state of the defect localization to the final state of healing, when the defect was completely filled. As explained above, differentiation is simulated by incremental changes of the elastic Young's modulus.

The elastic Young's modulus, in turn, is changed in dependence of a mechanical stimulus (compressive strains). Therefore, the algorithm uses as input data the minimum principal strains after equilibrium at each material point (total number of nodes) in an intact model. These input data are written in form of a formatted external ASCII file. This file contains information about the element number, the node number, the signal magnitude (minimum principal strains, pore pressure or fluid velocity) and the initial material name. These data are then used for defining the middle of the trilinear curve as shown in Fig. 2.4. The equilibrium of the intact situation is altered by the creation of an osteochondral defect. Aim of the algorithm is then to reestablish equilibrium by using a stimulus calculated after comparison of the current minimum principal strain with the minimum principal strains known from the intact situation. As explained above, the algorithm uses the parameters defined in the trilinear curves for each tissue calculated from histological sections to generate changes in the elastic modulus of Young.

The input data was obtained using the utility subroutine UVARM from ABAQUS. This utility subroutine is called as many times as increments defined in the load step multiplied by the number of nodes and multiplied by the number of desired variables to be visualized. As explained above (description of the tissue differentiation model) one load step consists of 6 increments. The intact situation for a flat interface for example contained 1564 nodes. The variables represent the values that should be known after the FEM analysis. In this case six variables were of interest: three principal strains (maximal, medial and minimum), two fluid velocities (fluid velocity in the X direction and fluid velocity in the Y direction) and pore pressure. In consequence the preanalysis subroutine for this model was called 56304 times (1564 nodes * 6 increments * 6 variables). It is important to know this value in order to set the required variables in the environment files of an ABAQUS user appropriately (see Annex 1).

These variables are known as user variables for material information. The variables are calculated, stored in memory after each increment and written in an independent formatted external ASCII file for each variable. In this form after preanalysis of the intact model the corresponding signal information (minimum principal strains) for each node and iteration was recorded. Additionally the element number, node number, increment number and material name were added to this file.

The “user subroutine” (Annex 2) written to simulate healing can now be used since the minimum principal strains and the tissue type for an intact situation are given. After variable definition and dimensioning of necessary arrays, this subroutine contains three principal parts: in the first part, all tissue types (initials and expected to be formed) are defined by limits of maximal and minimal values of Young’s modulus. In the second part all necessary values to define the points conforming the trilinear curves for each tissue and the factors for growth and resorption are given. The third part contains the rhombuses of decisions, in which the current strain values are analyzed and the elastic modulus of Young is calculated and updated after each iteration (schema shown in Fig. 2.5). The last part is related to the manipulation and storage of each variable used in the algorithm.

The finite element method solves the integral equations generated for the osteochondral defect model with the method of the displacements using an algorithm of optimization. This optimization procedure changes the mean bandwidth[7] in the solution matrix. Thus, the solution for each node is made following the sequence suggested by the optimization procedure. In this form the ascending numerical sequence defined by the mesh topography could not be used. Therefore, in the algorithm a mechanism was implemented to verify that the current node to be analyzed is the same one as read from the intact situation. To guarantee this, some additional files are created to compare and to write element and node information.

The elastic Young modulus, which represents the grade of healing at each step, was associated with a state variable (SDV in ABAQUS). A state variable implies that its associated value is stored in a temporal memory field and could be used in a mathematical formula in combination with other numbers or state variables. A state variable can be iteratively saved in memory when its value is associated to a field variable. In this case, its value could be used iteratively in the input model data. Thus, the elastic Young modulus is calculated as a state variable, saved in a field variable and used to show the history of the material stiffness during healing simulation. The input data of the model is thereby updated and will be rewritten after each iteration. However, changes associated with each state variable are performed at the last increment, when the total compressive load applied on the joint during a step was completed. During load application the fluids inside the tissue were exuded to attenuate the compressive load. When a load cycle is completed, new elastic Young’s modulus are calculated for each

[7] Mean bandwidth: denoted by B. If a matrix of order N stored in accordance with the skyline format (skymatrix) use S memory locations, the ratio B=S/N is called the mean bandwidth.

tissue type. Poisson's ratio and permeability can then be changed. Thus, the values of these mechanical material properties are adopted in dependence to the tissue type. Tissue differentiation stops when minimum principal strains and tissue types are the same in the defect model as in the intact one. Thus, when a tissue achieves values of the dead zone, the stimulus is set to zero. The last Young modulus is then maintained unchanged during the rest of the healing simulation.

Tissue differentiation is regulated through changes in the elastic modulus of Young principally in accordance to the quantity of stimulus required to achieve the strain field encountered in an equilibrium state. So, this process is started and maintained until all tissues achieve the strain field previously determined in an intact situation. The "center point" of the trilinear curve is the minimum principal strain value for an intact situation in a node with the same coordinates as in the defect model. Obviously the mesh for the intact model and the defect model needs to be identical. Healing can then be described as the intention of convergence of an injured joint to achieve a healthy state represented by the intact model under determined mechanical conditions. As a result, it proved to be feasible to program chondrocyte activity as a biological response to a new local mechanical environment generated when articular damage occurs.

Only for flat a joint, implementation of a treatment of numerical viscosity at the elements conforming the defect wall was necessary. Numerical viscosity reduces possible inconsistencies of Hook's law at the interface defect wall-host tissues. Such inconsistencies are commonly attributed to singularities in the strain values after load application between two materials in contact, whose elastic Young's modulus shows a drastic difference (in its values). This numerical instability can create a shock transition zone. In the flat model the instability was formed not only due to a jump in the material properties at the interface between the connective tissue – cancellous bone (0.2 vs. 1750 MPa) and connective tissue – cartilage (0.2 vs. 10MPa), but also due to a high strain concentration at the defect vertex. Numerical viscosity is a well-documented procedure applied in several cases when the discontinuity is detectable. Numerical viscosity was then applied to smooth the mechanical response of the affected region (3% of the total number of the elements of TA, Fig. 2.6).

2.2.4.1 Additional tools developed for analysis of the data

Some additional tools including mesh generation and treatment of the results were created during the project:

A PYTHON routine was written to convert the IGES data information generated from PRO/Engineer to represent the histological sections as B–Splines to composite curves readable in Marc/mentat. This information was used to perform the finite element mesh in Marc/mentat.

A PYTHON routine was written to convert the mesh information (elements with its node connectivity, nodes coordinates, and material sets) created from Marc/mentat to a readable format to be used as input data in ABAQUS.

In PYTHON language a routine was developed to write changes of the elastic modulus of Young, calculated after each iteration in each material point, in an external ASCII file.

A PYTHON routine was written to create the steps information automatically to the input data of the defect model to be analyzed.

In MATLAB a short routine was developed to read this data and quantify each tissue type after each iteration.

3 Results

3.1 Bone-joint mechanics (humerus project)

In the first part of the project, the study of intact and fractured proximal humeri under physiological loads, the following results were obtained:

3.1.1 Fixation stiffness *in vitro* and in the simulation

This model was validated by comparison between the stiffness obtained *in vitro* with the stiffness calculated in a numerical model. For comparison the obtained *in vitro* values are rewritten here: seven specimens fixated with the LCP-PH were mechanically tested *in vitro* in axial compression and torsion. From these measurements the average stiffness in the axial direction was calculated to be 957.5 ± 398.21 N/mm and in torsion to 0.48 ± 0.11 Nm/°. The specimen of poor bone quality selected for finite element analysis had an *in vitro* axial stiffness of 830.2 N/mm and a torsional stiffness of 0.53 Nm/° and those specimens selected to represent the reference bone had an axial stiffness of 927.2 N/mm and a torsional stiffness of 0.64 Nm/°. The corresponding finite element analyses realized in this work (humerus project) yielded a compressive stiffness of 846.4 N/mm and a torsional stiffness of 0.52 Nm/° for a poor bone quality and 1047.9 N/mm and 0.59 Nm/° for the reference bone. The composite stiffness between experiment (*in vitro*) and finite element analysis (this work) for the specific bones differed in compression by a maximum of 13% and in torsion by a maximum of 7.8 %.

3.1.2 Straining of intact and fractured proximal humerus under physiological loads

The intact humeri bones were loaded mainly in compression with superimposed bending and torsion (Fig. 3.1).

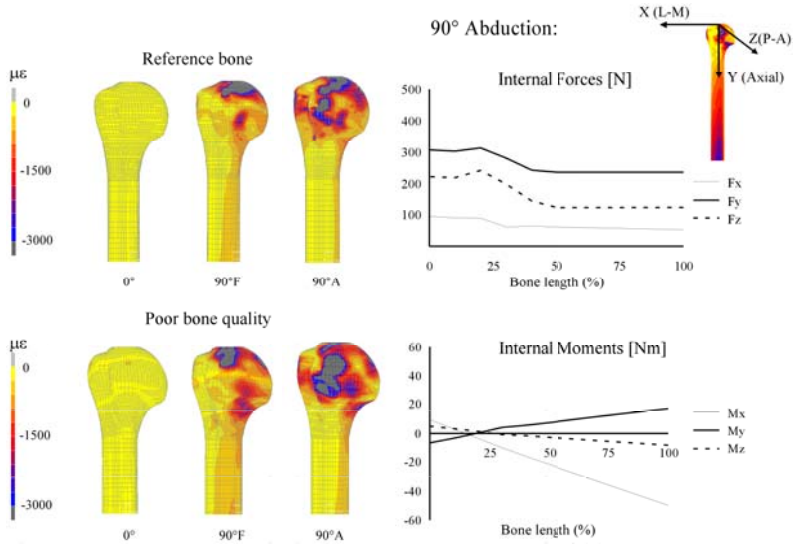

Fig. 3.1: Finite element model of the proximal humerus under physiological-like loading conditions. Minimum principal strains of the bone surface are given for the neutral position (left), 90° forward flexion (center) and for 90° abduction (right).

In this figure both intact specimens, the reference bone and poor bone quality were compared under different physiological-like loading conditions.

For the intact situation and 90° abduction the maximal strain values were found in the cortical bone. Strains were further increased in the specimen with poor bone quality under 90° abduction.

Even though the strains differed in value, the strain patterns were comparable between the neutral position, 90° abduction and 90° forward flexion under physiological-like loading conditions in the defect situation (Fig. 3.2). Comparing the strains obtained in the cortical bone (percentage of elements) for the different simulated physiological cases 90° abduction showed the largest strain values, followed by 90° forward flexion (Fig. 3.3). The lowest strain values were found for the neutral position (Fig. 3.3).

The strain distribution (percentage of elements) in the cancellous bone loaded in 90° abduction, were moderated in the specimen with reference bone quality (8% ≥ 1000 με, Fig. 3.4). The strain values were lower than the limits reported from *in vivo* data (Frost, 1987; Lanyon, et al., 1975; Lanyon, 1976). For the same physiological loading condition the specimen with poor bone quality showed a significant increment in the number of elements with high strain magnitudes (38% ≥ 1000 με, Fig. 3.4). A similar result was found in the surface strain distribution. For the specimen with the poor quality the strain pattern was similar but noticeably increased in magnitude compared with the specimen with reference bone quality. The modeling of the muscles as single force vectors implies a local overestimation of the strains close to the muscle attachments. This effect was considerably more pronounced in the osteoporotic specimen compared to the reference bone.

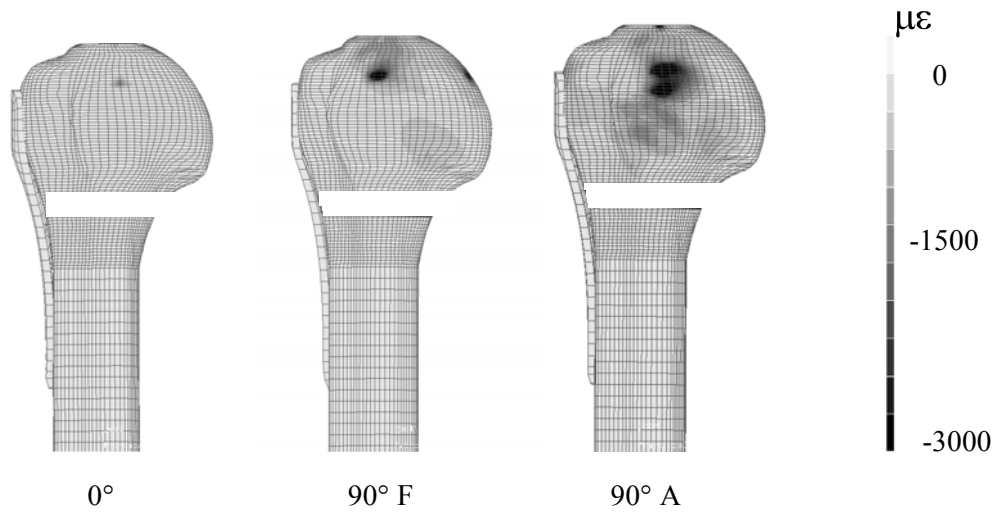

Fig. 3.2: Minimum principle strains at the anterior bone surface. Osteoporotic, poor quality bone with a bone defect stabilized by an angle stable osteosynthetic device is shown for three different arm positions: 0°, 90° forward flexion (F) and 90° abduction (A).

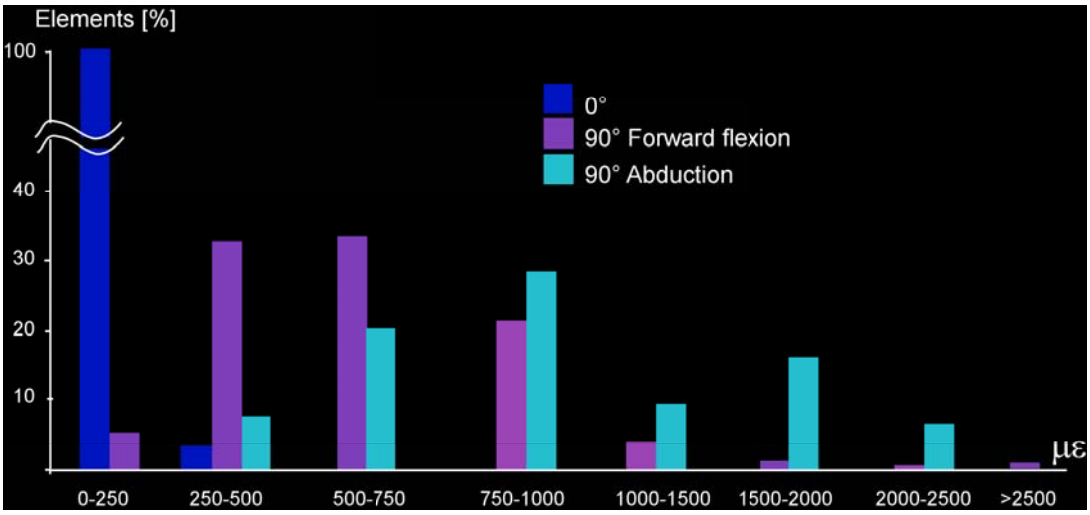

Fig. 3.3: Distribution of cortical bone elements for different strain ranges. Strains are given as minimum principal strain values for different arm positions under physiological-like loading conditions for the specimen with poor bone quality and a 5 mm osteotomy at the level of the surgical neck of the humerus.

The specimens stabilized with a LCP-PH were not strained in a different manner: Strains of the cancellous bone were increased (> 20%) in the fractured situation compared with the intact one. However, the strain values were significantly increased in the specimen with lower bone density (Fig. 3.4). These results were reported by (Maldonado, et al., 2003).

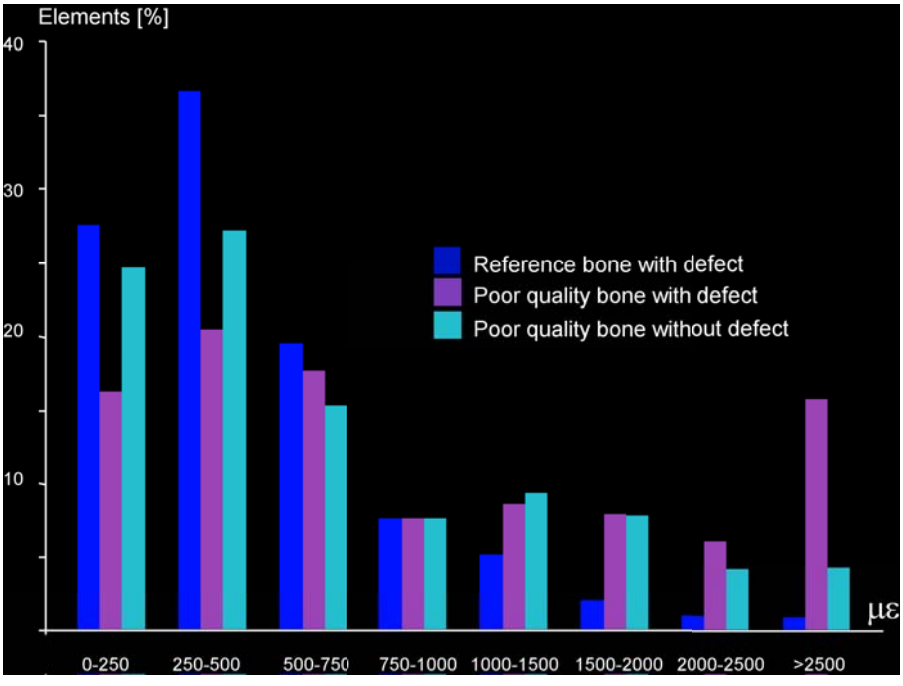

Fig. 3.4: Distribution of cancellous bone elements for different strain ranges. Strains are given as minimum principal strain values during 90° abduction for a specimen with reference bone quality and defect, and a specimen of poor bone quality, both with and without defect. Defects were stabilized using an angle-stable osteosynthetic device.

3.2 Osteochondral healing (Galileo project)

3.2.1 Strain Analysis

As explained in the material and methods section it was necessary to perform a numerical analysis of the histological sections for developing the tissue differentiation model (Fig. 3.5). Factors for growth and resorption as well as the points of the trilinear curve for each tissue type were calculated. Additionally, strains of the different tissues formed during healing were determined for the first time. The compressive field of strains in the initial defect situation was determined as well.

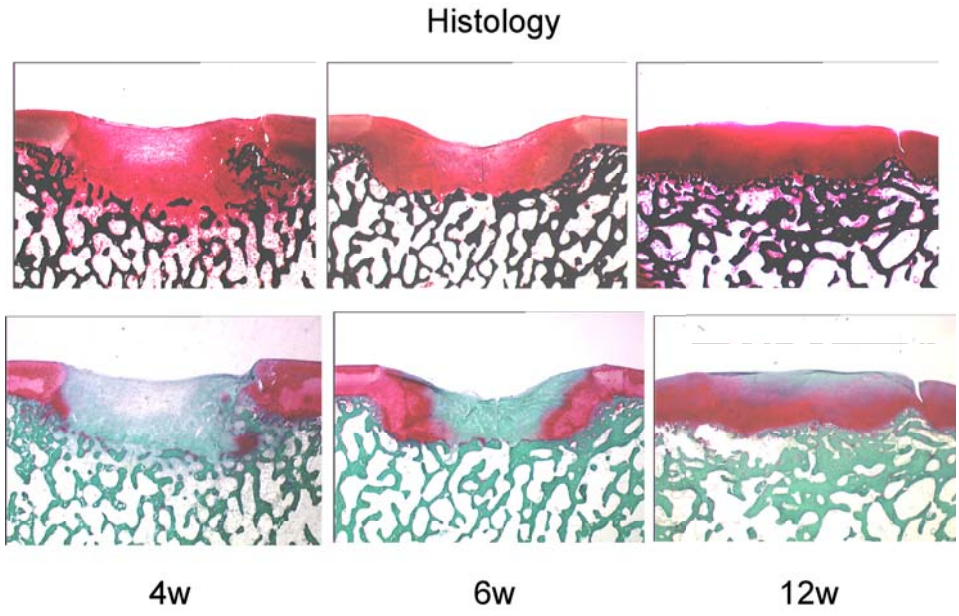

Fig. 3.5: Histological sections of osteochondral defect healing at 4, 6 and 12 weeks stained with Safranin-Orange von Kossa (top) and Safranin-light green (bottom). 4th week: First cartilage cells at the defect wall as well as a resorption region at the basis are visible. 6th week: the cartilage growths from the lateral borders of the defect. It is calcified forming cancellous bone as far as the subchondral plate. Fibrous tissue fills the defect with low formation of hyaline cartilage. At the center a defect region can be seen. 12th week: the cancellous bone has completely regrown; the fibrous tissue is differentiated to hyaline cartilage (Bail, et al., 2003; Duda, et al., 2005).

3.2.1.1 Histological sections

Using the finite element method histological sections of osteochondral healing were numerically analyzed. Values of minimum principal strains for each tissue type at the three points selected in the animal experimentation were obtained as follows:

At the 4th week (Fig. 3.6) strain concentrations at the interface cartilage subchondral bone were found. Maximal compressive strain values of –2.0e-2 at the interface cartilage-connective tissue were registered. At the defect center these values decreased to –1.7e-2 in the connective tissue. Strain values of up to –1.2e-2 were obtained at the defect wall in the regions

corresponding to the places of first cartilage differentiation. At the defect basis compressive strains values between –0.8e-2 and –1.0e-2 were achieved in the connective tissue after subchondral bone resorption.

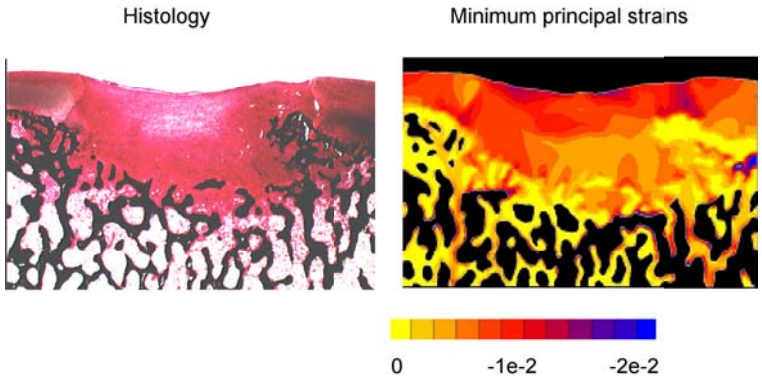

Fig. 3.6: Left: histology at the 4th week, stained with Safranin-Orange von Kossa. Right: Straining of the formed tissues during healing in a selected histological section at the 4th week.

At the 6th week (Fig. 3.7) the first cartilage regions grew and reached the defect basis in a centripetal filling configuration. The minimum principal strains at the defect wall were then reduced by up to 15 %. The minimum principal strains at the defect center were reduced from -1.7e-2 to –1.2e-2. In the transition region between the defect center and the cartilage at the wall, the minimum principal strains varied between –1.5e-2 and –1.3e-2. Minor values of minimum principal strains were found in the area where the newly formed cartilage was differentiated to pre-cancellous bone. The connective tissue at the resorption region in the defect basis was replaced by hyaline cartilage. Minimum principal strains were then changed to –0.5e-2.

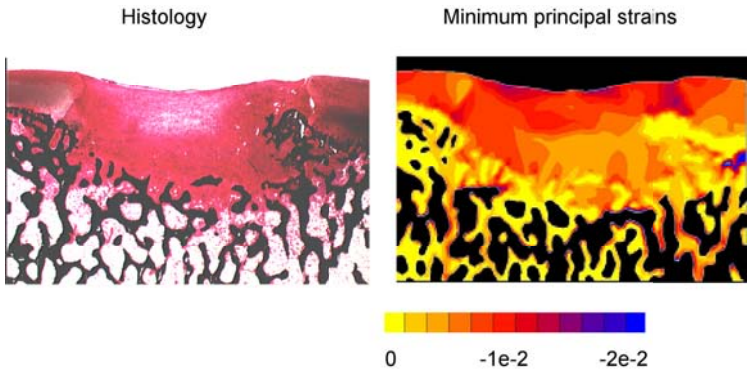

Fig. 3.7: Left: histology at the 6th week, stained with Safranin-O vK. Right: Straining of the formed tissues during healing in a selected histological section at the 6th week.

At the 12th week (Fig. 3.8) the minimum principal strain values at the defect wall were reduced by up to 12% when the fibrous cartilage was replaced by hyaline cartilage. At the defect center the connective tissue was replaced by fibrous tissue and minimum principal strains between –

0.5e-2 and –0.6e-2 were found. The defect basis was completely filled with subchondral bone and thereby the minimum principal strains were reduced by up to –0.2e-2.

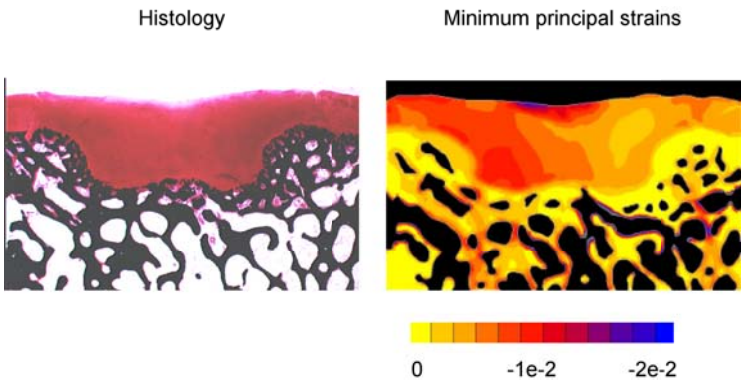

Fig. 3.8: Left: histology at the 12th week, stained with Safranin-O vK. Right: Straining of the formed tissues during healing in a selected histological section at the 12th week.

High average strain values were registered in the bone marrow areas at the subchondral bone. The compressive strain magnitudes varied between –2.0e-2 and –2.5e-2 at the 4th week. Only minor variations were registered during healing. At the 6th week these values varied between –1.7e-2 to –2e-2 and were maintained constant until the 12th week. The maximal strain values registered in the total model were –1.09e-1 at the 4th week, -5.42e-2 at the 6th week and –4.23e-2 at the 12th week. These values were found in regions localized between the interface bone marrow and cancellous bone.

The averages of the rate of change in the minimum principal strains at each control point (4, 6, and 12 weeks) were calculated. These rates defined the factors for growth and resorption for each tissue type observed during healing *in vivo*. These values were used to update the elastic modulus of Young as explained above (material and methods, the tissue differentiation model) and were reported in the table 2.2.

Additionally as shown in Fig 3.9, a scheme representing the initial defect was drawn on the digitized histological section in order to compare the localization and magnitudes of the straining during defect filling. That is, the remaining host tissues are not shown. The newly formed regions (resorption or connective tissue at the basis) and their strain distribution are particularly recognizable. The blue-violet zones at the interface host-new tissue and at the center indicate zones of strain concentration due to strong changes in the mechanical properties of the related tissues. Compressive loads produce high strain values at the center of the defect where the tissues will be differentiated into stiffer tissues. The identification of zones of high biological activity during osteochondral healing (resorption, differentiation, growth) related with drastic variations in the magnitudes of compressive tissue straining was for the first time confirmed and reported in this work.

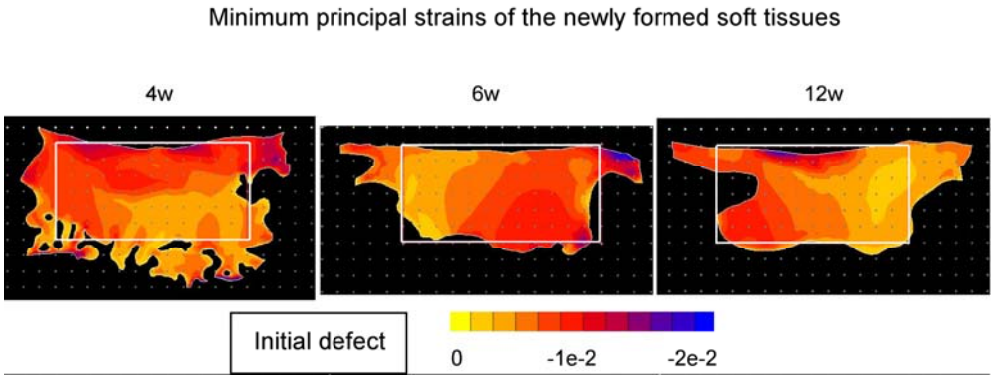

Fig. 3.9: Straining of the newly differentiated soft tissues at the defect region during healing after numerical analysis of histological sections at 4 (left), 6 (center), and 12 weeks (right). The quadrilateral represents the initial defect (∅ = 6mm, depth = 2mm).

3.2.1.2 Defect model

Observing the strain pattern an unloaded region at the defect base (680 με, 27% of intact), and an increased strain field at the circumference of the osteochondral defect (5000 με, 200% of intact; Fig. 3.10) were seen. Minor differences in the straining were found when the defect size was varied. An increment of 0.8 mm in the defect diameter produced an increment of 12% in the strain field and an increment of 10% was obtained when the depth was enlarged by 0.4mm.

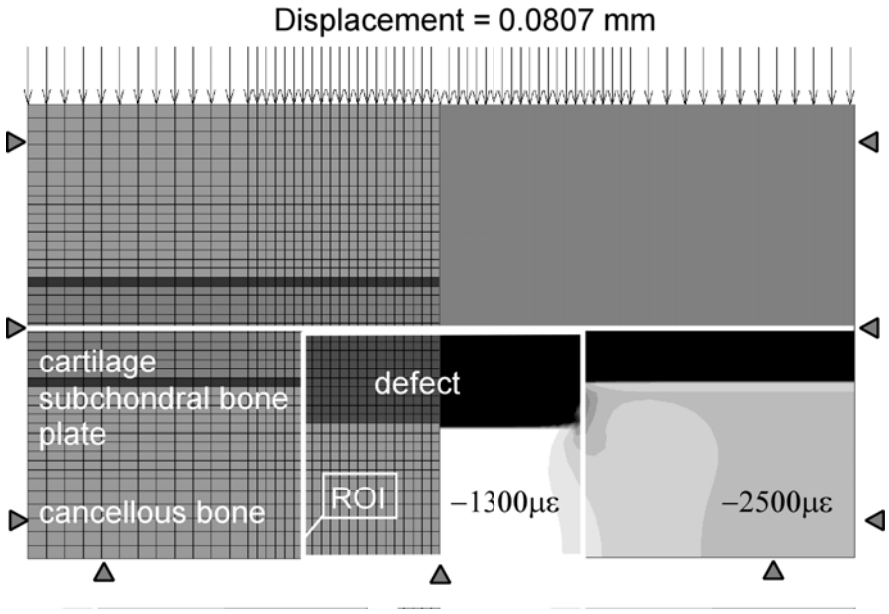

Fig. 3.10: Straining of the initial defect situation.

3.2.2 Comparison of the simulated healing to spontaneous repair *in vivo*

Qualitatively, the differentiation model resembles healing as observed in histology (Fig. 3.11). The healing pattern showed “centrifugal-shaped” growth from the defect borders to the center, resorption at the defect basis, and a remaining unfilled region at the center of the defect (Fig.

3.5): after the 4th week the defect was filled with connective tissue in a non structural array, showing the first tissues at the interface of the defect wall, at the 6th week the connective tissue was differentiated to fibrous tissue in a well defined structural array and a small percentage of hyaline cartilage. At the 12th week part of the fibrous tissue was differentiated to hyaline cartilage.

Quantitatively, the differentiation model showed amounts of new-formed tissues comparable with those obtained in the histomorphometrical findings.

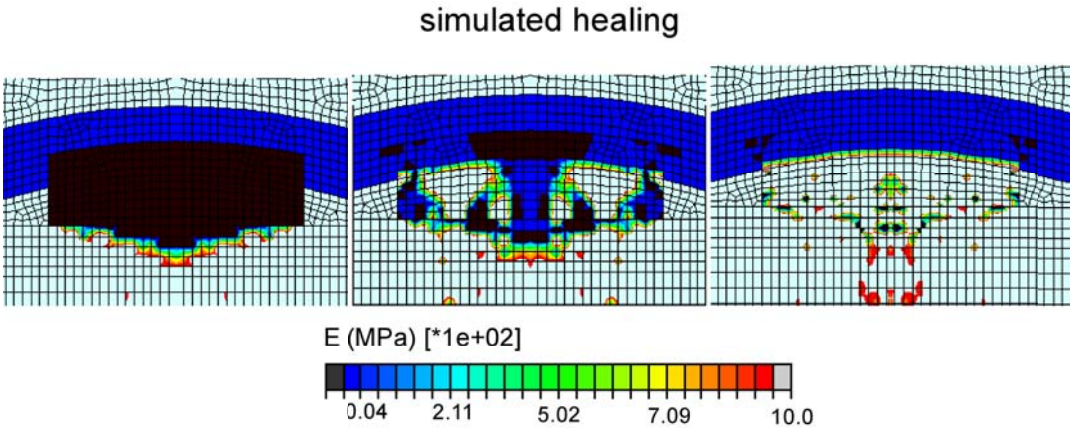

Fig. 3.11: Simulation of osteochondral defect healing. The selected iterations correspond to the histological staining after 4 (top), 6 (center) and 12 weeks (bottom).

After qualitative matching of the simulated healing with the observations of histology and similar amounts of differentiated tissues in the simulated healing with the histomorphometrical analysis, the differentiation model was considered to be validated. Only after validation can the differentiation model be used to analyze the influence of mechanical conditions on osteochondral healing.

3.3 Influence of mechanical conditions on osteochondral healing

3.3.1 Influence of the defect size

During simulated osteochondral defect healing, tissue straining led to an increase of the material properties and successively to a filling of the defect. The filling occurred from the circumference of the defect and with resorption of the defect base (Fig. 3.11). In the simulated healing the tidemark (subchondral bone plate) of the osteochondral defect area was re-established by a defect healing from the surrounding trabecular bone rather than a bone apposition from the defect base. Analyzing the defect size, which allows healing, the following results were found: when the defect depth was increased by 50% it was filled with 5% of hyaline cartilage. An increase of 33% in the defect width produced 20% of hyaline cartilage. No hyaline cartilage formation was registered when the cartilage thickness was increased by 15% (Fig. 3.12). In no case was the defect completely filled with hyaline cartilage. However, qualitatively the healing pattern did not show significant differences.

Simulated healing appears to be stable: Growth occurred without oscillations around a specific tissue type but showed smooth variations from the initial defect to the final healing stages. The defect filling occurred mainly during the first 50 iterations (approx. 70% of the initial defect area). Between the iteration 51-150, the healing rate decreased and hence only minor variations in the elastic modulus of Young were observed after the 50th iteration. Contrarily, to the observation after the 12 weeks in the *in vivo* situation, the model predicted full defect filling. The complete defect filling occurred later (approx. iteration 112) when the defect width was increased compared with a model of increased defect depth (approx. iteration 72). When the cartilage stiffness was increased, filling of the defect was observed approx. in the 68th iteration (Fig. 3.12).

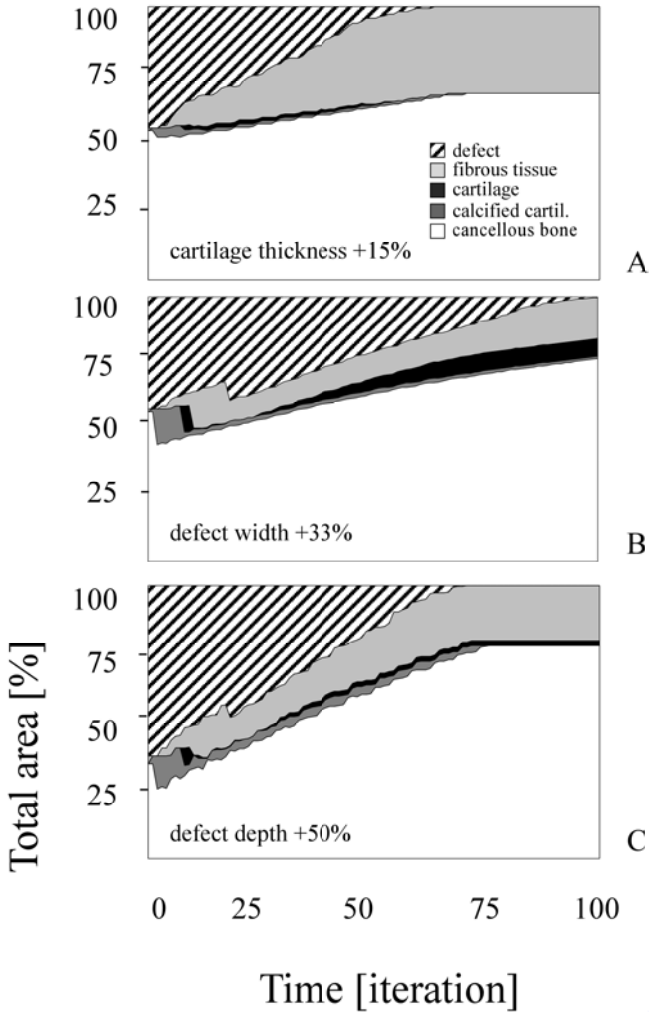

Fig. 3.12: Simulated osteochondral defect healing: With an increased cartilage thickness only fibrous tissue was generated (A). When the defect width was increased, only slight variations compared to the initial healing prediction were found (B). When the depth was increased only fibrous tissue formation was predicted (C).

For all models minor variations in the quantified newly formed tissues at the equilibrium point were found. No changes in the material properties were registered in the remaining tissues (cartilage and cancellous bone) compared to the initial values. A slight stiffness reduction or

"zone of influence" at the subchondral bone surrounding the defect was observed in all models. These results were reported by (Duda, et al., 2005). After the initial resorption at the defect base, the adaptive finite element analysis predicted a restoration of the tidemark and a complete defect filling after 100 iterations. This pattern of healing appeared to be independent of the specific defect geometry or loading configuration used (Fig. 3.12). When the defect size was varied the resorption area was comparable for both models (12% vs. 15%). This area was smaller when the cartilage thickness was increased (7%). Only in the initial defect and the larger defect situation (defect width +33%) did the adaptive finite element analysis predict cartilage formation.

3.3.2 Influence of the local joint curvature

The healing pattern was in general qualitatively comparable to the findings of the examination of the histological sections. The following stages of healing were registered both *in vivo* and in the simulation: initial cartilage formation at the defect wall, centripetal filling starting at the lateral borders at the interface defect-cancellous bone and resorption at the basis of the cancellous bone even a slight reduction of the stiffness in the remaining bone (Fig. 3.5). This general behavior appeared to be independent of the joint curvature (Fig 3.11, Fig. 3.13).

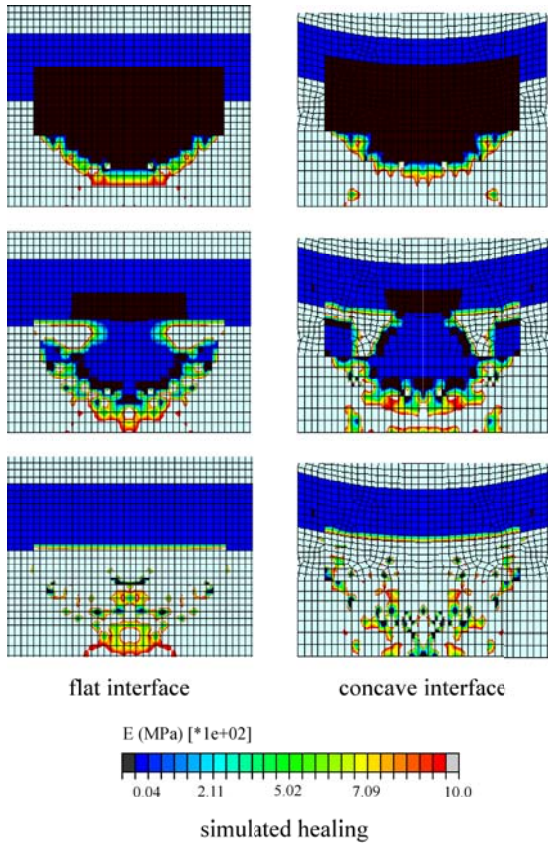

Fig. 3.13: Simulated healing process. Left: Healing process in a flat interface. Right: Healing process in a concave interface. The healing pattern appears to be independent of the local geometry. Time points compared approximately from top to bottom: 4, 6 and 12 weeks in the animal experiment.

However, the amount of the individual tissues formed was different between models during simulated healing (Fig. 3.14 – 3.17). After equilibrium was reached, only minor differences remained (< 10%).

Compared to the total number of iterations required to achieve equilibrium (150), a high percentage of the defect (90%) was filled relatively fast in the case of a flat and a convex interface and slightly slower in a concave interface. This level was reached approximately after the first 41 iterations in a flat interface, first 47 iterations in a convex interface and first 60 iterations in a concave interface. In the case of a flat interface the pre-cancellous bone becomes stiffer and was gradually differentiated to cancellous bone (approx. iterations 41-81). After equilibrium, approx. 25% of the newly formed cartilage showed a hyaline consistence (Fig. 3.14). Although the equilibrium was achieved, a remaining unfilled defect area prevailed (approx. 10%).

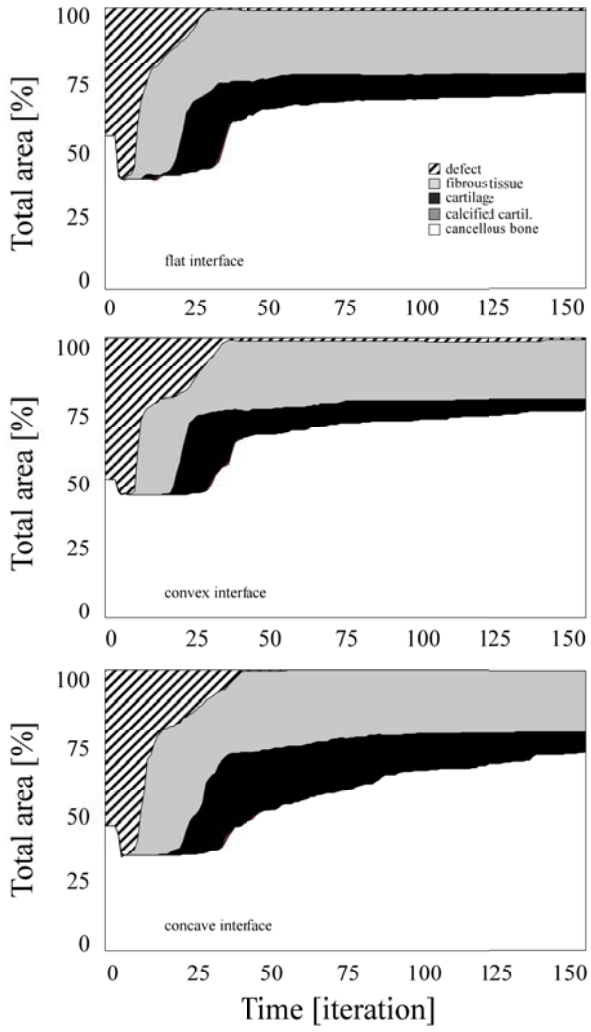

Fig. 3.14: Tissue quantification during healing. Top: flat interface. Center: convex interface. Bottom: concave interface. The mechanical conditions in a concave interface (bottom) appear to be more favorable for healing based on the larger quantity of differentiated hyaline cartilage.

More hyaline cartilage was formed in the concave model during simulated healing. The maximum percentage of hyaline cartilage during the simulations was smaller (27%) but occurred earlier (approx. iteration 26) in the convex than in the concave model (40%, approx. iteration 40). In the histomorphometric analysis a maximum of 33.1 ± 13.2% of hyaline cartilage was registered in the 12^{th} week (Duda, et al., 2005). After resorption, the newly formed cancellous bone at the defect base showed in general a 35% higher stiffness in the concave interface compared with the convex ones. However, these values were in both cases up to 20% smaller than the original bone stiffness. For both models an increase of 15% in the stiffness was observed in the remaining cartilage surrounding the defect compared to flat geometry.

In the case of a flat surface, approximately 25% of the total area (TA) at the defect basis (Fig. 3.14) was reabsorbed. In the case of a concave interface, this area was higher (approx. 18%) compared with the convex surface (approx. 5%). The reabsorbed bone area was restored more rapidly in the convex situation (approx. iteration 28) compared with the flat (approx. iteration 40) and the convex situation (approx. iteration 50).

As shown in the figure 3.14, the stiffness of each tissue type during simulated healing was determined. The tissues were identified and classified according to the values given in the table 2.2. However, in order to analyze the evolution of the newly formed tissues, which were localized in the initial defect area, these limits were redefined. For example, for the cancellous bone stiffness initially limited between 825.1 y 2300 MPa, two limits were then labeled inside this range: (825.1 – 1500) MPa and (1500.1 – 2300) MPa. Similarly, new limits were defined for the calcified cartilage: from (12.1 – 825) MPa these limits were extended to (12.1-25, 25.1-100, 100.1-500, 500.1-825) MPa. For hyaline cartilage the initial range (8.1 – 12) MPa was extended to (8.1-9, 9.1-10, 10.1-11, 11.1-12) MPa. Fibrous cartilage was subdivided from (3.1-8.0) MPa to (3.1-4, 4.1-5, 5.1-6, 6.1-7, 7.1-8) MPa. The initial limits of the defect tissue (0.2-3) MPa remained unchanged (Fig. 3.15, 3.16, 3.17). Since the stiffness of each tissue type during healing was written in an ASCII file it was not necessary to run the algorithm again to quantify the percentage of the elements corresponding to each redefined limit. In this form, a more precise quantification of the joint curvature effect on healing can be determined.

A relation between the bone quality reached and the stiffness of the newly differentiated cartilage tissue was established. Comparing the convex model with the concave one, it can be seen clearly that although the percentage of cancellous bone with stiffness between 1500.1 and 2300 MPa (superior quality) is slowly higher in the model with a convex curvature (Fig.3.15), the quantity and quality of the newly formed hyaline cartilage is higher in the concave model (Fig. 3.16). It is important to note that although the defect filling occurs roughly at the same “time” (iteration) for the concave and the convex model, the differentiation for the fibrous, hyaline and cancellous bone tissue occurs more slowly (requires more iterations) in the concave case (Fig. 3.15 vs. Fig. 3.16). That is, the slope of differentiation from one tissue type to another was slower in the concave case compared with the convex one.

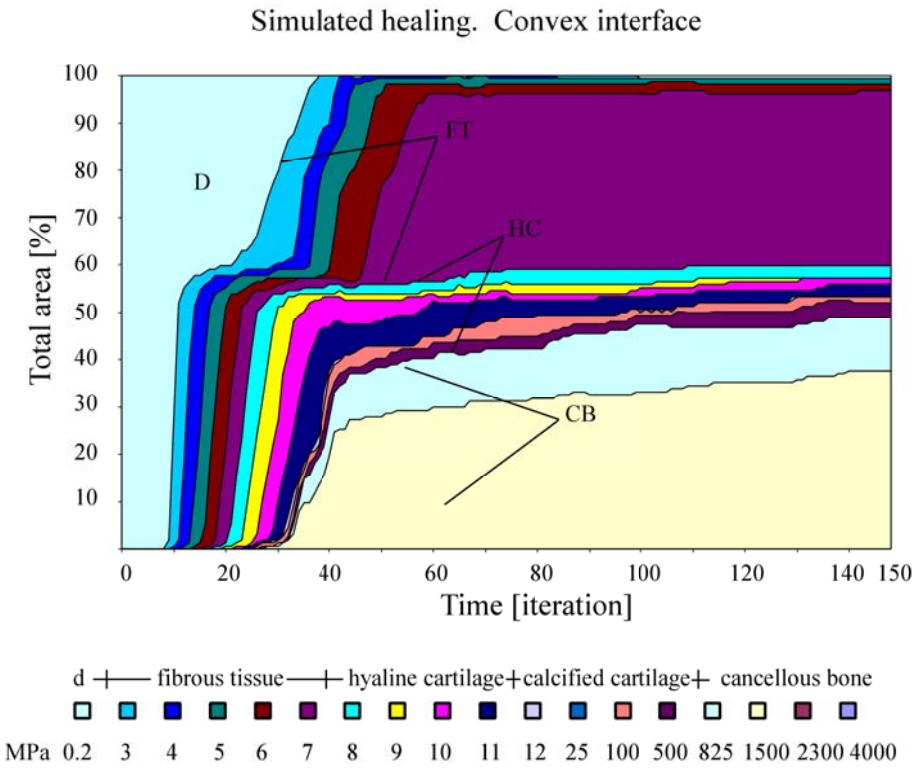

Fig. 3.15: Simulated healing for a convex interface. For each tissue type, the range of the maximal and minimal values of the stiffness was subdivided. The slope for tissue differentiation and the quantity of reached stiffnesses during healing are illustrated.

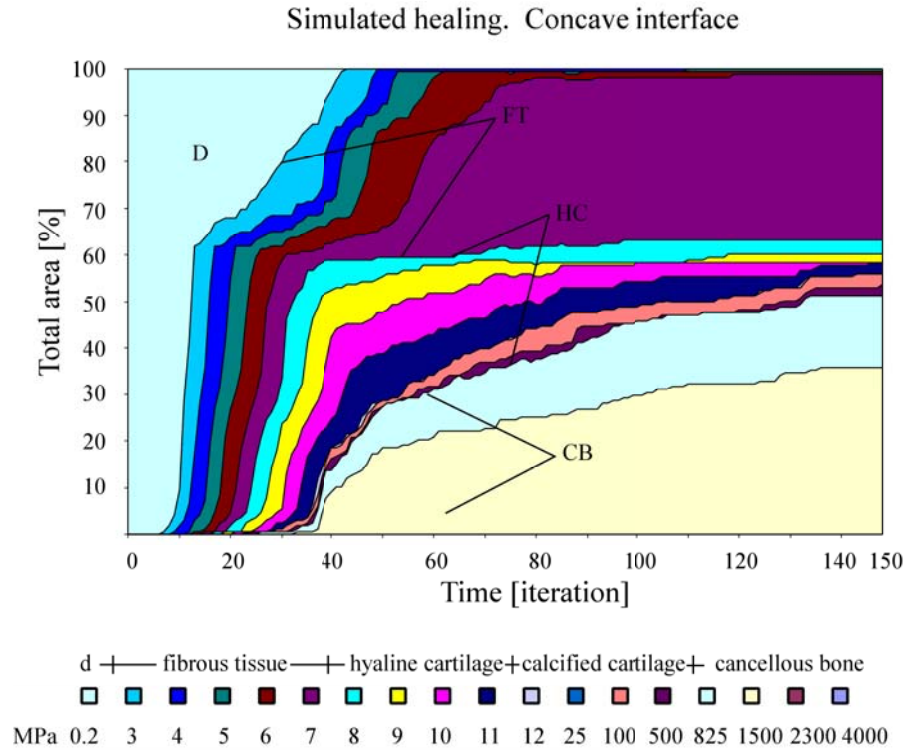

Fig. 3.16: Quantification of stiffnesses reached (tissue types) and slope of differentiation during simulated healing for a concave interface.

Analyzing healing in the flat model (Fig. 3.17) the quantity of the different newly formed tissues, as expected, was similar to the convex model. Defect filling occurs approximately at the same iteration and the slope of differentiation is comparable with the convex model, too.

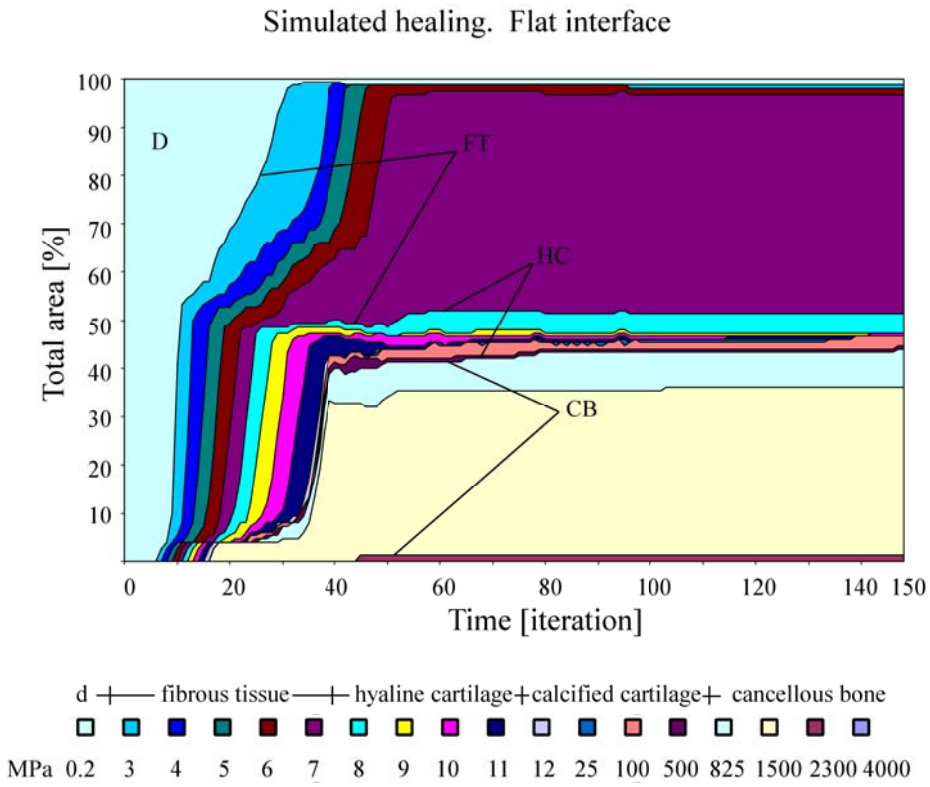

Fig. 3.17: Quantification of stiffnesses reached (tissue types) and slope of differentiation during simulated healing for a flat interface.

Variations in the joint curvature altered the quality of the remaining cancellous bone surrounding the defect. During the first iterations a reduction in the stiffness of the cancellous bone was observed in a region localized under the defect, which was extended from the defect basis to the distal horizontal border of the model (from 1750MPa to approx. 850MPa). This “zone of influence” was registered in all models (Fig. 3.11, Fig. 3.13). Inside this zone the cancellous bone proximal to the defect basis was differentiated to connective tissue forming the characteristic bone resorption observed *in vivo*. The flat interface showed the lowest percentage of affected elements (10%), followed by the convex interface with 19% and for the concave interface with 32%.

The zone of influence in the subchondral bone at the defect basis was differentiated to tissues of higher stiffness (from 850MPa to 1700MPa). After resorption the bone region was differentiated from connective tissue to other tissue types with higher elastic Young’s modulus until the original bone stiffness was achieved. However, a minor percentage of the rest of the cancellous bone inside this zone of influence surrounding the horizontal border, where the mechanical boundary condition were applied, showed a lower mechanical quality compared with the native cancellous bone stiffness. In a convex interface a maximal reduction of 52.8% in the mechanical properties of the cancellous bone was registered between the iterations 1 – 43

in 7% of the elements. After the iteration 43 the cancellous bone stiffness gradually increased to achieve the original stiffness. In a concave interface in 25% of the elements conforming this region a reduction of up to 69% was observed until the iteration 85. After the iteration 85 the stiffness of cancellous bone was restored to the original values. In a flat interface 12% of the elements diminished its mechanical stiffness of up to 65% during the first 28 iterations. After the iteration 28 the initial stiffness was gradually reestablished (Fig. 3.14).

During healing, active resorption zones, at the defect basis, were observed in the cancellous bone. These zones seemed to be more active than observed in the remaining cancellous bone. The cancellous bone stiffness was gradually reduced changing its tissue type to pre-cancellous bone, cartilage, fibrous tissue and finally to connective tissue. These resorption zones achieved a maximal percentage of 25.5% of the total area for a concave curvature (iteration 53), followed by the convex one with 10.6% (iteration 48). A maximum of 7% of the total area of the cancellous bone elements in the total area (TA) (iteration 46) were differentiated to connective tissue in the model with a flat curvature (Fig. 3.14). The patterns of these remaining defect regions in the cancellous bone were analyzed (Fig. 3.11, Fig. 3.13). Size and localization of these zones varied in dependence to the joint curvature. In total three zones, with different sizes and localizations, were observed. The region (Z1) is localized at the interface defect wall - remaining cartilage tissue. The second resorption region Z2 was localized in the center of the defect limiting at the axisymmetric axis of the model (Z2). The third region (Z3) was observed in a zone localized between the regions Z1 y Z2 (Fig. 3.18).

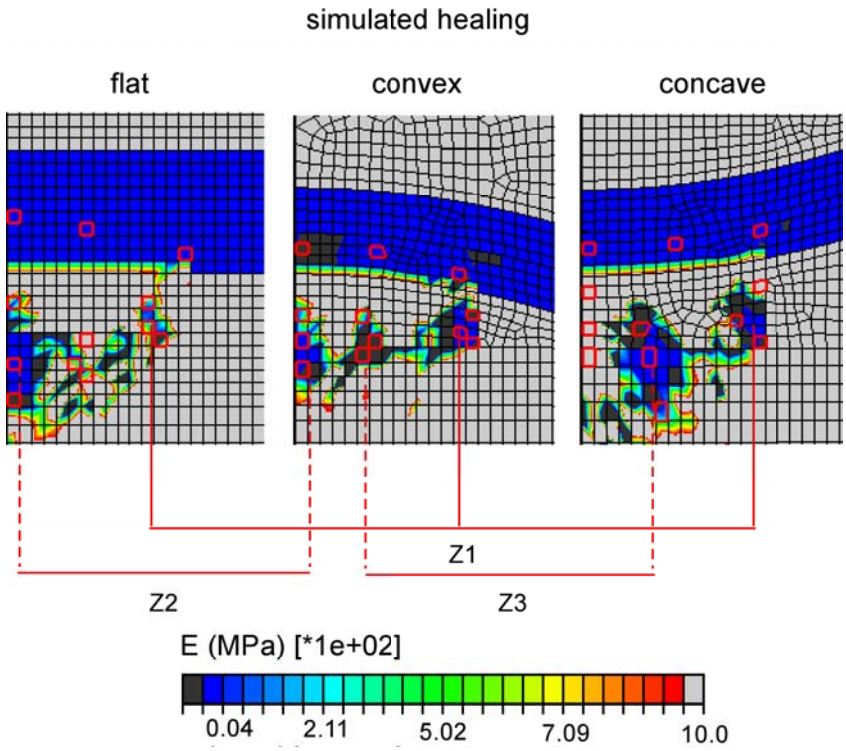

Fig. 3.18: Resorption regions observed in the cancellous bone (Z1, Z2, Z3) during simulated osteochondral healing. Specific elements at the same regions, remarked in red, were select to compare its differentiation pattern.

In the flat joint resorption regions, type Z1 and Z2 were formed. In the convex joint curvature all resorption types were observed: Z1, Z2 y Z3, while in the concave interface only resorption regions type Z1 and Z3 were registered. After a maximum of 46 iterations for a flat interface, 67 iterations for a convex interface and 115 iterations for a concave interface, these regions started to fill themselves with cancellous bone (Fig. 3.14). After equilibrium, a remaining area of 12% of unfilled cancellous bone for a flat interface, 4% for a convex interface and 0% for a concave interface was observed. Looking at the interface defect wall to cancellous bone (original) (Fig. 3.14) in a convex joint, 5% of the elements of the total defect area are still almost undifferentiated after the first 20 iterations. This zone was changed to fibrous tissue between the iterations 21 – 39. Finally, after iteration 39 it was differentiated to cancellous bone. In a concave surface, although generally the repair process appeared to be slightly slower than observed for the convex model, these events were comparable. So, at the same interface in the concave surface the connective tissue remained undifferentiated until iteration 29. It was differentiated to fibrous tissue at iteration 61 and to cancellous bone at iteration 120. At this interface (defect wall to cancellous bone) only minor changes were observed in a flat interface. The interface defect wall to host cartilage remained 37.5% partially unfilled in a convex surface (Fig. 3.11). In the concave geometry, 29.4% of the area remained unfilled during the first healing stages (iterations 16 - 25). After 26 iterations, the percentage of the unfilled elements was reduced by up to 2% and stayed constant during the rest of the healing process. At this interface minor variations were observed in a flat interface.

Fluid flow and pore pressure were studied as possible mechanical stimulus to simulate tissue differentiation (Fig. 3.19).

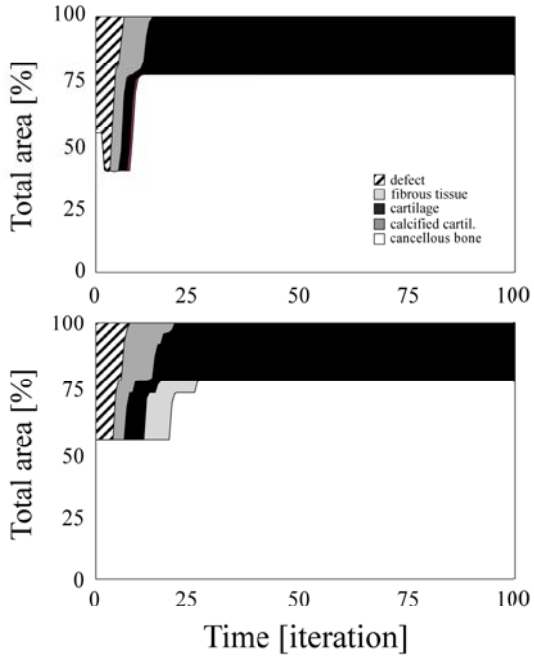

Fig. 3.19: Pore pressure (top) and fluid flow (bottom) as mechanical stimuli to simulate differentiation. Fluid flow was unable to reproduce the characteristic resorption region at the defect basis.

These fluid related mechanical parameters were unable to reproduce some characteristics of the healing process observed *in vivo*. In the simulation, pore pressure used as mechanical stimulus for differentiation appears to fill the defect very fast without formation of fibrous tissue. Fluid flow, used as mechanical stimulus, fills the defect without resorption of the cancellous bone at the defect basis, which was a typical feature of the *in vivo* healing process.

3.3.3 Influence of the defect fillings stiffness

Comparing the quality of the formed tissues during healing, when the defect was filled with a biomaterial, the use of a plug with the same stiffness as defined for the cancellous bone (P1) allowed calcified and hyaline cartilage formation (Fig. 3.20). A reduction of 50% of the material stiffness (P2) produced a decrease in the mechanical quality of the newly differentiated cartilage (Fig. 3.21). The remaining cartilage showed a diminution of approximately 35% of its original mechanical stiffness independent of the plug used.

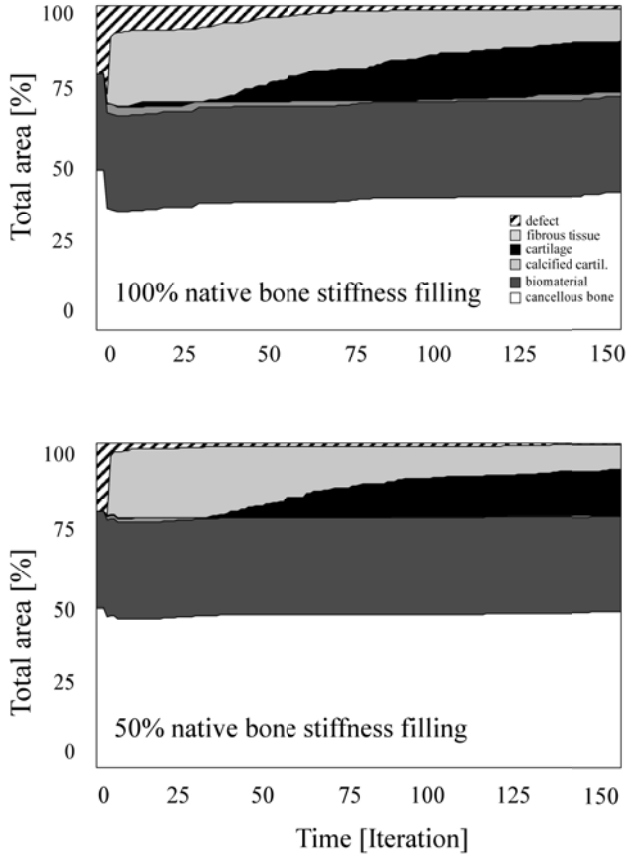

Fig. 3.20: Tissue quantification during healing using defect fillings. Top: Graft with the same stiffness as the cancellous bone (P1). Bottom: Graft with a stiffness of 50% of the cancellous bone (P2). Although a higher percentage of resorption is observed in P1, it shows a higher percentage of hyaline cartilage compared with P2. Additionally it shows calcified cartilage formation.

In the defect region, a calcified cartilage layer was newly formed and maintained during healing only when a biomaterial with the same native bone stiffness was used (Fig. 3.20). When the stiffness was reduced by 50%, a minor percentage of calcified cartilage was formed compared

with P1 (Iterations 1 – 38). A total degradation of the calcified cartilage was observed in this case, which disappeared approximately after iteration 38. Although the formed tissues varied in quantity, the strain pattern was comparable for both models. The first iterations of the healing process for P2 appeared to be lightly unstable. During the first 7 iterations (from 150 necessaries to achieve equilibrium) the material properties of the connective tissue (defect) showed oscillatory variations around of the maximal and minimal values of this tissue type, avoiding differentiation to fibrous tissue. After the 7th iteration this effect disappeared and stable growth was detected again. This effect was principally observed at the lateral surfaces of the biomaterial plug P2.

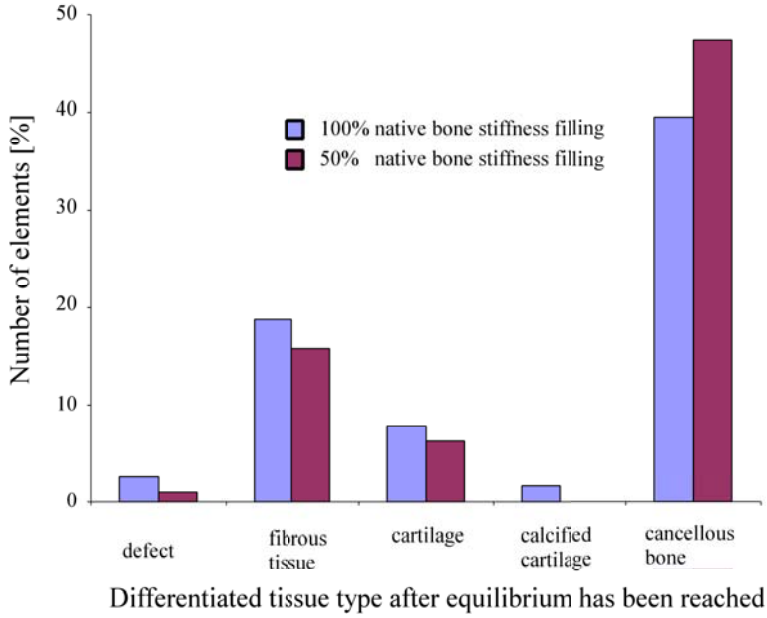

Fig. 3.21: Differentiated tissues after healing (equilibrium) using a cylindrical graft with two different stiffnesses: 100% and 50% of the cancellous bone stiffness are compared. The usage of defect fillings with the same stiffness than the cancellous bone forms tissues with a better mechanical quality during healing. However, a slight resorption at the cancellous bone is observed, as well as calcified cartilage differentiation.

For both models, the first cartilage “islands” were observed not only at the lateral wall defect, as observed in the osteochondral defects, but also at the center of the biomaterial plug. In P1, the defect was approximately 80% filled after 35 iterations. This filling consisted of approximately 95% fibrous tissue. Further into the healing process, up to 20% of the fibrous tissue was differentiated into hyaline cartilage after 75 iterations. At the equilibrium state, the defect was up to 95% filled, 30% of which was fibrous tissue and 70% hyaline cartilage. In P2, the defect was approximately 90% filled consisting only of fibrous tissue after 35 iterations. Halfway through the healing process (iteration 75), up to 15% of the fibrous tissue was differentiated into hyaline cartilage. However, at the equilibrium point, 45% of the newly formed tissue consisted of hyaline cartilage. A comparison of P1 and P2 after equilibrium (at approx. iteration 150) showed that 12% more cancellous bone had formed in P2.

4 Discussion

4.1 Discussion of the method

4.1.1 Bone-joint mechanics (humerus project)

Strain distribution of intact and fractured human humeri was evaluated after simulation of three common physiological load situations for two different bone qualities. The muscle attachments were considered as simple points (nodes) where the corresponding loads (vectors) acted. The advantage of this simplified load representation is a fast evaluation of the muscle direction while its effect on the bone-joint strain behavior can still be retrieved. Its principal disadvantage is, however, to induce elevated punctual deformations in the nodes where the muscles were attached, including a small area of influence delimited for the position of the Gauss points[8] used in the finite element analysis to evaluate the strain field. However, this study has demonstrated that the influence of the bone quality is more important for the straining than the theoretical effect of overestimation produced by the muscle attachments. This may be concluded because in the physiological situations analyzed, regions of higher deformations were observed at the bone surface in zones without muscles directly attached compared to regions with muscle attachments. This finding implies that the susceptibility of a region to suffer fractures correlates more closely with the local bone quality than with muscle attachments on it, and it could explain why fracture patterns are hardly predictable based only on a study of their local physiological load condition. As a result, this could clarify why in elder patients, whose bone quality is frequently affected by osteoporosis, spontaneous fractures could occur without the incidence of a predetermined or critical physiological situation.

However, a more realistic model should consider muscle attachments as surfaces of loads and the internal reconstruction of the trabecular bone network. Maybe the pattern of the straining, in the zones of influences where the muscles are attached, could be affected due to the possibility that such a zone could have a poor bone quality at the cortical but could be connected via trabecular network with a zone of a better mechanical quality. In this case its strain pattern could be better in comparison with the hypothetical situation, in which this cortical region has an acceptable mechanical quality but lacks a continuous trabecular network (osteoporosis). Considering a surface of load to simulate muscle attachments with a three-dimensional trabecular network reconstruction can show how large this effect will be. Thus, as was demonstrated in this study, the mechanical configuration (strain pattern) for particular patients under the same physiological conditions was primarily affected by bone quality.

In the model only proximal muscles were considered. This fact produced, as observed in Fig. 3.1, a remaining component of moment in each one of the three principal load directions in the distal region. However, the humeral bone should be in equilibrium and the sum of loads and

[8] Gauss points: points of interpolation inside of a finite element in which the equilibrium equation are applied.

moments in the center of rotations of bone should be zero (center of the bone head, and condyles). Since the CT scans of the bone were performed in the proximal region, information about the distal region was not available. Therefore the bone was extended and the points of rotation were translated to two points localized approximately at the same length as the condyle, but near the centerline of the bone shaft as encountered in reality. Thus, to achieve the moment of equilibrium an increase of the force was necessary. Equilibrium was then reestablished by imposing a pair of forces producing moments with the same magnitude and inverse directions as the remaining moments. This method generated a local distortion of the area containing the points of load application. However, this effect disappeared approximately in the first third of the distal humerus. So, this effect does not have any influence on the results of the straining obtained in the proximal region. The results and conclusions determined in this study are thus valid and sufficient to learn more about the bone – joint mechanics evaluated in intact and fractured humeri bones.

4.1.2 Osteochondral healing (Galileo project)

4.1.2.1 On the selection of Young's elastic modulus to simulate differentiation

Differentiation was simulated by variation of the elastic modulus of Young. It is known that a relation between this mechanical parameter and the healthy state of the cartilage exists. Osteoarthrosis (OA), a common disease that affects the cartilage, could for example cause a diminution of the tensile properties of this tissue as shown in Table 4.1.

	Normal (MPa)	Fibrilled (MPa)	OA (MPa)
superficial	7.8	7.2	1.4
medial	4.9	7.5	0.85
depth	4.0	4.9	2.11

Table 4.1: Tensile properties of the human femoral condyle cartilage. The elastic modulus of Young is affected due to pathological conditions of the cartilage (Mow and Ratcliffe, 1997).

These variations have been associated with a disruption in the collagen fibrils in the solid matrix (Mow and Ratcliffe, 1997). Therefore, the selection of the elastic modulus of Young to represent the state of repair in osteochondral defects appears to be appropriate. Additionally, in an indirect manner it demonstrates the internal state of the collagen matrix by transmitting the mechanical signals after load application.

Moreover, most of the published tissue differentiation models used change Young's elastic modulus as the parameter to represent growth or resorption during healing. This feature allows a comparison between the reported findings of these studies and the those encountered in this project.

In this project ABAQUS was used to simulate healing using the finite element method. The

elastic modulus of Young was defined as a field variable. This implies that the mechanical stimulus for differentiation of each tissue is newly calculated when all tissue stiffnesses making up the joint region have been actualized after an iteration. However, *in vivo* studies do not determine the time of occurrence or the manner in which differentiation for each tissue type sets in. Moreover, to analyze how these changes take place requires considering a microenvironment that affects cells. Such environmental conditions at this microlevel are not yet precisely known. To assume continuous fields representing the joint and changing their mechanical properties at each tissue type was sufficient to demonstrate the hypotheses formulated in this project. *In vivo* experiments of osteochondral healing demonstrated that different tissues appear to have different rates to achieve each healing phase. The healing velocity depends on the type and number of cells in each tissue and their connectivity to cells of other tissues. In the created tissue differentiation model, the implementation of factors for growth and resorption calculated from numerical analysis of histological sections reproduce this fact.

More recently, interdisciplinary research of osteochondral healing is aimed to clarify how this cell communication pathway is initiated, maintained and when required, disabled. Simultaneously over the last years, the attention given to mechanical conditions influencing these cell communication-response pathways to stimulate healing has increased. In this project the tissues making up the joint were modeled as a continuum and its mechanical behavior was assumed to follow the rule of mixtures (a rule to explain the mechanical behavior of materials constituted by a fluid and a solid phase). This approach has been traditionally used in soil mechanics and more recently has been employed to describe and simulate the mechanical behavior of biphasic tissues.

4.1.2.2 On the selection of biphasic soil behavior to represent cartilage mechanics.

To simulate differentiation, the biphasic mixture model of Mow and co-workers (Huang, et al., 2001; Huang, et al., 2003; Mow, et al., 1989) was used in this project. This model supposes cartilage to be a biphasic incompressible material composed of a solid and a fluid phase. This treatment is consistent with the cartilage composition (approx. 80% water, and 20% collagen matrix). Recent models have been published representing cartilage even as a triphasic material in which not only mechanical but also electrochemical events are taken into account. However, sufficient information that allows the usage of the corresponding electrical properties of the cartilage for simulation of healing still does not exist.

In the Mow theory, when a continuum is exposed to compressive loads, the fluids inside (e.g. 80% of cartilage consist of water) are exudated, thereby producing high hydrostatic pressures. This hydrostatic pressure is a mechanical response that counteracts the external acting load to avoid possible damage of the solid phase by overloading. This behavior has been observed in the cartilage, too. The fluid phase appears to be an important factor regulating the mechanical chondrocyte response under compressive loads. The biphasic behavior of cartilage could be analyzed using concepts from soil mechanics. Parameters defining biphasic cartilage

properties have been well documented and measured in *in vitro* experiments. Thus, more realistic material properties for cartilage (biphasic) and the employment of a widely used theory (soil mechanics) to explain cartilage behavior were used in the present project.

Osmotic pressure is not taken into account in this theory. Basic concepts concerning the interaction of the ion charges between the collagen matrix and chondrocyte membrane has only recently been understood. Some cellular influx and efflux pathways have been identified. However, it is still unknown how mechanical signals in these pathways are transduced into biological responses. Experimental models and *in vitro* measurements of cell cultured chondrocyte stimulated with different patterns of mechanical loads (Lee, et al., 2002; Smith, et al., 2004; Suh, et al., 1995) (e.g. intermittent hydrostatic pressure, shear stresses) showed different responses in dependence of the type of load used. Intermittent hydrostatic pressure appears to increase matrix protein whereas shear stresses induce molecular changes related to apoptosis (Smith, et al., 2004). Mow and his group have proposed a triphasic theory or rule of mixtures to explain cartilage behavior. The absence of standard parameters (e.g. electrical response or its interaction with mechanical signals) describing triphasic composition of cartilage implies a difficulty in the incorporation of this mechanical behavior into a continuous joint model. Therefore, its usage in a differentiation model with predictive capabilities is obviously still not feasible.

Biphasic material properties on the other hand already reproduce the healing process observed in histology. Perhaps the use of a triphasic theory could be first tested experimentally and then incorporated into a computational approach in the future. Models evaluating the microenvironment of a chondrocyte or a determined tissue type as a triphasic material could be developed and compared with a biphasic one.

4.1.2.3 Convergence during healing simulation

In order to guarantee convergence during simulated healing, an equation to calculate the minimal time limit allowed in an increment has been employed. This equation is recommended in the user manual of ABAQUS for models with highly non-linear mechanical behavior. The appropriate selection of this minimal time turned out to be important, because it avoids formation of singular points in the solution and thereby avoids the implementation of additional smoothing algorithms during healing simulation. Up to now, reported tissue differentiation models to simulate fracture healing (Lacroix and Prendergast, 2002) and osteochondral healing (Kelly and Prendergast, 2004) used such smoothing algorithms in order to avoid drastic changes in the evolution of the tissue stiffness. Although the effect of this simplification on the healing pattern has not been clarified. Such a “tissue average” behavior does not exist *in vivo*.

4.1.2.4 On the selection of mechanical conditions to evaluate repair

In clinical practice, the influence of mechanical conditions on healing has until recently not been considered to be important, although some research groups have studied this topic alone in particular (Li, et al., 2001; Quinn, et al., 1998; Waldman, et al., 2003; Wang, et al., 2002; Wong and Carter, 2003), established a link between biomechanical and biochemical loads (Lai, et al., 1998) or determined a relation between biomechanical loads and gene activity (Valhmu, et al., 1998).

The influence of mechanical conditions during healing of osteochondral defects by animal models was corroborated; and at a more profound level, the microenvironment of chondrocytes cultures stimulated under controlled mechanical loads (bioreactors) was analyzed (Chen CT, et al., 2003; Martin, et al., 1999). *In vitro* studies have shown that cyclic compressive loading on chondrocytes appears to increase hydrostatic pressure, matrix deformation and fluid flow. These changes in the extracellular environment stimulate aggrecans and protein synthesis. In the present project, simulated compressive loads were applied and the corresponding tissue deformations, which are mechanically related to the strain fields, determined. The mechanical conditions imposed at the initial defect situation were maintained during repair. Gait analysis in the animal model demonstrated that the load transmission after and before defect creation was almost the same with a slight reduction during the first 6 days after surgery. Therefore no variations in the initial load were performed during healing simulation. Although the contact boundary condition during repair was not determined in the animal experimentation, it was supposed to be constant (frictionless) during simulated healing.

This study demonstrates the importance of mechanical conditions for understanding and evaluating healing, and hence justifies the usage of a differentiation model able to evaluate the influence of each parameter individually or simultaneously, which is impossible using *in vitro* experiments only.

4.1.2.5 On the selected cases to be analyzed

The cases were selected according to the following criteria: 1. To answer controversial questions, such as the maximum defect size able to start spontaneous healing or the consequence of increased thickness, 2. To understand why osteochondral defects occur more frequently on specific geometrical surfaces and 3. To include recent treatments for osteochondral defect healing, such as the usage of defect fillings. After the validation of the tissue differentiation model, these selected examples showed the versatility of the algorithm developed in this project.

4.1.2.6 On the quantification of the differentiated tissues during healing

The selection of a specific area, TA in fig 2.6, to quantify tissues during healing allows a comparison of the effect of the mechanical conditions on repair for the different analyzed cases.

Data from these areas complement the qualitative analyses (comparison of simulated healing to histology) giving more complete information about the healing state and its behavior after changes in the mechanical boundary conditions. The representation of the tissues is based on a continuous field in which the strain field was measured. This representation could even be extrapolated to show the active regions during healing without the requirement of a detailed geometrical representation of the subchondral bone or the different structural-related zones of the cartilage (superficial, middle and deep zone).

As shown in Figures 3.15 to 3.17, the algorithm is able to handle different ranges of stiffnesses for each tissue type. These stiffnesses can then be assigned to a specific tissue type more precisely. In this way, the effect of the cancellous bone quality on the quantity and quality of the newly differentiated cartilage can be determined. This ability to predict a widely heterogeneous distribution mitigates the possible effects on the simulated healing when an initial homogeneous characterization is used for the material properties of the model (instead of different stiffnesses as a function of cartilage depth).

4.1.2.7 On the algorithm

This study has demonstrated that the usage of an algorithm to analyze the influence of mechanical conditions on healing can be applied successfully to simulated clinical situations. The principal advantages of the algorithm are 1. It allows the determination of the straining of each tissue type necessary for healing with adequate mechanical properties, which cannot be determined *in vivo,* and 2. It is able to predict the type and localization of each tissue during healing. On the other hand, a disadvantage of the model is the lack of a more precise correspondence between the increment step and the real time in which healing occurs. Although by comparing the histomorphometric analysis and the quantification of the simulated healing, it was possible to establish a correspondence between simulated iterations and the real time in which healing occurred during animal experimentation (days, weeks), it is not certain that the same relation may still be valid after months or years.

Generally, algorithms to simulate healing could be tested by their application to an intact situation. In such a case it is expected that remodeling should not take place. However, because this model uses the intact situation as equilibrium state, the minimum principal strains used as a basis for comparison with the current strain values in the defect model or evaluated model are the same.

4.2 Discussion of the results

4.2.1 Bone-joint mechanics (humerus project)

For the selected bone specimens, the influence of bone quality and physiological loads on the magnitude and distribution of tissue strain was quantified. The strain magnitudes are influenced principally by bone quality and to a lesser degree by activity (0° neutral position, 90° abduction, 90° forward extension). The small average difference of only ± 6 % between the measured and

the calculated stiffnesses shows that numerical tools can be used to analyze the influence of bone quality of fractured and intact humeri under physiological loads. Maximum strain values were found for 90° abduction. The strain magnitudes for this arm position were considerably larger (25%) in the weak bone with low values of density distribution (average 0.26 gm/cm^2, DEXA) than in the reference humerus (average 0.49 gm/cm^2, DEXA).

Comparing the total group of humeri, the specimen with low-density values (DEXA= 0.26gm/cm2) showed a low axial stiffness and average torsional stiffness. In contrast, the specimen with a better density distribution showed an average axial stiffness and a high torsional stiffness. The range of measured straining could be considered to represent the maximum and minimum strain values possible for different bone qualities under physiological loads. However, the analysis of more specimens could still allow a better description of the spectrum of the straining.

Even though the analyzed implant (LCP-PH) was quite flexible compared to conventional osteosynthetic devices for the proximal humerus (T-plate, nails), cancellous tissue straining increased due to osteosynthetic treatment. The weak bone stock was found to be more strained than the healthy counterparts. In this respect implant design considerations should not only account for implant stabilization in healthy but also in weak bone stock. Normally this aspect has not been considered in the pre-clinical evaluation of osteosynthese. Also specific or individual models created from QCT data allow to choose osteosynthetic devices which could guarantee an adequate load transmission avoiding strain peaks in the surrounding tissues and lead to homogeneous straining of the remaining trabecular network, especially in osteoporotic patients. Bone models that assume homogeneous material property distributions are not able to show critical conditions or regions of strain concentration. To know the localization of such regions could become important in the study of bone mechanics and their interaction with a selected predesigned osteosynthese. As a result, the consideration of bone density distribution for modeling bones appears to be important.

The study of physiological loads in human bones improved our understanding of their mechanical behavior, taking specific characteristics such as geometry and bone quality into consideration (Maldonado, et al., 2003). In the majority of biomechanical studies so far, the analysis of the different physiological activities was performed without consideration of bone quality. Normally the bone is modeled as being homogeneous, isotropic and with a linear elastic behavior defined by a unique value of Young's modulus.

In the first part of this project, an analysis of different physiological loads using the finite element method in two humeral bones with inhomogeneous density distribution was performed. The results showed that the influence of the bone quality on the strain pattern was significant. Under the same mechanical conditions, a poor bone quality produces a higher strain concentration than a bone with a more favorable density distribution. After comprehension of the mechanical constrains which could influence bone behavior, the study of osteochondral defects at the joint was performed. Having demonstrated the influence of mechanical conditions

on bone behavior, it was necessary to establish the local effects of mechanical conditions on healing, for example those of joint geometry.

4.2.2 Osteochondral healing (Galileo project)

In order to estimate the local effects on healing (joint curvature, defect geometry), osteochondral defects resembling the local joint geometry observed in the experiments were analyzed. The fact that different amounts of hyaline and fibrous tissue were formed when changes in the defect size, local joint geometry or stiffness of the defect fillings were made is evidence of the influence of mechanical conditions on healing.

Although ground reaction forces of all animals were registered during healing, its complex musculoskeletal load situation remains unknown. However, chondrocyte activity is principally promoted by compressive loads and therefore the assumption of only axial forces loading the model was considered to be sufficient to simulate osteochondral healing. How chondrocytes may respond under compressive loads is summarized in a theory supporting the tissue differentiation model developed in this project.

4.2.2.1 Theory supporting the tissue differentiation model

Stem cells operate as mechanotransducers that are differentiated and develop under hydrostatic pressures and high deformations. Since the first phase of the healing process of an osteochondral defect is characterized by an high percentage of fluids, which allows higher deformations and which are rich in osteoprogenitor and stem cells, it is imaginable that cells could respond to the corresponding mechanical conditions: higher pressures (80% water under compressive loads) as a reaction mechanism and higher deformations as consequence of the action of external loads. Due to the dependence of the defect size, only a limited number of cells exists. These cells feel the dynamically acting external loads so they necessarily need an evolution into a tissue with better stiffness, which allows transmission of the external loads without collapse of the newly formed tissues. Thereby stem cells are transformed to connective tissue, which is able to fulfill these specific mechanical conditions: The fluids in the soft tissues react to hydrostatic pressure and simultaneously allow maximal deformations. In this case an unstructured and laxed connective tissue is differentiated first to a structured and stiffer tissue, whose task is to transmit the external loads more efficiently, and finally, as response to the high pressure, into a tissue rich in fibroblast. This evolution of mechanical reaction could explain why the first cartilage formation is observed at the bottom and at the defect walls: The fluids inside the newly formed tissues under compression are moving laterally in a similar way as in the case of confined compression, moreover the deformations are maximal at the defect vertex (geometry, drastic changes in the elastic Young's modulus). This combination of higher pressures and deformations stimulates differentiation from connective tissue to fibrous tissue. In this sense it is possible to identify characteristic values of hydrostatic pressures and deformations for each tissue type that allows differentiation of each tissue into the next stiffer one. In this manner, the elastic modulus of Young for each tissue will be increased or

decreased depending on the current state of hydrostatic pressures and deformations. Cartilage consists of 80% water, and therefore, both the influence of the hydrostatic pressure and the action of mechanical deformations are important factors to be considered while analysing osteochondral repair. The cartilage cells seem to react faster in the first phases of the healing process, and decrease their rate of differentiation when the basis of the defect is filled with a stiffer tissue.

4.2.2.2 Straining of histological sections

The numerical analysis of histological sections turned out to be a helpful tool to understand the biological response of the tissues under specific mechanical conditions. Additionally, the determination of factors for growth and resorption from *in vivo* data as well as the points of tissue-specific trilinear curves allowed a matching of simulated healing to the observed *in vivo* repair. The use of numerical analysis of histological sections represents an advance in the development of tissue differentiation models by reducing the necessity of initial assumptions (hypothetical factors for differentiation) or the use of additional procedures (smooth functions, stiffness averages, etc.).

A relation between the range of strains calculated during healing and the differentiated tissue type observed in histology was established. Hence, strain concentrations were registered at the interface cartilage-connective tissue and at the defect basis, in the same regions as those where the first newly differentiated tissues were observed *in vivo*.

Between the 4th week and the 6th week, a zone of high straining was observed at the resorption region in the defect basis. This could indicate the necessity to define another tissue type between connective tissue and the fibrous tissue. Between the 6th and the 12th week, another recognizable straining zone was detected between the newly formed cancellous bone tissue and the hyaline cartilage indicating that the definition of another transition - tissue type between these tissues, that is the pre-cancellous bone - was appropriate.

In the 12th week, the strain concentration at the interface between the newly formed cartilage and the remaining cartilage tended to disappear indicating the reestablishment of the continuity in the mechanical properties of the hyaline cartilage. The possible knowledge of the range of strains at each time step allowed the determination of a quantitative relation between the material properties and the mechanical behavior of each tissue type. The permanent strain concentration at the interface defect cartilage at the 4th and 12th week disappeared when, after centrifugal filling, the remaining connective tissue at the defect center was replaced by fibrous tissue. According to the simulation of bone marrow areas in the subchondral region, the strain distribution at the defect basis seems to be reduced in dependence on the size of the marrow areas. A reduction of 17% in the compressive strains at the defect basis was measured between the 6th and the 12th week.

4.2.2.3 Influence of mechanical conditions on osteochondral healing

4.2.2.3.1 On the influence of the defect size on osteochondral healing

The geometry of osteochondral defects appears to influence the pattern of cartilage repair. In no case was a total restoration of the defect observed. An increase in the defect depth leads to minor formation of hyaline cartilage than when the defect width was increased.

Some *in vivo* studies have already been performed in order to study the influence of defect size on healing (Brown, et al., 1991; Jackson, et al., 2001; Shahgaldi, 1998). While Brown and his group studied the influence of the defect width, Jackson und Shahgaldi have analyzed spontaneous repair in large defect models. These studies have established that certainly a maximal dimension (depth or width) exists in which after an initial defect filling with fibrous tissue, damage at the cartilage and hence, later even in the subchondral region is observed. In the case of large defects a direct proportional relation between depth and damage was established (large defects appear to produce more damage). Maybe this is related to the number of cells or BMU necessary to remodel and to repair injured tissues. Considering this possibility, the latest techniques for the treatment of large defect areas include the usage of biomaterials alone or in combination with cells to promote cartilage and subchondral bone restoration. Although the effect of the biological process on healing has not been taken into account in the differentiation model, it was possible to predict a low percentage of hyaline cartilage formation and a degradation of the surrounding subchondral bone for the initial model situation in agreement with *in vivo* observations. These results suggest that structural and mechanical conditions are important and could be responsible for the type of the tissues formed during healing. Mechanical conditions affecting healing should be evaluated for treatment of osteochondral defects.

The fact that no hyaline cartilage formation was observed when its thickness was increased, or that a minor percentage was formed after geometrical changes of the defect implies that the selection of a treatment should take into account the localization, size and shape of the defect and the joint region in which the defect is localized. Additionally, the lack of hyaline cartilage formation warned about the importance of an appropriate selection of the region in which the defect could be surgically created in animal experimentation. The usage of a region with a very thin cartilage thickness, for example, could produce a faulty healing outcome by fast transmission of the compressive loads to the subchondral bone, which could reduce the mechanical stimulus.

4.2.2.3.2 Influence of the local joint curvature and usage of defect fillings on healing

This study has demonstrated that changes in the local joint surface curvature alter the process of healing. The mechanical environment around the defect during healing causes strong variations in the mechanical signal, in accordance with changes in the joint curvature. Additionally it was shown that the simulated healing after defect filling using a biomaterial with the same mechanical stiffness as the native subchondral bone proved to be better than in the

case of a biomaterial with a reduced stiffness (50% of the native bone). The effect of the stiffness of a predesigned biomaterial to fill the defect could be used as a parameter to analyze the healing outcome after biomaterial implantation.

Minimum principal strains selected as stimulus together with the usage of a factor (growth and resorption) for differentiation managed to reproduce the healing pattern observed in histology. In fact, the model agreed qualitatively with the histology and was quantitatively comparable to the histomorphometrical analysis (Duda, et al., 2005).

During healing, material frontiers are continuously in movement, reducing gradually the required stimulus to achieve the equilibrium state. Therefore the apparent “rate of healing” was reduced approximately after iteration 41, when the defect was filled to a higher percentage (Fig. 3.14). This behavior was comparable to the *in vivo* situation, where a higher percentage of the defect was filled between the 4^{th} and the 6^{th} week and was completely filled between the 6^{th} and the 12^{th} week. Thus, apparently the rate of filling depends on the current healing state: it was higher during the first weeks and was reduced at the final stages of healing.

The quality of the cartilage and its stiffness vary according to its localization, as indicated by others (Krishnan, et al., 2003; Laasanen, et al., 2003; Mow and Ratcliffe, 1997; Nieminen, et al., 2004; Wu and Herzog, 2002). So, different joints in the same individual entity (human or animal) have shown local variations in structure (geometry and material properties) and thereby in mechanical behavior. However, until today the more frequent occurrences of osteochondral defects at convex joint surfaces have not been related to the local mechanical environment. Although few clinical reports discuss the low rate of occurrence of osteochondral defects on concave surfaces, it is generally associated with mechanical factors without further explanation (Exner, et al., 1991; Hjelle, et al., 2002; Ueblacker, et al., 2004). This study is the first to demonstrate that this may be related to the mechanical stimulus for healing. In fact, the quantity of hyaline cartilage formation during healing simulation was affected by changes in the joint surface curvature (Fig. 3.14, Fig. 3.15, Fig. 3.16, Fig. 3.17).

After redefinition (subdivision) of the original stiffness ranges for the newly formed tissues in the defect area, it was demonstrated that a relation between the quality of the newly formed cancellous bone and its slope of differentiation (increments required to jump to another tissue type) and the quantity of the differentiated hyaline cartilage exists. Apparently changes in the joint curvature produce alterations in the differentiated cancellous bone tissue and in the rate of differentiation for the soft tissues. Higher quantities of differentiated tissues with better quality were formed under slower rates of differentiation. Concave joint surfaces showed a slower rate of differentiation for the cancellous bone and a higher quantity of hyaline cartilage with stiffnesses near to the upper limit (better quality) than observed in the case of convex joint surface (Fig. 3.15 vs. 3.16). Since the mechanical boundary conditions in a model with a flat joint “curvature”, taking into account the localization of the initial defect, are more similar to the convex joint curvature, the healing response observed for a flat model was comparable with the convex model. However, the rate of differentiation for the fibrous cartilage tissue was slower in

the flat model. It is possible that a strong correlation between the mechanical conditions and the rate of differentiation for each tissue exists. If the mechanical conditions can be regulated during the healing process, the rate of differentiation could be regulated, too. Thereby the quantity and the quality of the newly formed hyaline cartilage, which is essential to avoid damage of the joint, could be improved. The mechanical response of different joint curvatures and therefore the quantity of the differentiated tissues appears to be remarkably different under the same loads. The algorithm allowed quantifying such differences (rate of differentiation, quantity of formed hyaline cartilage), establishing a link between the mechanical response of a specific joint curvature and the obtained simulated healing.

A continuity of material properties in the layers under an osteochondral defect, which operates as a basis for the newly formed cartilage, is important for the development of a tissue with adequate mechanical quality for load transmission. This process is indicated by the quantity of the hyaline cartilage formed during the defect healing (Fig. 3.20; Fig. 3.21). In fact, hyaline cartilage formation occurs earlier (approx. iteration 11), i.e., when plug and cancellous bone have the same stiffness as when a considerable difference in their elastic Young's modulus exists (Fig. 3.20). Although the resorption was less than 5% at the subchondral bone basis of the defect for both models, the fact that this value was slightly higher in a plug with the same mechanical quality than the cancellous bone could imply the necessity for further analysis. Perhaps the definition of border conditions between the plug and the cancellous bone could be improved, for example the press-fit force, applyed to implant the plug, could be defined in dependence on the stiffness of the defect filling used or the plug porosity could be modeled heteregoneus depending on its stiffness distribution. The consideration of this last parameter should affects the response of the interface at the defect basis. A relation between the resorption areas and healing outcome (hyaline cartilage formation) could be thereby established.

Some differentiation models have been developed to study osteochondral healing (Duda, et al., 2005; Kelly and Prendergast, 2004), fracture repair (Bailon-Plaza and van der Meulen, 2001; Claes and Heigele, 1999; Lacroix and Prendergast, 2002) or remodeling around implants (Kerner, et al., 1999; van Rietbergen, et al., 1993). In these studies the influence of biomechanical conditions in combination with biological growth factors affecting healing have been established, as shown by Bailon-Plaza and co-workers. The healing patterns reported in the literature (Jackson, et al., 2001) were similar to the one obtained in the animal model of Bail et al. (Bail, et al., 2003). The resorption region or subchondral bone remodeling at the defect basis was a typical characteristic observed during the first stages of osteochondral repair (Jackson, et al., 2001). A differentiation model for osteochondral healing simulation should thus be able to reproduce this feature as well. The tissue differentiation model presented in this thesis is the only one that reproduces this effect. The predicted resorption agrees very well with the corresponding experiments.

Some studies have analyzed the usage of scaffolds and the incorporation of growth factors to generate collagen type II during osteochondral repair, which is present in hyaline cartilage. Lee

J.W and co-workers (Lee, et al., 2004) found that TGF-ß1, BMP-2 and growth differentiation factor 5 (GDF–5) could “induce rapidly” type II collagen expression. Indrawattana (Indrawattana, et al., 2004) and Ma (Ma, et al., 2003) reported similar results using different growth factors applied alone or in combination. These studies have demonstrated the possibility of improving the quality of the repaired tissue. However, there is not enough information that can be incorporated in a tissue differentiation model to predict its effect on osteochondral repair. Using *in vitro* culture and by developing sophisticated bioreactors, the effect of mechanical conditions on chondrocytes has clearly been demonstrated: The type of load and form of application influences the viability of chondrocytes. Shear stresses, and overloading for example are responsible for apoptosis or cell degeneration whereas intermittent compressive loads appear to promote differentiation (Bueno, et al., 2004; D'Lima, et al., 2001; Smith, et al., 2004). However, a difficult point in this *in vitro* evaluation is the measurement of isolated effects for each load condition. It is very difficult not only to apply shear alone or bending alone without the incidence of an unexpected load component, but it is also possible that measurements in the media in which cells are stimulated to proliferate may induce an additional mechanical stimulus whose effect on differentiation can be determined only with difficulty.

The differentiation model developed in this project has so far not been used in the specific case of isolated cell groups. However, this point is discussed in order to show that maybe the study of mechanical conditions on healing through the usage of such models seems to be more promising for determining which mechanical environment has a considerable effect to improve healing.

In a pilot study fluid flow and pore pressure, used as mechanical stimulus for differentiation, were incapable of reproducing the qualitative and quantitative healing process observed *in vivo* lacking the characteristic resorption region at the defect base observed in histology. Only minimum principal strains were able to cause this effect of resorption. The mechanical stimuli of the fluid related parameters were obviously not sufficient to produce resorption, generating an imbalance between the resorption and the growth region defined in the trilinear curve. Hence, the consideration of only compressive loads acting at the joint might be insufficient to recreate the complex mechanical environment present in a joint. Additionally, the amount of growth stimulus was higher in comparison with the values obtained when minimum principal strains were used as stimuli producing an effect of apparent “accelerated” healing. In fact, defect filling was completed after only 25 iterations, which was very quick in comparison with 166 iterations required in the case of minimum principal strains. However, with improved boundary conditions for the fluids these parameters should principally reproduce resorption as well.

An aspect to be considered is the relation between strain and permeability during healing simulation. Permeability is a property that involves microstructural aspects of cellular activity as shown in recent investigations. Its effect on the mechanics of the joint tissues is measurable and well known. Changes in the cartilage’s permeability have a remarkable influence on its capacity to support compressive loads by generating hydrostatic pressures. Some researchers

concluded that for degenerative diseases, changes in the porosity of the cartilage tissue are associated with losses of the water content, which leads to a reduction in its permeability. The consideration of this parameter in the development of a tissue differentiation model turned out to be very important in analyzing how changes in the elastic properties occur, inducing changes in the strain fields. These changes can be considered as an indirect indicator of healing. In the present study a correspondence between the state of healing and the current permeability was established. However, for two reasons, it was not possible to find a more exact relation between the state of tissue permeability and its healthiness. First, the material properties during healing were not measured in the animal experimentation, and second, because permeability was defined in dependence of the current elastic modulus of Young at each iteration and not with the current strain at each material point. Some studies have focused on establishing a relationship between strains and permeability based on *in vitro* experiments allowing the development of a theory of this biological process. In initial results, an explicit mathematical relation of these factors was proposed. However, further *in vitro* studies would be necessary to implement the corresponding equations in a tissue differentiation model.

The resorption regions in the cancellous bone are strongly influenced by variations in the joint curvature. Based on the quantity of the newly formed cartilage, this study has shown that concave curvatures could provide a more favorable environment for healing compared to convex surfaces. The concave model showed minor areas of resorption forming during healing simulation. The fact that areas of cartilage and fibrous tissue observed in the cancellous bone during defect healing are higher in a convex curvature compared with the concave one might suggest that mechanical conditions are responsible for the creation and maintenance of these regions (Z1, Z2 and Z3: Fig 3.18). Perhaps a relationship exists between the mechanics of differentiation, the mechanical quality of the underlying subchondral bone and the quantity of hyaline cartilage that could be differentiated during spontaneous repair.

4.3 Comparison with other studies

Prendergast developed a differentiation model to simulate fracture healing. His group made an extension of the initial proposed model and applied it to analyze osteochondral healing treated with grafts. The related work was published some months after the first results of this thesis. Prendergast used his differentiation model to investigate the possible optimal mechanical properties of a material to be used as defect filling. The differentiation model proposed by the Prendergast group presents not only some weaknesses in the concept but also lacks relevant characteristics observed in histological analysis of animal models. Comparing the results obtained in this work to the model proposed by Kelly and Prendergast, a predetermined combination of fluid velocity and shear strains to predict the differentiated tissue during repair results not only in a strong dependence on the initially selected material properties but also, as was our own experience using fluid flow as mechanical stimulus, makes it impossible for the model to reproduce resorption at the defect basis. Additionally, the usage of two parameters (fluid velocity versus shear strains) as stimuli for tissue differentiation during healing makes it difficult to extrapolate such a linear relation between the fluid velocity and the shear strain to an

in vivo situation. The tissue differentiation model used in the present study has shown that the usage of only minimum principal strains as mechanical stimuli achieves an acceptable correlation with the histomorphometrical data and reproduces the histological findings in animal models of osteochondral repair. Additionally, our differentiation model allows a large spectrum of strains to be defined only by the initial configuration. A redefinition of the limiting values for strains associated with specific tissue types during the run of the model is thus not necessary.

Huiskes's model has been widely used to study bone behavior. Its description of growth and remodeling simulation during and after medical device implantation has shown results very close to the observed findings in medical practice. In this study it was demonstrated that cartilage differentiation certainly could be explained as well according to the same principles as those developed by Huiskes with only some modifications. An important point was the determination of factors for growth and resorption from numerical analysis of the histological sections which were used in combination with a mechanical stimulus as proposed by Huiskes's to simulate differentiation. The selection of compressive strains as mechanical stimulus indubitably demonstrated a strong influence in the course and rate of the healing outcome.

4.4 Clinical relevance

The models analyzed in this thesis should also help to explain why osteochondral defects are more frequently reported in joints with convex surfaces. In fact, it was found that the local mechanical environment affects the type of tissues after differentiation tissues. A validated tissue differentiation model is able to predict how the mechanical stiffness of a biomaterial influences the quality and quantity of the newly formed tissues during healing, allowing to choose the appropriate biomaterial with matching mechanical properties for joint functionality.

Patient specific models taking into account the different regions, thicknesses and radii of the cartilage for joint reconstruction, as well as the specific physiological loads could be helpful in developing a more profound link between the mechanical conditions and the complex biological process during osteochondral healing. Alternatively it could be possible to determine for a specific patient (given geometry, density bone distribution, and cartilage mechanical properties) the external load required to obtain the greatest percentage of hyaline cartilage formation. In this case, physiological load conditions must be simulated.

To date, some methods exist to determine the state of the repair process such as arthroscopic examinations to verify if the defect is filled or if the graft is integrated with the surroundings tissues. Latest techniques include biomarkers in joint fluids in combination with MRI to check joint damage, quantity of collagen type II, or to look for the presence of macromolecules such as a cartilage oligomeric protein, which is normally interpreted as pathological changes during healing (Poole, 2003), as indirect indicators of the healing state. However, in practice it should be desirable to develop technical procedures to measure the mechanical properties of engineered cartilage during healing in order to compare and improve the treatment of osteochondral defects.

5 Conclusion

As a first step preceding the development of the differentiation model, during the analysis of the bone-joint behavior, it was demonstrated that bone quality is an important aspect to be considered. There are two possibilities of exploring the influence of this parameter on healing exist. It is possible to analyze the effect produced after changes in the initial elastic modulus of Young of the subchondral bone region, either by modeling the subchondral bone as a continuous field and to compare the amount and quality of the predicted tissues, or by constructing a detailed subchondral bone architecture with bone density distribution of different knee specimens. Independently of the selected way, the influence of the bone quality could clearly be established.

The healing of osteochondral defects is strongly influenced by mechanical conditions. Although the tissue differentiation model developed in this project used a simplified geometrical representation of the knee to analyze 1. the effect of changes in the defect size, 2. the influence of the local joint curvature and 3. the effect of using biomaterials to fill the defect, the results obtained were sufficient to predict the type of the newly differentiated tissues formed during healing. In every case, alterations in the mechanical environment produced measurable changes in the healing outcome. The defect was always filled with a mixture of hyaline and fibrous cartilage and never solely with hyaline cartilage, which was confirmed by clinical studies.

The results suggest that the mechanical environment required for osteochondral healing changes when the joint curvature is varied. It seems that the concave model resulted in the formation of cartilage of a higher quality (i.e. more hyaline cartilage was formed and the mechanical stiffness was higher) than with the convex model, but the rate of differentiation of the cancellous bone was slower than with the convex model. Comparing the stiffnesses of the surrounding tissues, the concave model resulted in tissues of a higher quality than with the convex model. However, no large differences were observed between the simulated healing patterns of the defects on concave and convex surfaces.

The algorithm meant that it was possible to find a mechanical explanation for the less favorable clinical outcome of defects localized on convex surfaces in comparison to those on concave ones. However, further analyses (for example in the form of longer, well documented animal experimentation) are necessary before such an algorithm can be applied to clinical cases. The effects of stiffness on healing should be taken into account when designing a biomaterial for filling osteochondral defects. The appropriate stiffness of this biomaterial could be determined preoperatively depending on the quantity and quality of predicted healing.

The differentiation model developed in this project could play a role in evaluating clinical situations by comparing the predicted healing and the observed process after surgery; thus detailed documentation of the healing process over a long time can be obtained.

This technique could be developed even further for use in conjunction with patient-specific data to predict the outcome of osteochondral repair. Although osteochondral repair is a very complex biological process, it appears to be important to consider mechanical factors that affect healing and that the process can be predicted accurately.

6 Future works

The tissue differentiation model developed allows deeper insight into further subjects related to osteochondral healing. Various interesting applications of this technique may be analyzed in the future. Some possibilities for further research are briefly discussed below.

6.1 Future works related to the usage of the tissue differentiation model

1. The tissue differentiation model could be used to determine the load condition that permits the largest formation of hyaline cartilage. A sensitive analysis could then be performed in which the design variable is the load and the other parameters should remain unchanged.
2. In this project two different stiffness conditions of a defect filling were analyzed: A plug with 100% of the native subchondral bone stiffness and another with 50% of the native subchondral bone stiffness. The differentiation model could be used to determine an inhomogeneous stiffness of the defect filling so that different elastic modulus for the plug material properties could be suggested to construct such an implant.
3. The plug geometry could be analyzed to reduce stress concentrations. The use of a plug with rounded borders at the basis could be necessary. Consequently, before the implant can be used it may be recommendable to smooth the defect geometry to achieve the same plug geometry. The differentiation model could show the effect of an optimized assembly interface defect-plug on osteochondral healing.
4. Patient data could be used to construct the geometry and density distribution of the joint region in order to analyze the more favorable healing prediction from the tissue differentiation model after simulation of different treatments.

6.2 Future works related to the algorithm

Permeability is a material property related to the fluid mechanics behavior of a biphasic-modeled tissue. In the algorithm permeability is updated in dependence on the current material property. It is recommendable to change the permeability dependence so that this parameter may be updated in relation to the current strain values.

6.3 Future works related with the finite element model

1. In the finite element model, the defect size is very large compared with the joint size. Perhaps the influence of the boundary conditions on the remaining tissues is overestimated. Modeling a large joint region could produce a reduction of the “zone of influence” observed at the cancellous bone subjacent to the osteochondral defect. Although this reduction is actually only 15% of the initial subchondral bone stiffness and then incrementally reestablished to the original value, the zone of influence achieves the upper model frontier.

2. Since the analysis of joint curvature shows an influence of the stiffness of the remaining subchondral bone on the quantity and quality of the newly formed hyaline cartilage, it may be necessary to conduct a more detailed analysis of this region. The reconstruction of a system of the trabecular geometry of the subchondral bone region considering density distribution is recommended. The differentiation model should be able to show how this trabecular system is affected and how it influences the cartilage formation. Perhaps it could be demonstrated that a subchondral bone with poor bone quality decreases the percentage of hyaline cartilage formation.

7 References

1. Agneskirchner, J. D.; Hurschler, C.; Stukenborg-Colsman, C.; Imhoff, A. B. and Lobenhoffer, P. (2004): Effect of high tibial flexion osteotomy on cartilage pressure and joint kinematics: a biomechanical study in human cadaveric kneesWinner of the AGA-DonJoy Award 2004, Arch Orthop Trauma Surg 124 [9], pp. 575-84. Epub 2004 Aug 03.
2. Akens, M. K.; von Rechenberg, B.; Bittmann, P.; Nadler, D.; Zlinszky, K. and Auer, J. A. (2001): Long term in-vivo studies of a photo-oxidized bovine osteochondral transplant in sheep, BMC Musculoskelet Disord 2 [1], p. 9.
3. Aloia, J. F.; Vaswani, A.; Meunier, P. J.; Edouard, C. M.; Arlot, M. E.; Yeh, J. K. and Cohn, S. H. (1987): Coherence treatment of postmenopausal osteoporosis with growth hormone and calcitonin, Calcif Tissue Int 40 [5], pp. 253-9.
4. Ament, C. and Hofer, E. P. (2000): A fuzzy logic model of fracture healing, J Biomech 33 [8], pp. 961-8.
5. Appleyard, R. C.; Burkhardt, D.; Ghosh, P.; Read, R.; Cake, M.; Swain, M. V. and Murrell, G. A. C. (2003): Topographical analysis of the structural, biochemical and dynamic biomechanical properties of cartilage in an ovine model of osteoarthritis, Osteoarthritis and Cartilage 11 [1], pp. 65-77.
6. Appleyard, R. C.; Swain, M. V.; Khanna, S. and Murrell, G. A. (2001): The accuracy and reliability of a novel handheld dynamic indentation probe for analysing articular cartilage, Phys Med Biol 46 [2], pp. 541-50.
7. Aro, H.T. and Chao, E.Y.S. (1993): Bone-healing patterns affected by loading, fracture fragment stability, fracture type, and fracture site compression, Clinical Orthopaedics and Related Research 293, pp. 8-17.
8. Arokoski, J. P.; Jurvelin, J. S.; Vaatainen, U. and Helminen, H. J. (2000): Normal and pathological adaptations of articular cartilage to joint loading, Scand J Med Sci Sports 10 [4], pp. 186-198.
9. Bader, D. L.; Kempson, G. E.; Egan, J.; Gilbey, W. and Barrett, A. J. (1992): The effects of selective matrix degradation on the short-term compressive properties of adult human articular cartilage, Biochim Biophys Acta 1116 [2], pp. 147-154.
10. Bae, Won C.; Law, Amanda W.; Amiel, David and Sah, Robert L. (2004): Sensitivity of Indentation Testing to Step-Off Edges and Interface Integrity in Cartilage Repair, Annals of Biomedical Engineering 32 [3], pp. 360-369.
11. Bagge, M. (2000): A model of bone adaptation as an optimization process, J Biomech 33 [11], pp. 1349-57.
12. Bail, H.; Klein, P.; Kolbeck, S.; Krummrey, G.; Weiler, A.; Schmidmaier, G.; Haas, N. P. and Raschke, M. J. (2003): Systemic application of growth hormone enhances the early healing phase of osteochondral defects--a preliminary study in micropigs, Bone 32 [5], pp. 457-467.
13. Bailon-Plaza, A.; Lee, A. O.; Veson, E. C.; Farnum, C. E. and van der Meulen, M. C. (1999): BMP-5 deficiency alters chondrocytic activity in the mouse proximal tibial growth plate, Bone 24 [3], pp. 211-6.
14. Bailon-Plaza, A. and van der Meulen, M. C. (2001): A mathematical framework to study the effects of growth factor influences on fracture healing, J Theor Biol 212 [2], pp. 191-209.
15. Barry, F. P. (2003): Mesenchymal stem cell therapy in joint disease, Novartis Found Symp 249, pp. 86-96; discussion 96-102, 170-4, 239-41.
16. Barry, Frank P. and Murphy, J. Mary (2004): Mesenchymal stem cells: clinical applications and biological characterization, The International Journal of Biochemistry & Cell Biology 36 [4], pp. 568-584.
17. Beaupré, G. S.; Stevens, S. S. and Carter, D. R. (2000): Mechanobiology in the development, maintenance, and degeneration of articular cartilage, J Rehabil Res Dev 37 [2], pp. 145-51.

18. Benjamin, M. and Ralphs, J. R. (2004): Biology of Fibrocartilage Cells, International Review of Cytology Volume 233 pp. 1-45, Academic Press.
19. Bobic, V. (1999): Treatment of Full Thickness Injuries in Articular Cartilage, International Society of Arthroscopy, Knee Surgery and Orthopaedic Sports Medicine (ISAKOS).
20. Boschetti, F.; Pennati, G.; Gervaso, F.; Peretti, G. M. and Dubini, G. (2004): Biomechanical properties of human articular cartilage under compressive loads, Biorheology 41 [3-4], pp. 159-166.
21. Breinan, H. A.; Minas, T.; Hsu, H. P.; Nehrer, S.; Sledge, C. B. and Spector, M. (1997): Effect of cultured autologous chondrocytes on repair of chondral defects in a canine model, J Bone Joint Surg Am 79 [10], pp. 1439-51.
22. Brittberg, M. (1999): Autologous chondrocyte transplantation, Clin Orthop [367 Suppl], pp. S147-55.
23. Brittberg, M.; Lindahl, A.; Nilsson, A.; Ohlsson, C.; Isaksson, O. and Peterson, L. (1994): Treatment of deep cartilage defects in the knee with autologous chondrocyte transplantation [see comments], N Engl J Med 331 [14], pp. 889-95.
24. Brittberg, M.; Tallheden, T.; Sjogren-Jansson, B.; Lindahl, A. and Peterson, L. (2001): Autologous chondrocytes used for articular cartilage repair: an update, Clin Orthop [391 Suppl], pp. S337-48.
25. Brittberg, M. and Winalski, C. S. (2003): Evaluation of cartilage injuries and repair, J Bone Joint Surg Am 85-A [Suppl 2], pp. 58-69.
26. Broom, N. D. and Poole, C. A. (1982): A functional-morphological study of the tidemark region of articular cartilage maintained in a non-viable physiological condition, J Anat 135 [Pt 1], pp. 65-82.
27. Brown, T. D.; Pope, D. F.; Hale, J. E.; Buckwalter, J. A. and Brand, R. A. (1991): Effects of osteochondral defect size on cartilage contact stress, J Orthop Res 9 [4], pp. 559-67.
28. Buckwalter, J. A. (1983): Articular cartilage, Instr Course Lect 32, pp. 349-70.
29. Buckwalter, J. A. (1995): Osteoarthritis and articular cartilage use, disuse, and abuse: experimental studies, J Rheumatol 43 (Suppl), pp. 13-15.
30. Buckwalter, J. A. (1999): Evaluating methods of restoring cartilaginous articular surfaces, Clin Orthop [367 Suppl], pp. S224-38.
31. Buckwalter, J. A. (2002): Articular cartilage injuries, Clin Orthop [402], pp. 21-37.
32. Buckwalter, J. A. (2003): Integration of science into orthopaedic practice: implications for solving the problem of articular cartilage repair, J Bone Joint Surg Am 85-A [Suppl 2], pp. 1-7.
33. Buckwalter, J. A. and Brown, T. D. (2004): Joint injury, repair, and remodeling: roles in post-traumatic osteoarthritis, Clin Orthop [423], pp. 7-16.
34. Buckwalter, J. A. and Mankin, H. J. (1998): Articular cartilage repair and transplantation, Arthritis Rheum 41 [8], pp. 1331-1342.
35. Buckwalter, J. A. and Mankin, H. J. (1998): Articular cartilage. Part I: tissue design and chondrocyte-matrix interactions, Instr Course Lect 47, pp. 477-486.
36. Buckwalter, J. A. and Mankin, H. J. (1998): Articular cartilage. Part II: degeneration and osteoarthritis, repair, regeneration, and transplantation, Instr Course Lect 47, pp. 487-504.
37. Buckwalter, J. A. and Mankin, H. J. (1998): Articular cartilage: tissue design and chondrocyte-matrix interactions, Instr Course Lect 47, pp. 477-486.
38. Buckwalter, J. A.; Martin, J. A.; Olmstead, M.; Athanasiou, K. A.; Rosenwasser, M. P. and Mow, V. C. (2003): Osteochondral repair of primate knee femoral and patellar articular surfaces: implications for preventing post-traumatic osteoarthritis, Iowa Orthop J 23, pp. 66-74.
39. Buckwalter, J. A.; Mow, V. C. and Ratcliffe, A. (1994): Restoration of Injured or Degenerated Articular Cartilage, J Am Acad Orthop Surg 2 [4], pp. 192-201.
40. Buckwalter, J. A.; Saltzman, C.; Brown, T. and Schurman, D. J. (2004): The impact of osteoarthritis: implications for research, Clin Orthop [427 Suppl], pp. S6-S15.

41. Buckwalter, Joseph A. M. D. and Brown, Thomas D. P. H. D. (2004): Joint Injury, Repair, and Remodeling: Roles in Post-Traumatic Osteoarthritis. [Report], Clinical Orthopaedics & Related Research June 1 [423], pp. 7-16.
42. Bueno, E. M.; Bilgen, B.; Carrier, R. L. and Barabino, G. A. (2004): Increased rate of chondrocyte aggregation in a wavy-walled bioreactor, Biotechnol Bioeng 28, p. 28.
43. Burstein, D. and Gray, M. (2003): New MRI techniques for imaging cartilage, J Bone Joint Surg Am 85-A [Suppl 2], pp. 70-7.
44. Butler, D. L.; Shearn, J. T.; Juncosa, N.; Dressler, M. R.; Hunter, S. A.; Buckwalter, J. and Schurman, D. J. (2004): Functional tissue engineering parameters toward designing repair and replacement strategies, Clin Orthop [427 Suppl], pp. S190-9.
45. Cancedda, R.; Dozin, B.; Giannoni, P. and Quarto, R. (2003): Tissue engineering and cell therapy of cartilage and bone, Matrix Biol 22 [1], pp. 81-91.
46. Carter, D. R.; Beaupre, G. S.; Wong, M.; Smith, R. L.; Andriacchi, T. P.; Schurman, D. J. and Smith, R. L. (2004): The mechanobiology of articular cartilage development and degeneration, Clin Orthop [427 Suppl], pp. S69-77.
47. Carter, D. R. and Hayes, W. C. (1976): Bone compressive strength: the influence of density and strain rate, Science 194 [4270], pp. 1174-6.
48. Carter, D. R. and Wong, M. (2003): Modelling cartilage mechanobiology, Philos Trans R Soc Lond B Biol Sci 358 [1437], pp. 1461-71.
49. Case, N. D.; Duty, A. O.; Ratcliffe, A.; Muller, R. and Guldberg, R. E. (2003): Bone formation on tissue-engineered cartilage constructs in vivo: effects of chondrocyte viability and mechanical loading, Tissue Eng 9 [4], pp. 587-96.
50. Chen CT; Fishbein KW; Torzilli PA; Hilger A; Spencer RGS and WE, Horton (2003): Matrix fixed-charge density as determined by magnetic resonance microscopy of bioreactor-derived hyaline cartilage correlates with biochemical and biomechanical properties, Arthritis and Reumathism 48 [4], pp. 1047-1056.
51. CHEN, MIN-HUEY and BROOM, NEIL (1998): On the ultrastructure of softened cartilage: a possible model for structural transformation, J Anatomy 192 [3], pp. 329-341.
52. Chu, C. R.; Coutts, R. D.; Yoshioka, M.; Harwood, F. L.; Monosov, A. Z. and Amiel, D. (1995): Articular cartilage repair using allogeneic perichondrocyte-seeded biodegradable porous polylactic acid (PLA): a tissue-engineering study, J Biomed Mater Res 29 [9], pp. 1147-1154.
53. Chu, Y.; Elias, J. J.; Duda, G. N.; Frassica, F. J. and Chao, E. Y. (2000): Stress and micromotion in the taper lock joint of a modular segmental bone replacement prosthesis, J Biomech 33 [9], pp. 1175-1179.
54. Claes, L. E.; Heigele, C. A.; Neidlinger-Wilke, C.; Kaspar, D.; Seidl, W.; Margevicius, K. J. and Augat, P. (1998): Effects of mechanical factors on the fracture healing process, Clin Orthop 355 Suppl, pp. 132-147.
55. Claes, L.; Eckert-Hubner, K. and Augat, P. (2002): The effect of mechanical stability on local vascularization and tissue differentiation in callus healing, Journal of Orthopaedic Research 20 [5], pp. 1099-1105.
56. Claes, L.E. and Heigele, C.A. (1999): Magnitudes of local stress and strain along bony surfaces predict the course and type of fracture healing, Journal of Biomechanics 32 [3], pp. 255-266.
57. Cook, S. D.; Salkeld, S. L.; Popich-Patron, L. S.; Ryaby, J. P.; Jones, D. G. and Barrack, R. L. (2001): Improved cartilage repair after treatment with low-intensity pulsed ultrasound, Clin Orthop [391 Suppl], pp. S231-43.
58. Costa, C.; Brokaw, J. L.; Wang, Y. and Fodor, W. L. (2003): Delayed rejection of porcine cartilage is averted by transgenic expression of alpha1,2-fucosyltransferase, Faseb J 17 [1], pp. 109-11. Epub 2002 Nov 15.
59. Csönge, Lajos; Bravo, Daniel; Newman-Gage, Helen; Rigley, Theodore; Conrad, Ernest U.; Bakay, András; Strong, D. Michael and Pellet, Sándor (2002): Banking of osteochondral allografts, Part II. Preservation of Chondrocyte Viability During Long-Term Storage, Cell and Tissue Banking 3 [3], pp. 161-168.
60. D'Lima, D. D.; Hashimoto, S.; Chen, P. C.; Colwell, C. W., Jr. and Lotz, M. K. (2001):

Impact of mechanical trauma on matrix and cells, Clin Orthop [391 Suppl], pp. S90-9.

61. Duda, G.N.; Maldonado, Z.; Klein, P.; Heller, M.; Burns, J. and Bail, H. (2005): On the Influence of Mechanical Conditions in Osteochondral Defect Healing, Journal of Biomechanics 38 [4], pp. 843-851.
62. Ebisawa, K.; Hata, K.; Okada, K.; Kimata, K.; Ueda, M.; Torii, S. and Watanabe, H. (2004): Ultrasound enhances transforming growth factor beta-mediated chondrocyte differentiation of human mesenchymal stem cells, Tissue Eng 10 [5-6], pp. 921-9.
63. Eckstein, F.; Reiser, M.; Englmeier, K. H. and Putz, R. (2001): In vivo morphometry and functional analysis of human articular cartilage with quantitative magnetic resonance imaging--from image to data, from data to theory, Anat Embryol (Berl) 203 [3], pp. 147-73.
64. Evans, P. J.; Miniaci, A. and Hurtig, M. B. (2004): Manual punch versus power harvesting of osteochondral grafts, Arthroscopy 20 [3], pp. 306-310.
65. Exner, G. U.; Meyer, C. and Elsig, J. P. (1991): Osteochondrosis dissecans of concave joint surfaces: roof of shoulder joint, tibial plateau, distal tibia, Z Orthop Ihre Grenzgeb 129 [4], pp. 302-304.
66. Fortier, L. A.; Balkman, C. E.; Sandell, L. J.; Ratcliffe, A. and Nixon, A. J. (2001): Insulin-like growth factor-I gene expression patterns during spontaneous repair of acute articular cartilage injury, J Orthop Res 19 [4], pp. 720-8.
67. Franz, T.; Hasler, E. M.; Hagg, R.; Weiler, C.; Jakob, R. P. and Mainil-Varlet, P. (2001): In situ compressive stiffness, biochemical composition, and structural integrity of articular cartilage of the human knee joint, Osteoarthritis and Cartilage 9 [6], pp. 582-592.
68. Frederick H. Silver and Bradica, Gino (2002): Mechanobiology of cartilage: how do internal and external stresses affect mechanochemical transduction and elastic energy storage?, Biomechanics and Modeling in Mechanobiology 1 [3], pp. 219-238.
69. Frost, H. M. (1987): Bone "mass" and the "mechanostat": a proposal, Anat Rec 219 [1], pp. 1-9.
70. Frost, H. M. and Jee, W. S. (1994): Perspectives: a vital biomechanical model of the endochondral ossification mechanism, Anat Rec 240 [4], pp. 435-46.
71. Fuentes-Boquete, I.; Lopez-Armada, M. J.; Maneiro, E.; Fernandez-Sueiro, J. L.; Carames, B.; Galdo, F.; de Toro, F. J. and Blanco, F. J. (2004): Pig chondrocyte xenoimplants for human chondral defect repair: an in vitro model, Wound Repair Regen 12 [4], pp. 444-52.
72. Fung, Y.C. (1993): Biomechanics: Mechanical properties of living tissues, 2. ed., Springer, New York.
73. Ghadially, J. A. and Ghadially, F. N. (1975): Evidence of cartilage flow in deep defects in articular cartilage, Virchows Arch B Cell Pathol 18 [3], pp. 193-204.
74. Ghivizzani, S. C.; Oligino, T. J.; Robbins, P. D. and Evans, C. H. (2000): Cartilage injury and repair, Phys Med Rehabil Clin N Am 11 [2], pp. 289-307.
75. Giannini, S.; Vannini, F. and Buda, R. (2002): Osteoarticular grafts in the treatment of OCD of the talus: mosaicplasty versus autologous chondrocyte transplantation, Foot Ankle Clin 7 [3], pp. 621-633.
76. Goldsmith, A. A. J.; Hayes, A. and Clift, S. E. (1996): Application of finite elements to the stress analysis of articular cartilage, Medical Engineering & Physics 18 [2], pp. 89-98.
77. Gole, Madhura D.; Poulsen, Dan; Marzo, John M.; Ko, Seung-Hee and Ziv, Israel (2004): Chondrocyte viability in press-fit cryopreserved osteochondral allografts, Journal of Orthopaedic Research 22 [4], pp. 781-787.
78. Graichen, H.; von Eisenhart-Rothe, R.; Vogl, T.; Englmeier, K. H. and Eckstein, F. (2004): Quantitative assessment of cartilage status in osteoarthritis by quantitative magnetic resonance imaging: technical validation for use in analysis of cartilage volume and further morphologic parameters, Arthritis Rheum 50 [3], pp. 811-6.
79. Grande, D. A.; Mason, J.; Light, E. and Dines, D. (2003): Stem cells as platforms for delivery of genes to enhance cartilage repair, J Bone Joint Surg Am 85-A [Suppl 2], pp. 111-6.

80. Griffith, L. G. and Naughton, G. (2002): Tissue engineering--current challenges and expanding opportunities, Science 295 [5557], pp. 1009-14.
81. Guilak, F. (2000): The deformation behavior and viscoelastic properties of chondrocytes in articular cartilage, Biorheology 37 [1-2], pp. 27-44.
82. Guilak, F.; Butler, D. L. and Goldstein, S. A. (2001): Functional tissue engineering: the role of biomechanics in articular cartilage repair, Clin Orthop [391 Suppl], pp. S295-305.
83. Guilak, F. and Mow, V. C. (2000): The mechanical environment of the chondrocyte: a biphasic finite element model of cell-matrix interactions in articular cartilage, J Biomech 33 [12], pp. 1663-1673.
84. Guo, X. E. (2001): Mechanical Properties of Cortical and Cancellous Bone Tissue, Cowin, S. C., Bone Mechanics Handbook, 2nd Edition. ed., pp. 10-8 10-18, CRC Press LLC, Boca Raton, Florida.
85. Hall, MC. (1963): The structure of the upper end of the humerus with reference to osteoporotic changes in senescence leading to fractures, Canad Med Ass J 88, pp. 290-294.
86. Hangody, L.; Kish, G.; Karpati, Z.; Szerb, I. and Udvarhelyi, I. (1997): Arthroscopic autogenous osteochondral mosaicplasty for the treatment of femoral condylar articular defects. A preliminary report, Knee Surg Sports Traumatol Arthrosc 5 [4], pp. 262-7.
87. Hangody, L.; Kish, G.; Karpati, Z.; Udvarhelyi, I.; Szigeti, I. and Bely, M. (1998): Mosaicplasty for the treatment of articular cartilage defects: application in clinical practice, Orthopedics 21 [7], pp. 751-6.
88. Hangody, L.; Rathonyi, G. K.; Duska, Z.; Vasarhelyi, G.; Fules, P. and Modis, L. (2004): Autologous osteochondral mosaicplasty. Surgical technique, J Bone Joint Surg Am 86-A [Suppl 1], pp. 65-72.
89. Hangody, Laszlo and Fules, Peter (2003): Autologous Osteochondral Mosaicplasty for the Treatment of Full-Thickness Defects of Weight-Bearing Joints: Ten Years of Experimental and Clinical Experience, J Bone Joint Surg Am 85-A [Suppl 2], pp. 25-32.
90. Hattori, K.; Takakura, Y.; Morita, Y.; Takenaka, M.; Uematsu, K. and Ikeuchi, K. (2004): Can ultrasound predict histological findings in regenerated cartilage?, Rheumatology (Oxford) 43 [3], pp. 302-305. Epub 2003 Oct 29.
91. Heiner, Anneliese D. and Martin, James A. (2004): Cartilage responses to a novel triaxial mechanostimulatory culture system, Journal of Biomechanics 37 [5], pp. 689-695.
92. Hepp, P.; Lill, H.; Bail, H.; Korner, J.; Niederhagen, M.; Haas, N. P.; Josten, C. and Duda, G. N. (2003): Where should implants be anchored in the humeral head?, Clin Orthop [415], pp. 139-47.
93. Hibbit; Karlsson, J. and Sorensen, M. T. (2003): ABAQUS user's manual.
94. Hidaka, Chisa; Goodrich, Laurie R.; Chen, Chih-Tung; Warren, Russell F.; Crystal, Ronald G. and Nixon, Alan J. (2003): Acceleration of cartilage repair by genetically modified chondrocytes over expressing bone morphogenetic protein-7, Journal of Orthopaedic Research 21 [4], pp. 573-583.
95. Hinterwimmer, S.; von Eisenhart-Rothe, R.; Siebert, M.; Welsch, F.; Vogl, T. and Graichen, H. (2004): Patella kinematics and patello-femoral contact areas in patients with genu varum and mild osteoarthritis, Clin Biomech (Bristol, Avon) 19 [7], pp. 704-10.
96. Hiraki, Y.; Shukunami, C.; Iyama, K. and Mizuta, H. (2001): Differentiation of chondrogenic precursor cells during the regeneration of articular cartilage, Osteoarthritis Cartilage 9 [Suppl A], pp. S102-8.
97. Hjelle, K.; Solheim, E.; Strand, T.; Muri, R. and Brittberg, M. (2002): Articular cartilage defects in 1,000 knee arthroscopies, Arthroscopy 18 [7], pp. 730-734.
98. Hjertquist, S. O. and Lemperg, R. (1971): Histological, autoradiographic and microchemical studies of spontaneously healing osteochondral articular defects in adult rabbits, Calcif Tissue Res 8 [1], pp. 54-72.
99. Horký, D. (1993): The Submicroscopic Structure of Articular Cartilage in the Adult Pig, Acta Vet. Brno 62, pp. 9-18.

100. Huang, Chun-Yuh; Mow, Van C. and Ateshian, Gerard A. (2001): The Role of Flow-Independent Viscoelasticity in the Biphasic Tensile and Compressive Responses of Articular Cartilage, Journal of Biomechanical Engineering 123 [5], pp. 410-417.

101. Huang, Chun-Yuh; Soltz, Michael A.; Kopacz, Monika; Mow, Van C. and Ateshian, Gerard A. (2003): Experimental Verification of the Roles of Intrinsic Matrix Viscoelasticity and Tension-Compression Nonlinearity in the Biphasic Response of Cartilage, Journal of Biomechanical Engineering 125 [1], pp. 84-93.

102. Huiskes, R. (1990): The various stress patterns of press-fit, ingrown and cemented femoral stems, Clin.Orthop 261, pp. 27-38.

103. Huiskes, R. (1997): Total joint replacement: on innovation, ambition, courage, irony and morsellized bone, of course, Iowa Orthop J 17, pp. 130-133.

104. Huiskes, R. (1997): Validation of adaptive bone-remodeling simulation models, Stud Health Technol Inform 40, pp. 33-48.

105. Huiskes, R. (2000): If bone is the answer, then what is the question?, J Anat 197 [Pt 2], pp. 145-156.

106. Huiskes, R.; Ruimerman, R.; van Lenthe, G. H. and Janssen, J. D. (2000): Effects of mechanical forces on maintenance and adaptation of form in trabecular bone, Nature 405 [6787], pp. 704-706.

107. Huiskes, R.; Weinans, H.; Grootenboer, H.J.; Dalstra, M.; Fudala, B. and Sloof, T.J. (1987): Adaptive bone remodeling theory applied to prosthetic-design analysis, J.Biomech. 20, pp. 1135-1150.

108. Hunziker, E. B. (1999): Articular cartilage repair: are the intrinsic biological constraints undermining this process insuperable?, Osteoarthritis Cartilage 7 [1], pp. 15-28.

109. Hunziker, E. B. (2002): Articular cartilage repair: basic science and clinical progress. A review of the current status and prospects, Osteoarthritis and Cartilage 10 [6], pp. 432-463.

110. Hunziker, E. B.; Quinn, T. M. and Hauselmann, H. -J. (2002): Quantitative structural organization of normal adult human articular cartilage, Osteoarthritis and Cartilage 10 [7], pp. 564-572.

111. Hunziker, E. B.; Wagner, J. and Studer, D. (1996): Vitrified articular cartilage reveals novel ultra-structural features respecting extracellular matrix architecture, Histochem Cell Biol 106 [4], pp. 375-82.

112. Ikenoue, T.; Trindade, M. C.; Lee, M. S.; Lin, E. Y.; Schurman, D. J.; Goodman, S. B. and Smith, R. L. (2003): Mechanoregulation of human articular chondrocyte aggrecan and type II collagen expression by intermittent hydrostatic pressure in vitro, J Orthop Res 21 [1], pp. 110-6.

113. Indrawattana, N.; Chen, G.; Tadokoro, M.; Shann, L. H.; Ohgushi, H.; Tateishi, T.; Tanaka, J. and Bunyaratvej, A. (2004): Growth factor combination for chondrogenic induction from human mesenchymal stem cell, Biochem Biophys Res Commun 320 [3], pp. 914-9.

114. Jackson, D. W.; Lalor, P. A.; Aberman, H. M. and Simon, T. M. (2001): Spontaneous repair of full-thickness defects of articular cartilage in a goat model. A preliminary study, J Bone Joint Surg Am 83-A [1], pp. 53-64.

115. Jackson, D. W.; Simon, T. M. and Aberman, H. M. (2001): Symptomatic articular cartilage degeneration: the impact in the new millennium, Clin Orthop [391 Suppl], pp. S14-25.

116. Johnson, L. L. (2001): Arthroscopic abrasion arthroplasty: a review, Clin Orthop [391 Suppl], pp. S306-17.

117. Johnstone, B. and Yoo, J. U. (1999): Autologous mesenchymal progenitor cells in articular cartilage repair, Clin Orthop [367 Suppl], pp. S156-62.

118. Jones, Wendy R.; Ping Ting-Beall, H.; Lee, Greta M.; Kelley, Scott S.; Hochmuth, Robert M. and Guilak, Farshid (1999): Alterations in the Young□s modulus and volumetric properties of chondrocytes isolated from normal and osteoarthritic human cartilage, Journal of Biomechanics 32 [2], pp. 119-127.

119. Kääb, M. J.; Ito, K.; Clark, J. M. and Nötzli, H. P. (1998): Deformation of articular

cartilage collagen structure under static and cyclic loading, J Orthop Res 16 [6], pp. 743-751.

120. Kaar, T. K.; Fraher, J. P. and Brady, M. P. (1998): A quantitative study of articular repair in the guinea pig, Clin Orthop [346], pp. 228-43.

121. Kelly, D. J. and Prendergast, P. (2004): Using a Mechano-Regulation Model for Tissue Differentiation to Design an Optimized Scaffold for Osteochondral Defect Repair, ESB2004, Bosch.

122. Keogh, C. F.; Wong, A. D.; Wells, N. J.; Barbarie, J. E. and Cooperberg, P. L. (2004): High-resolution sonography of the triangular fibrocartilage: initial experience and correlation with MRI and arthroscopic findings, AJR Am J Roentgenol 182 [2], pp. 333-6.

123. Kerner, J.; Huiskes, R.; van Lenthe, G. H.; Weinans, H.; van Rietbergen, B.; Engh, C. A. and Amis, A. A. (1999): Correlation between pre-operative periprosthetic bone density and post-operative bone loss in THA can be explained by strain-adaptive remodelling, Journal of Biomechanics 32 [7], pp. 695-703.

124. Klein, P. (2001): Histologische, immunhistologische und histomorphometrische Untersuchungen der Wirkung von Systemisch appliziertem speziesspezifischen Wachstumshormon auf einen osteochondralen Knorpeldefekt am Yucatan-Minischwein, Unfall und Wiederherstellungschirurgie Charité - Campus Virchow Klinikum, Freien Universität, Berlin.

125. Koay, Eugene J.; Shieh, Adrian C. and Athanasiou, Kyriacos A. (2003): Creep Indentation of Single Cells, Journal of Biomechanical Engineering 125 [3], pp. 334-341.

126. Korhonen, R. K.; Laasanen, M. S.; Toyras, J.; Rieppo, J.; Hirvonen, J.; Helminen, H. J. and Jurvelin, J. S. (2002): Comparison of the equilibrium response of articular cartilage in unconfined compression, confined compression and indentation, Journal of Biomechanics 35 [7], pp. 903-909.

127. Korhonen, R. K.; Wong, M.; Arokoski, J.; Lindgren, R.; Helminen, H. J.; Hunziker, E. B. and Jurvelin, J. S. (2002): Importance of the superficial tissue layer for the indentation stiffness of articular cartilage, Medical Engineering & Physics 24 [2], pp. 99-108.

128. Kornaat, P. R.; Doornbos, J.; van der Molen, A. J.; Kloppenburg, M.; Nelissen, R. G.; Hogendoorn, P. C. and Bloem, J. L. (2004): Magnetic resonance imaging of knee cartilage using a water selective balanced steady-state free precession sequence, J Magn Reson Imaging 20 [5], pp. 850-6.

129. Korstjens, C. M.; Nolte, P. A.; Burger, E. H.; Albers, G. H.; Semeins, C. M.; Aartman, I. H.; Goei, S. W. and Klein-Nulend, J. (2004): Stimulation of bone cell differentiation by low-intensity ultrasound--a histomorphometric in vitro study, J Orthop Res 22 [3], pp. 495-500.

130. Krishnan, Ramaswamy; Park, Seonghun; Eckstein, Felix and Ateshian, Gerard A. (2003): Inhomogeneous Cartilage Properties Enhance Superficial Interstitial Fluid Support and Frictional Properties, But Do Not Provide a Homogeneous State of Stress, Journal of Biomechanical Engineering 125 [5], pp. 569-577.

131. Kuroki, H.; Nakagawa, Y.; Mori, K.; Ikeuchi, K. and Nakamura, T. (2004): Mechanical effects of autogenous osteochondral surgical grafting procedures and instrumentation on grafts of articular cartilage, Am J Sports Med 32 [3], pp. 612-20.

132. Kuroki, H.; Nakagawa, Y.; Mori, K.; Ohba, M.; Suzuki, T.; Mizuno, Y.; Ando, K.; Takenaka, M.; Ikeuchi, K. and Nakamura, T. (2004): Acoustic stiffness and change in plug cartilage over time after autologous osteochondral grafting: correlation between ultrasound signal intensity and histological score in a rabbit model, Arthritis Res Ther 6 [6], pp. R492-504. Epub 2004 Sep 14.

133. Laasanen, M. S.; Toyras, J.; Korhonen, R. K.; Rieppo, J.; Saarakkala, S.; Nieminen, M. T.; Hirvonen, J. and Jurvelin, J. S. (2003): Biomechanical properties of knee articular cartilage, Biorheology 40 [1-3], pp. 133-140.

134. Laasanen, M. S.; Toyras, J.; Vasara, A. I.; Hyttinen, M. M.; Saarakkala, S.; Hirvonen, J.; Jurvelin, J. S. and Kiviranta, I. (2003): Mechano-acoustic diagnosis of cartilage degeneration and repair, J Bone Joint Surg Am 85-A [Suppl 2], pp. 78-84.

135. Lacroix, D. and Prendergast, P. (2002): A mechano-regulation model for tissue

differentiation during fracture healing: analysis of gap size and loading, Journal of Biomechanics 35 [9], pp. 1163-1171.

136. Lai, W. M.; Gu, W. Y. and Mow, V. C. (1998): On the conditional equivalence of chemical loading and mechanical loading on articular cartilage, J Biomech 31 [12], pp. 1181-5.

137. Lane, J. G.; Massie, J. B.; Ball, S. T.; Amiel, M. E.; Chen, A. C.; Bae, W. C.; Sah, R. L. and Amiel, D. (2004): Follow-up of osteochondral plug transfers in a goat model: a 6-month study, Am J Sports Med 32 [6], pp. 1440-50. Epub 2004 Jul 20.

138. Lanyon, L. E.; Hampson, W. G. J.; Goodship, A. E. and Shah, J. S. (1975): Bone deformation recorded in vivo from strain gauges attached to the human tibial shaft, Acta Orthop Scand. 46, pp. 256-268.

139. Lanyon, L.E. (1976): The measurements of bone strain "in vivo", Acta Orthop Belg, Suppl 1, pp. 98-108.

140. Lauritzen, J. B.; Schwarz, P.; Lund, B.; McNair, P. and Transbol, I. (1993): Changing incidence and residual lifetime risk of common osteoporosis-related fractures, Osteoporos Int 3 [3], pp. 127-32.

141. Lee, Jong Eun; Kim, Ko Eun; Kwon, Ick Chan; Ahn, Hyun Jeong; Lee, Sang-Hoon; Cho, Hyunchul; Kim, Hee Joong; Seong, Sang Chul and Lee, Myung Chul (2004): Effects of the controlled-released TGF-[beta]1 from chitosan microspheres on chondrocytes cultured in a collagen/chitosan/glycosaminoglycan scaffold, Biomaterials 25 [18], pp. 4163-4173.

142. Lee, R. B.; Wilkins, R. J.; Razaq, S. and Urban, J. P. (2002): The effect of mechanical stress on cartilage energy metabolism, Biorheology 39 [1-2], pp. 133-43.

143. Leipzig, N. D. and Athanasiou, K. A. (2005): Unconfined creep compression of chondrocytes, J Biomech 38 [1], pp. 77-85.

144. Li, K. W.; Williamson, A. K.; Wang, A. S. and Sah, R. L. (2001): Growth responses of cartilage to static and dynamic compression, Clin Orthop [391 Suppl], pp. S34-48.

145. Li, L. P. and Herzog, W. (2004): Strain-rate dependence of cartilage stiffness in unconfined compression: the role of fibril reinforcement versus tissue volume change in fluid pressurization, Journal of Biomechanics 37 [3], pp. 375-382.

146. Li, L. P.; Herzog, W.; Korhonen, R. K. and Jurvelin, J. S. (2005): The role of viscoelasticity of collagen fibers in articular cartilage: axial tension versus compression, Medical Engineering & Physics 27 [1], pp. 51-57.

147. Lill, H.; Hepp, P.; Gowin, W.; Oestmann, J. W.; Korner, J.; Haas, N. P.; Josten, C. and Duda, G. N. (2002): Age- and gender-related distribution of bone mineral density and mechanical properties of the proximal humerus, Rofo Fortschr Geb Rontgenstr Neuen Bildgeb Verfahr 174 [12], pp. 1544-50.

148. Lill, H.; Hepp, P.; Hoffmann, J.E.; Laborowicz, J.; Engel, T.; Josten, C. and Duda, G.N. (2001): Neue Implantate zur Stabilisierung proximaler Humerusfrakturen – Eine vergleichende in-vitro Studie, Osteosynthese International 9, pp. 1-9.

149. Lill, H.; Hepp, P.; Korner, J.; Josten, C. and Duda, G.N. (2001): Histomorphometrische und biomechanische Analyse in unterschiedlichen Regionen des proximalen Humerus, Chirurgisches Forum 30, pp. 395-398.

150. Lill, H.; Hepp, P.; Korner, J.; Kassi, J. P.; Verheyden, A. P.; Josten, C. and Duda, G. N. (2003): Proximal humeral fractures: how stiff should an implant be? A comparative mechanical study with new implants in human specimens, Arch Orthop Trauma Surg 123 [2-3], pp. 74-81. Epub 2003 Feb 12.

151. Lill, H.; Hepp, P.; Rose, T.; Konig, K. and Josten, C. (2004): The angle stable locking-proximal-humerus-plate (LPHP) for proximal humeral fractures using a small anterior-lateral-deltoid-splitting-approach - technique and first results, Zentralbl Chir 129 [1], pp. 43-8.

152. Loboa, E.G; Wren, T.A.L.; Beaupré, G.S. and Carter, B. G. (2003): Mechanobiology of soft skeletal tissue differentiation—a computational approach of a fiber-reinforced poroelastic model based on homogeneous and isotropic simplifications, Biomechanics and Modeling in Mechanobiology 2 [2], pp. 83-6.

153. Luyten, F. P. (2004): Mesenchymal stem cells in osteoarthritis, Curr Opin Rheumatol 16 [5], pp. 599-603.

154. Lysaght, M. J. and Hazlehurst, A. L. (2004): Tissue engineering: the end of the beginning, Tissue Eng 10 [1-2], pp. 309-20.

155. Lysaght, M. J. and Reyes, J. (2001): The growth of tissue engineering, Tissue Eng 7 [5], pp. 485-93.

156. Lyyra-Laitinen, T.; Niinimaki, M.; Toyras, J.; Lindgren, R.; Kiviranta, I. and Jurvelin, J. S. (1999): Optimization of the arthroscopic indentation instrument for the measurement of thin cartilage stiffness, Phys Med Biol 44 [10], pp. 2511-24.

157. Lyyra, T.; Jurvelin, J.; Pitkanen, P.; Vaatainen, U. and Kiviranta, I. (1995): Indentation instrument for the measurement of cartilage stiffness under arthroscopic control, Med Eng Phys 17 [5], pp. 395-9.

158. Lyyra, T.; Kiviranta, I.; Vaatainen, U.; Helminen, H. J. and Jurvelin, J. S. (1999): In vivo characterization of indentation stiffness of articular cartilage in the normal human knee, J Biomed Mater Res 48 [4], pp. 482-7.

159. Ma, H. L.; Hung, S. C.; Lin, S. Y.; Chen, Y. L. and Lo, W. H. (2003): Chondrogenesis of human mesenchymal stem cells encapsulated in alginate beads, J Biomed Mater Res 64A [2], pp. 273-81.

160. Maldonado, Zully M.; Seebeck, Jorn; Heller, Markus O. W.; Brandt, Doris; Hepp, Pierre; Lill, Helmut and Duda, Georg N. (2003): Straining of the intact and fractured proximal humerus under physiological-like loading, Journal of Biomechanics 36 [12], pp. 1865-1873.

161. Marti, C. B.; Gautier, E.; Wachtl, S. W. and Jakob, R. P. (2004): Accuracy of frontal and sagittal plane correction in open-wedge high tibial osteotomy, Arthroscopy 20 [4], pp. 366-72.

162. Martin, I.; Obradovic, B.; Freed, L. E. and Vunjak-Novakovic, G. (1999): Method for quantitative analysis of glycosaminoglycan distribution in cultured natural and engineered cartilage, Ann Biomed Eng 27 [5], pp. 656-62.

163. Meinel, Lorenz; Karageorgiou, Vassilis; Fajardo, Robert; Snyder, Brian; Shinde-Patil, Vivek; Zichner, Ludwig; Kaplan, David; Langer, Robert and Vunjak-Novakovic, Gordana (2004): Bone Tissue Engineering Using Human Mesenchymal Stem Cells: Effects of Scaffold Material and Medium Flow, Annals of Biomedical Engineering 32 [1], pp. 112-122.

164. Mikic, B. and Carter, D. R. (1995): Bone strain gage data and theoretical models of functional adaptation, J Biomech 28 [4], pp. 465-9.

165. Miller, P. D.; Bonnick, S. L. and Rosen, C. J. (1996): Consensus of an international panel on the clinical utility of bone mass measurements in the detection of low bone mass in the adult population, Calcif Tissue Int 58 [4], pp. 207-14.

166. Ming, Zhang; Zheng, Y. P. and Mak, Arthur F. T. (1997): Estimating the effective Young's modulus of soft tissues from indentation tests--nonlinear finite element analysis of effects of friction and large deformation, Medical Engineering & Physics 19 [6], pp. 512-517.

167. Mow, V. C.; Gibbs, M. C.; Lai, W. M.; Zhu, W. B. and Athanasiou, K. A. (1989): Biphasic indentation of articular cartilage--II. A numerical algorithm and an experimental study, J Biomech 22 [8-9], pp. 853-61.

168. Mow, V.C. and Ratcliffe, A. (1997): Structure and function of articular cartilage and meniscus, Mow, V.C. and Hayes, W.C., Basic Orthopaedics Biomechanics, 2. ed., pp. 113-179, Lippincott-Raven, Philadelphia.

169. Mullender, M. G. and Huiskes, R. (1995): Proposal for the regulatory mechanism of Wolff's law, J Orthop Res 13 [4], pp. 503-12.

170. Müller, M. E.; Nazarian, S. and Koch, P. (1989): Clasification AO des Fractures, Springer, Ed, Berlin, Heidelber, New York.

171. Nam, E. K.; Makhsous, M.; Koh, J.; Bowen, M.; Nuber, G. and Zhang, L. Q. (2004): Biomechanical and histological evaluation of osteochondral transplantation in a rabbit model, Am J Sports Med 32 [2], pp. 308-16.

172. Naruse, Kouji; Urabe, Ken; Mukaida, Tomoyuki; Ueno, Takeshi; Migishima, Fujio; Oikawa, Astuhiko; Mikuni-Takagaki, Yuko and Itoman, Moritoshi (2004): Spontaneous differentiation of mesenchymal stem cells obtained from fetal rat circulation, Bone 35 [4], pp. 850-858.

173. Neer, C.S. (1970): Displaced Proximal Humeral Fractures. Part I. Classification and Evaluation, J Bone Joint Surg Am 52, pp. 1077-1089.

174. Nehrer, S. and Minas, T. (2000): Treatment of articular cartilage defects, Invest Radiol 35 [10], pp. 639-46.

175. Nehrer, S.; Spector, M. and Minas, T. (1999): Histologic analysis of tissue after failed cartilage repair procedures, Clin Orthop 365 [365], pp. 149-62.

176. Newman, A. P. (1998): Articular cartilage repair, Am J Sports Med 26 [2], pp. 309-24.

177. Nieminen, H. J.; Saarakkala, S.; Laasanen, M. S.; Hirvonen, J.; Jurvelin, J. S. and Toyras, J. (2004): Ultrasound attenuation in normal and spontaneously degenerated articular cartilage, Ultrasound Med Biol 30 [4], pp. 493-500.

178. Nieminen, Miika T.; Toyras, Juha; Laasanen, Mikko S.; Silvennoinen, Johanna; Helminen, Heikki J. and Jurvelin, Jukka S. (2004): Prediction of biomechanical properties of articular cartilage with quantitative magnetic resonance imaging, Journal of Biomechanics 37 [3], pp. 321-328.

179. Nigg, B. and Herzog, W. (1994): Biomechanics of the Musculo-Skeletal System., John Wiley and Sons, Ltd,, John Wiley and Sons, Ltd,, England.

180. Nishikori, T.; Ochi, M.; Uchio, Y.; Maniwa, S.; Kataoka, H.; Kawasaki, K.; Katsube, K. and Kuriwaka, M. (2002): Effects of low-intensity pulsed ultrasound on proliferation and chondroitin sulfate synthesis of cultured chondrocytes embedded in Atelocollagen gel, J Biomed Mater Res 59 [2], pp. 201-6.

181. O'Driscoll, S. W. (1998): The healing and regeneration of articular cartilage, J Bone Joint Surg Am 80 [12], pp. 1795-812.

182. O'Driscoll, S. W. (1999): Articular cartilage regeneration using periosteum, Clin Orthop [367 Suppl], pp. S186-203.

183. O'Driscoll, S. W. (2001): Preclinical cartilage repair: current status and future perspectives, Clin Orthop [391 Suppl], pp. S397-401.

184. O'Driscoll, S. W. and Fitzsimmons, J. S. (2001): The role of periosteum in cartilage repair, Clin Orthop [391 Suppl], pp. S190-207.

185. O'Driscoll, S. W.; Keeley, F. W. and Salter, R. B. (1988): Durability of regenerated articular cartilage produced by free autogenous periosteal grafts in major full-thickness defects in joint surfaces under the influence of continuous passive motion. A follow-up report at one year, J Bone Joint Surg Am 70 [4], pp. 595-606.

186. O'Driscoll, S. W. and Salter, R. B. (1986): The repair of major osteochondral defects in joint surfaces by neochondrogenesis with autogenous osteoperiosteal grafts stimulated by continuous passive motion. An experimental investigation in the rabbit, Clin Orthop [208], pp. 131-40.

187. Oreffo, R. O. C. and Triffitt, J. T. (1999): Future potentials for using osteogenic stem cells and biomaterials in orthopedics, Bone 25 [1], pp. 5S-9S.

188. Ozgocmen, S.; Kiris, A.; Kocakoc, E.; Ardicoglu, O. and Kamanli, A. (2004): Evaluation of metacarpophalangeal joint synovitis in rheumatoid arthritis by power Doppler technique: relationship between synovial vascularization and periarticular bone mineral density, Joint Bone Spine 71 [5], pp. 384-8.

189. Park, Seonghun; Costa, Kevin D. and Ateshian, Gerard A. (2004): Microscale frictional response of bovine articular cartilage from atomic force microscopy, Journal of Biomechanics 37 [11], pp. 1679-1687.

190. Pascher, A.; Palmer, G. D.; Steinert, A.; Oligino, T.; Gouze, E.; Gouze, J. N.; Betz, O.; Spector, M.; Robbins, P. D.; Evans, C. H. and Ghivizzani, S. C. (2004): Gene delivery to cartilage defects using coagulated bone marrow aspirate, Gene Ther 11 [2], pp. 133-41.

191. Perez, Pablo and Santos, Andres (2004): Undersampling to acquire nuclear magnetic resonance images, Medical Engineering & Physics 26 [6], pp. 523-529.

192. Petersen, J.; Ruecker, A.; D., von Stechowm; Adamietz, P.; Poertner, R.; Rueger, J. M. and Meenen, N. M. (2003): Present and Future Therapies of Articular Cartilage Defects, European Journal of Trauma 29 [1], pp. 1-10.

193. Poole, A. R. (2003): What type of cartilage repair are we attempting to attain?, J

Bone Joint Surg Am 85-A [Suppl 2], pp. 40-44.

194. Poole, A. R.; Kojima, T.; Yasuda, T.; Mwale, F.; Kobayashi, M. and Laverty, S. (2001): Composition and structure of articular cartilage: a template for tissue repair, Clin Orthop [391 Suppl], pp. S26-33.

195. Porter, Scott E. M. D.; Stull, Douglass M. D.; Kneisl, Jeffrey S. M. D. and Frick, Steven L. M. D. (2004): Informed Consent Is Not Routinely Documented for Procedures Using Allografts. [Article], Clinical Orthopaedics & Related Research June 1 [423], pp. 287-290.

196. Prendergast, P. J. (1997): Finite element models in tissue mechanics and orthopaedic implant design, Clin Biomech (Bristol, Avon) 12 [6], pp. 343-366.

197. Prendergast, P. J. and Huiskes, R. (1995): The biomechanics of Wolff's law: recent advances, Ir J Med Sci 164 [2], pp. 152-4.

198. Prendergast, P. J.; Huiskes, R. and Soballe, K. (1997): ESB Research Award 1996. Biophysical stimuli on cells during tissue differentiation at implant interfaces, J Biomech 30 [6], pp. 539-48.

199. Prendergast, P. J.; van Driel, W. D. and Kuiper, J. H. (1996): A comparison of finite element codes for the solution of biphasic poroelastic problems, Proc Inst Mech Eng [H] 210 [2], pp. 131-6.

200. Quinn, T. M.; Grodzinsky, A. J.; Buschmann, M. D.; Kim, Y. J. and Hunziker, E. B. (1998): Mechanical compression alters proteoglycan deposition and matrix deformation around individual cells in cartilage explants, J Cell Sci 111 [Pt 5], pp. 573-83.

201. Raimondi, M.; Boschetti, F.; Falcone, N.; Fiore, G.B.; Remuzzi, A.; Marinoni, E.; Marazzi, M. and Pietrabissa, R. (2001): Mechanobiology of engineered cartilage cultured under a quantified fluid-dynamic environment, Biomechanics and Modeling in Mechanobiology 1 [1], pp. 69-82.

202. Ramallal, M.; Maneiro, E.; Lopez, E.; Fuentes-Boquete, I.; Lopez-Armada, M. J.; Fernandez-Sueiro, J. L.; Galdo, F.; De Toro, F. J. and Blanco, F. J. (2004): Xeno-implantation of pig chondrocytes into rabbit to treat localized articular cartilage defects: an animal model, Wound Repair Regen 12 [3], pp. 337-45.

203. Revell, W. J. and Heatley, F. W. (1988): Functional restoration of an articular surface using a heterotopic xenograft: biology of host-implant interactions in the canine patella, Biomaterials 9 [2], pp. 173-80.

204. Roughley, P. J. (2001): Age-associated changes in cartilage matrix: implications for tissue repair, Clin Orthop [391 Suppl], pp. S153-60.

205. Ruimerman, R.; Van Rietbergen, B.; Hilbers, P. and Huiskes, R. (2003): A 3-dimensional computer model to simulate trabecular bone metabolism, Biorheology 40 [1-3], pp. 315-320.

206. Rutherford, R.B.; Gu, K.; Racenis, P. and Krebsbach, P.H. (2003): Early Events: The In Vitro Conversion of BMP Transduced Fibroblasts to Chondroblasts, Connective Tissue Research 44 [Supplement 1/Supplement 1], pp. 117 - 123.

207. Saarakkala, S.; Korhonen, R. K.; Laasanen, M. S.; Toyras, J.; Rieppo, J. and Jurvelin, J. S. (2004): Mechano-acoustic determination of Young's modulus of articular cartilage, Biorheology 41 [3-4], pp. 167-79.

208. Saarakkala, S.; Toyras, J.; Hirvonen, J.; Laasanen, M. S.; Lappalainen, R. and Jurvelin, J. S. (2004): Ultrasonic quantitation of superficial degradation of articular cartilage, Ultrasound Med Biol 30 [6], pp. 783-92.

209. Saitoh, S.; Nakatsuchi, Y.; Latta, L. and Milne, E. (1994): Distribution of bone mineral density and bone strength of the proximal humerus, J Shoulder Elbow Surg 3, pp. 234-242.

210. Sakurakichi, Keisuke; Tsuchiya, Hiroyuki; Uehara, Kenji; Yamashiro, Teruhisa; Tomita, Katsuro and Azuma, Yoshiaki (2004): Effects of timing of low-intensity pulsed ultrasound on distraction osteogenesis, Journal of Orthopaedic Research 22 [2], pp. 395-403.

211. Salter, R. B.; Simmonds, D. F.; Malcolm, B. W.; Rumble, E. J.; MacMichael, D. and Clements, N. D. (1980): The biological effect of continuous passive motion on the healing of full-thickness defects in articular cartilage. An experimental investigation in the rabbit, J Bone Joint Surg [Am] 62 [8], pp. 1232-51.

212. Sarin, V. K. and Carter, D. R. (2000): Mechanobiology and joint conformity regulate endochondral ossification of sesamoids.[In Process Citation], J Orthop Res 18 [5], pp. 706-12.

213. Schmidt, W. A.; Schmidt, H.; Schicke, B. and Gromnica-Ihle, E. (2004): Standard reference values for musculoskeletal ultrasonography, Ann Rheum Dis 63 [8], pp. 988-94.

214. Scully, S. P.; Lee, J. W.; Ghert, P. M. A. and Qi, W. (2001): The role of the extracellular matrix in articular chondrocyte regulation, Clin Orthop [391 Suppl], pp. S72-89.

215. Seebeck, J.; Heller, M.; Schneider, E. and Duda, G.N. (2001): Influence of osteoporosis related morphological changes on tibial strains during walking, 4th Combined Meeting of the Orthopaedic Research Societies, Rhodos.

216. Sgaglione, Nicholas A. (2003): The biological treatment of focal articular cartilage lesions in the knee: future trends?, Arthroscopy: The Journal of Arthroscopic & Related Surgery 19 [Supplement 1], pp. 154-160.

217. Shahgaldi, B. Fariba (1998): Repair of large osteochondral defects: load-bearing and structural properties of osteochondral repair tissue, The Knee 5 [2], pp. 111-117.

218. Shapiro, F.; Koide, S. and Glimcher, M. J. (1993): Cell origin and differentiation in the repair of full-thickness defects of articular cartilage, J Bone Joint Surg Am 75 [4], pp. 532-53.

219. Shefelbine, Sandra J.; Augat, Peter; Claes, Lutz and Simon, Ulrich Trabecular bone fracture healing simulation with finite element analysis and fuzzy logic, Journal of Biomechanics In Press, Corrected Proof.

220. Silver, F. H. and Bradica, Gino (2002): Mechanobiology of cartilage: how do internal and external stresses affect mechanochemical transduction and elastic energy storage?, Biomechanics and Modeling in Mechanobiology 1 [3], pp. 219-238.

221. Smith, C. L. and Mansour, J. M. (2000): Indentation of an osteochondral repair: sensitivity to experimental variables and boundary conditions, J Biomech 33 [11], pp. 1507-1511.

222. Smith, R. L.; Carter, D. R.; Schurman, D. J. and Smith, R. L. (2004): Pressure and shear differentially alter human articular chondrocyte metabolism: a review, Clin Orthop [427 Suppl], pp. S89-95.

223. Steadman, J. R.; Rodkey, W. G. and Rodrigo, J. J. (2001): Microfracture: surgical technique and rehabilitation to treat chondral defects, Clin Orthop [391 Suppl], pp. S362-9.

224. Steinwachs, M. R. and Kreuz, P. C. (2003): [Combinations of different cartilage resurfacing techniques], Z Orthop Ihre Grenzgeb 141 [6], pp. 625-8.

225. Sterett, W. I. and Steadman, J. R. (2004): Chondral resurfacing and high tibial osteotomy in the varus knee, Am J Sports Med 32 [5], pp. 1243-9. Epub 2004 May 18.

226. Stone, K. R.; Ayala, G.; Goldstein, J.; Hurst, R.; Walgenbach, A. and Galili, U. (1998): Porcine cartilage transplants in the cynomolgus monkey. III. Transplantation of alpha-galactosidase-treated porcine cartilage, Transplantation 65 [12], pp. 1577-83.

227. Strunk, J.; Heinemann, E.; Neeck, G.; Schmidt, K. L. and Lange, U. (2004): A new approach to studying angiogenesis in rheumatoid arthritis by means of power Doppler ultrasonography and measurement of serum vascular endothelial growth factor, Rheumatology 7, p. 7.

228. Suh, J. K.; Li, Z. and Woo, S. L. (1995): Dynamic behavior of a biphasic cartilage model under cyclic compressive loading, J Biomech 28 [4], pp. 357-64.

229. Tibesku, C. O.; Szuwart, T.; Kleffner, T. O.; Schlegel, P. M.; Jahn, U. R.; Van Aken, H. and Fuchs, S. (2004): Hyaline cartilage degenerates after autologous osteochondral transplantation, Journal of Orthopaedic Research 22 [6], pp. 1210-1214.

230. Tis, John E.; Meffert, Rainer H.; Inoue, Nozomu; McCarthy, Edward F.; Machen, M. Shaun; McHale, Kathleen A. and Chao, Edmund Y. S. (2002): The effect of low intensity pulsed ultrasound applied to rabbit tibiae during the consolidation phase of distraction osteogenesis, Journal of Orthopaedic Research 20 [4], pp. 793-800.

231. Toyras, J.; Lyyra-Laitinen, T.; Niinimaki, M.; Lindgren, R.; Nieminen, M. T.;

Kiviranta, I. and Jurvelin, J. S. (2001): Estimation of the Young's modulus of articular cartilage using an arthroscopic indentation instrument and ultrasonic measurement of tissue thickness, J Biomech 34 [2], pp. 251-6.

232. Trickey, Wendy R.; Baaijens, Frank P. T.; Laursen, Tod A.; Alexopoulos, Leonidas G. and Guilak, Farshid Determination of the Poisson's ratio of the cell: recovery properties of chondrocytes after release from complete micropipette aspiration, Journal of Biomechanics In Press, Corrected Proof.

233. Trumble, Thomas M. D. and Verheyden, James M. D. (2004): Remodeling of Articular Defects in an Animal Model. [Report], Clinical Orthopaedics & Related Research June 1 [423], pp. 59-63.

234. Tsili, M. C. (2000): Theoretical solutions for internal bone remodeling of diaphyseal shafts using adaptive elasticity theory, Journal of Biomechanics 33 [2], pp. 235-239.

235. Ueblacker, P.; Burkart, A. and Imhoff, A. B. (2004): Retrograde cartilage transplantation on the proximal and distal tibia, Arthroscopy 20 [1], pp. 73-78.

236. Valhmu, W. B.; Stazzone, E. J.; Bachrach, N. M.; Saed-Nejad, F.; Fischer, S. G.; Mow, V. C. and Ratcliffe, A. (1998): Load-controlled compression of articular cartilage induces a transient stimulation of aggrecan gene expression, Arch Biochem Biophys 353 [1], pp. 29-36.

237. van den Berg, W. B.; van der Kraan, P. M.; Scharstuhl, A. and van Beuningen, H. M. (2001): Growth factors and cartilage repair, Clin Orthop [391 Suppl], pp. S244-50.

238. van der Helm, F.C.T. (1991): The shoulder mechanism. A dynamic approach. Ph.D. thesis, 0. ed., van der Helm, F.C.T., Ed, Delft University of Technology, Delft.

239. van der Helm, F.C.T. and Veenbaas, R. (1991): Modelling the mechanical effect of muscles with large attachment sites: application to the shoulder mechanism, J.Biomech. 24, pp. 1151-1163.

240. van der Meulen, Marjolein C. H. and Huiskes, Rik (2002): Why mechanobiology?: A survey article, Journal of Biomechanics 35 [4], pp. 401-414.

241. van Rietbergen, B.; Huiskes, R.; Weinans, H.; Sumner, D. R.; Turner, T. M. and Galante, J. O. (1993): ESB Research Award 1992. The mechanism of bone remodeling and resorption around press-fitted THA stems, J Biomech 26 [4-5], pp. 369-382.

242. Vena, P.; Verdonschot, N.; Contro, R. and Huiskes, R. (2000): Sensitivity Analysis and Optimal Shape Design for Bone-Prosthesis Interfaces in a Femoral Head Surface Replacement, Comput Methods Biomech Biomed Engin 3 [3], pp. 245-256.

243. von Rechenberg, B.; Akens, M. K.; Nadler, D.; Bittmann, P.; Zlinszky, K.; Kutter, A.; Poole, A. R. and Auer, J. A. (2003): Changes in subchondral bone in cartilage resurfacing--an experimental study in sheep using different types of osteochondral grafts, Osteoarthritis and Cartilage 11 [4], pp. 265-277.

244. von Rechenberg, B.; Akens, M. K.; Nadler, D.; Bittmann, P.; Zlinszky, K.; Neges, K. and Auer, J. A. (2004): The use of photooxidized, mushroom-structured osteochondral grafts for cartilage resurfacing--a comparison to photooxidized cylindrical grafts in an experimental study in sheep, Osteoarthritis Cartilage 12 [3], pp. 201-16.

245. Wakitani, S.; Goto, T.; Pineda, S. J.; Young, R. G.; Mansour, J. M.; Caplan, A. I. and Goldberg, V. M. (1994): Mesenchymal cell-based repair of large, full-thickness defects of articular cartilage, J Bone Joint Surg Am 76 [4], pp. 579-92.

246. Waldman, S. D.; Spiteri, C. G.; Grynpas, M. D.; Pilliar, R. M.; Hong, J. and Kandel, R. A. (2003): Effect of biomechanical conditioning on cartilaginous tissue formation in vitro, J Bone Joint Surg Am 85-A [Suppl 2], pp. 101-5.

247. Wang, C. C.; Guo, X. E.; Sun, D.; Mow, V. C.; Ateshian, G. A. and Hung, C. T. (2002): The functional environment of chondrocytes within cartilage subjected to compressive loading: a theoretical and experimental approach, Biorheology 39 [1-2], pp. 11-25.

248. Wang, M. and Yu, C. (2004): Silicone rubber: an alternative for repair of articular cartilage defects, Knee Surg Sports Traumatol Arthrosc 31, p. 31.

249. Wang, Xiaobo and Dumas, Genevieve A. (2002): Simulation of bone adaptive remodeling using a stochastic process as loading history, Journal of Biomechanics 35 [3], pp. 375-380.

250. Wang, Xuanhui; Grogan, Shawn P.; Rieser, Franz; Winkelmann, Verena; Maquet, Veronique; Berge, Martine La and Mainil-Varlet, Pierre (2004): Tissue engineering of biphasic cartilage constructs using various biodegradable scaffolds: an in vitro study, Biomaterials 25 [17], pp. 3681-3688.

251. Wei, X. and Messner, K. (1998): Age- and injury-dependent concentrations of transforming growth factor-beta 1 and proteoglycan fragments in rabbit knee joint fluid, Osteoarthritis Cartilage 6 [1], pp. 10-8.

252. Wong, M. and Carter, D. R. (2003): Articular cartilage functional histomorphology and mechanobiology: a research perspective, Bone 33, pp. 1-13.

253. Wu, J. Z. and Herzog, W. (2002): Elastic anisotropy of articular cartilage is associated with the microstructures of collagen fibers and chondrocytes, Journal of Biomechanics 35 [7], pp. 931-942.

254. Wu, J. Z.; Herzog, W. and Epstein, M. (1999): Modelling of location- and time-dependent deformation of chondrocytes during cartilage loading, J Biomech 32 [6], pp. 563-72.

255. Zannoni, C.; Mantovani, R. and Viceconti, M. (1998): Material properties assignment to finite element models of bone structures: a new method, Med Eng Phys 20 [10], pp. 735-40.

256. Zhang, Z. J.; Huckle, J.; Francomano, C. A. and Spencer, R. G. (2002): The influence of pulsed low-intensity ultrasound on matrix production of chondrocytes at different stages of differentiation: an explant study, Ultrasound Med Biol 28 [11-12], pp. 1547-53.

257. Zhang, Z. J.; Huckle, J.; Francomano, C. A. and Spencer, R. G. (2003): The effects of pulsed low-intensity ultrasound on chondrocyte viability, proliferation, gene expression and matrix production, Ultrasound Med Biol 29 [11], pp. 1645-51.

258. Zheng, Y. P.; Bridal, S. L.; Shi, J.; Saied, A.; Lu, M. H.; Jaffre, B.; Mak, A. F. and Laugier, P. (2004): High resolution ultrasound elastomicroscopy imaging of soft tissues: system development and feasibility, Phys Med Biol 49 [17], pp. 3925-38.

259. Zhurakovskii, I. P.; Ryzhov, A. I. and Komandenko, N. I. (2002): Pathomorphological Changes in Hyaline Cartilage during Focal Persistent Infection, Bulletin of Experimental Biology and Medicine 134 [4], pp. 414-417.

Annex 1

Most frequent error messages reported during the development of the tissue differentiation model and how they were solved.

IN ABAQUS:

1. Error code 11. This error is produced when an array is not appropriately dimensioned. The arrays should have the same order or size as the required field variables to be processed. The environment file should be conditioned simultaneously. Action: increase the dimension array in nodes*elements*required variables
2. Error code 6. The environment file has been not set appropriately. The variables pre-memory, standard_memory and max_history_request need to be increased in the abaqus environment file.
3. Convergence error. The analysis is stopped after a message reporting divergence in the solution. Solution: two aspects exist to be considered. First, change the element type. A non-Hourghess controlled element (see Abaqus user manual) could be appropriate to select when a non-geometry linearity approach is used in combination with biphasic behavior. If after the change of the element type the error message remains, the time limit defined in a step is not low enough, so that ABAQUS is required to find the solution. In the manual an equation is given to calculate this limit. (See section 5.5.1).

Unexpected material names are obtained in USDFLD (variable CMNAME) for some elements. Solution: Model contains parts and assemblies, and then elements are renumbered. Create model without parts and assemblies. Set the environment variable cae_no_parts_input_file=OFF.

Annex 2

The algorithm: Source code of the algorithm created to simulate tissue differentiation during healing of an osteochondral defect.

```
      SUBROUTINE USDFLD(FIELD,STATEV,PNEWDT,DIRECT,T,CELENT,
     1 TIME,DTIME,CMNAME,ORNAME,NFIELD,NSTATV,NOEL,NPT,LAYER,
     2 KSPT,KSTEP,KINC,NDI,NSHR,COORD,JMAC,JMATYP,MATLAYO,LACCFLA)

      INCLUDE 'ABA_PARAM.INC'

      INTEGER TNEN, TNE

      PARAMETER (NVAR=140000)
C TNEN= Total Number of Entities (Number of elem*Num. of Gauss points)
      PARAMETER (TNEN=6500)

C TNE= Total Number of Elements
      PARAMETER (TNE=1603)

C FL is the rate of convergence (to selected stimulus)
**      PARAMETER (FL=0.01)

C FL2, FL3 are the rate of change for the interface region
C (numerical viscosity)
      PARAMETER (FL2=0.001)
      PARAMETER (FL3=0.001)

C NREM: ID elements >= NREM goes not into remodelling
      PARAMETER (NREM=699)

*****
*** CN is the current material name: CMNAME for NOEL
*** AN is the previous material name: intact situation
*** BN is the previous material name to be use in the current model
*****
      CHARACTER*80 CMNAME,ORNAME,CPNAME
      CHARACTER*80 BN,B,CN,AN
      CHARACTER*9 ED
      CHARACTER*8 FLGRAY(15)
      CHARACTER*256 JOBNAME, OUTDIR

      DIMENSION FIELD(NFIELD),STATEV(NSTATV),DIRECT(3,3)
      DIMENSION T(3,3),TIME(2),CN(TNEN),AN(TNEN),BN(TNEN)
      DIMENSION ARRAY(15),JARRAY(15),JMAC(*),JMATYP(*),COORD(*)
      DIMENSION STIM(4), EP(3)
      DIMENSION PERC(3), S(3)


      INTEGER EN(TNE),EL(TNE),AE(TNE),SUMME,BUT(TNEN)
      INTEGER TOT,PLZ(TNE),SLZ(TNE)
      INTEGER NOD1(TNE),NOD2(TNE),NOD3(TNE),NOD4(TNE),CONT(4)


      REAL FL,DIF

      COMMON KOUNTER
      COMMON ST(NVAR,4,2)
      COMMON EN,NOD1,NOD2,NOD3,NOD4,EL,SUMME,BUT
      COMMON TOT,PLZ,SLZ
      COMMON AE,AN,CN,BN

      INTEGER JELEN(NVAR),NINTP(NVAR)

      DIMENSION CENTP(NVAR),LOCNUM(NVAR)
      DIMENSION INF(TNE)

      CHARACTER*75 NORM, CONNECT

      PARAMETER (ZERO=0.D0, ONE=1.D0)

      B = CMNAME
*********************************************************************
***
***  Definition of the element number and the integration point number
```

```
***
***  to check tissue differentiation process
***
************************************************************************
***   STIFFR =Constant defining the maximum rate of density change in HU
***   STIFFR =1
***   ELNUM  =Number of the element to be viewed in the msg file
      ELNUM    =  6
***   NOINT    = Number of the integration point to be examined.
      NOINT    = 1
***   SIG = negative signal for compressive stimuli
      SIG = -1

************************************************************************
***
***   Initial Path definitions
***
************************************************************************
***   NORM = Name of comparison file for physiological normals.

      NORM='/home/b/bexvega7/ABAQUS_JOBS/SIGNALS/ep1_cxc'
***   CONNECT = Name of the input file with the mesh data.
      CONNECT='/home/b/bexvega7/ABAQUS_JOBS/GEOM/cxab_elm.inp'
***      WRITE(7,*)'reading the signal'

************************************************************************
***   Opening all files
***
************************************************************************
      IF ((KSTEP.EQ.1).AND.(KINC.EQ.0).AND.(SUMME.EQ.0)) THEN
***         WRITE(7,*)'After summe'
*** status elements in the defect model
         OPEN(UNIT=102,
     *      FILE='/home/b/bexvega7/ABAQUS_JOBS/DATA/elem_state.inp')

*** creating and copying connectivity in other file from initial
*** job information
         OPEN(UNIT=104,STATUS='UNKNOWN',
     *      FILE='/home/b/bexvega7/ABAQUS_JOBS/DATA/connec.inp')
***  reading the initial job information

         OPEN(139,FILE=CONNECT, STATUS='OLD')
***         READ(139,800)ED
*** 800     FORMAT(A9)
***            IF (ED(1:9).EQ.'*Element,') THEN
C  I : Number of Elements
            DO 920 I=1,TNE
***               READ(139,900,END=930)EN(I),NOD1(I),NOD2(I),
***     *              NOD3(I),NOD4(I)
               READ(139,*,END=930)EN(I),NOD1(I),NOD2(I),
     *             NOD3(I),NOD4(I)
*** 900           FORMAT(I3,T5,I4,T10,I4,T15,I4,T20,I4)
               BUT(I)=1
***                  WRITE (104,910)EN(I),NOD1(I),NOD2(I),NOD3(I),NOD4(I)
               WRITE (104,*)EN(I),NOD1(I),NOD2(I),NOD3(I),NOD4(I)
*** 910              FORMAT(T5,I3,T10,I4,T15,I4,T20,I4,T25,I4)
 920        ENDDO
 930        CONTINUE
***            ENDIF
***  Id of all left connected elements
         OPEN(UNIT=105,STATUS='UNKNOWN',
     *      FILE='/home/b/bexvega7/ABAQUS_JOBS/DATA/left.inp')

*** Id of left connected elements in an interface region
         OPEN(UNIT=106,STATUS='UNKNOWN',
     *      FILE='/home/b/bexvega7/ABAQUS_JOBS/DATA/left_out.inp')
       WRITE(7,*)NOEL,KSTEP,KINC,EN(273),NOD1(273),CN(273)

         OPEN(UNIT=107,STATUS='UNKNOWN',
     *      FILE='/home/b/bexvega7/ABAQUS_JOBS/DATA/average.inp')

       FL=0.01

       SUMME = SUMME + 1
       WRITE(7,*)'files open here..'
       ENDIF

************************************************************************
```

```
***
***   STATEV(1) = Centre value of the dead zone in tri-linear curve
***   STATEV(2) = Intact value of stimulus of Cancellous bone
***   STATEV(3) = FAC (memory of actual stimulus before tri curve)
***   STATEV(4) = INITIAL Material property
***   STATEV(5-8) = TRI-LINEAR remodelling stimuli
***
**********************************************************************
      IF (NOEL.EQ.ELNUM.AND.NPT.EQ.NOINT) THEN
         WRITE (7,3000)KINC,KSTEP
 3000    FORMAT(/,'Start of increment ',I2,' in step ',I3)
      ENDIF

      IF(KSTEP.EQ.1.AND.KINC.EQ.1) THEN
         DO 50 L = 1,14
            STATEV(L) = 0.0
 50      END DO
      ENDIF
**********************************************************************
***
*** Establish the initial materials properties
***
*** file ID:129, Norm, ep1
***
**********************************************************************
      IF (KOUNTER.NE.1) THEN
       OPEN(129,FILE=NORM,STATUS='OLD')
         DO 40 N=1,NVAR
            READ(129,44,END=41)JELEN(N),NINTP(N),CENTP(N),AN(N)
 44         FORMAT(I5,I2,E12.5,T22,A)
            ST(JELEN(N),NINTP(N),2) = CENTP(N)
 40      ENDDO

 41      CONTINUE
         CLOSE(129)
         KOUNTER = 1
      ENDIF
**********************************************************************
***
*** WRITING ELEMENT INFORMATION (I)
***
***  Intact situation
***
**********************************************************************
      OPEN(UNIT=101,STATUS='UNKNOWN',
     *   FILE='/home/b/bexvega7/ABAQUS_JOBS/DATA/elements.inp')
         IF ((KSTEP.EQ.2).AND.(KINC.EQ.0)) THEN

***            WRITE (101,*)KSTEP

C AN is the previous material name (intact) and B is the actual material name(defect)
C NOEL is the actual element number (defect)
            DO 620, J=1, 6412
               IF (NOEL.EQ.JELEN(J)) THEN
                  BN(NOEL)=AN(J)
***                  WRITE (101,610)KSTEP,KINC,J,NOEL,JELEN(J),BN(NOEL),AN(NOEL),AN(J)
*** 610              FORMAT('KSTEP',T7,I3,T12,I3,T16,'J',
***     *                T19,I5,T27,I5,T34,I5,T41,A,T56,A,T71,A)
               ENDIF

 620        ENDDO

         ELSE
            CLOSE(101)
         ENDIF
**********************************************************************
***
***   Initial material definition STATEV(2)
***
**********************************************************************
      IF (KSTEP.EQ.1.AND.KINC.EQ.1) THEN
         STATEV(13) = ST(NOEL,NPT,2)

            IF (CMNAME.EQ.'DEFECT') THEN
               STATEV(2) = 0.2

            ELSE IF (CMNAME.EQ.'CAL_CART') THEN
               STATEV(2) = 20000
```

```
            ELSE IF (CMNAME.EQ.'CART') THEN
               STATEV(2) = 10

            ELSE IF (CMNAME.EQ.'SUBCHON') THEN
               STATEV(2) = 1750

            ELSE IF (CMNAME.EQ.'CARTILAGE') THEN
               STATEV(2) = 10

            ELSE IF (CMNAME.EQ.'SUBCHON_BONE') THEN
               STATEV(2) = 1750

            ELSE IF (CMNAME.EQ.'CALCIF_CART') THEN
               STATEV(2) = 20000

           ENDIF
          STATEV(4) = STATEV(2)
           IF (STATEV(2).LE.0.2) THEN
              STATEV(2) = 0.2
           ENDIF

      ENDIF

*********************************************************************
***
**      Updating the material properties
***
*********************************************************************
      IF (KSTEP.GE.2) THEN
         IF (STATEV(2).LE.3) THEN
            CMNAME='DEFECT'
         ELSE IF ((STATEV(2).GT.3).AND.(STATEV(2).LE.8)) THEN
            CMNAME='PRE_CARTILAGE'
         ELSE IF ((STATEV(2).GT.8).AND.(STATEV(2).LE.12)) THEN
            CMNAME='CARTILAGE'
         ELSE IF ((STATEV(2).GT.12).AND.(STATEV(2).LE.825)) THEN
            CMNAME='PRE_SUBCHON_BONE'
         ELSE IF ((STATEV(2).GT.825).AND.(STATEV(2).LE.2300)) THEN
            CMNAME='SUBCHON_BONE'
         ELSE IF ((STATEV(2).GT.2300).AND.(STATEV(2).LE.22E+03)) THEN
            CMNAME='CALCIF_CART'
         ENDIF
*** check          IF (KSTEP.GT.2.AND.NPT.EQ.NOINT) THEN
*** check            WRITE(7,*)'NEW_MAT',CMNAME
*** check          ENDIF
***          STATEV(10)=CMNAME
      ENDIF

*********************************************************************
***
***  Definition of the trilinear curve for each tissue type
***
*********************************************************************
***   Comparison model for physiological normals. Yes = 1, no = 0
***      NCOMP = 1

      IF ((CMNAME.EQ.'SUBCHON_BONE').OR.(CMNAME.EQ.'PRE_SUBCHON_BONE')) THEN
         PERC(1)= 0
         FL=ZERO
         BUT(NOEL)= 1
         PERC(2)= 0.555E-3
***         WRITE(7,*)'ciclo1',KSTEP,KINC,NPT

      ELSE IF (CMNAME.EQ.'CARTILAGE') THEN
         PERC(1) = 0.0001
         PERC(2) = 0.1295

      ELSE IF (CMNAME.EQ.'CALCIF_CART') THEN
         PERC(1) = 0.0001
         PERC(2) = 1.536e-4

      ELSE IF (CMNAME.EQ.'DEFECT') THEN
         PERC(1) = 0.00001
         PERC(2) = 0.1295

      ELSE
         PERC(1) = 0.0001
```

```
         PERC(2) = 0.1295
***         WRITE(7,*)'ciclo2',KSTEP,KINC,NPT
      ENDIF

************************************************************
***
***   Rate of change for the local strain in each Tissue
***
************************************************************
      IF ((BUT(NOEL).EQ.1).AND.(KSTEP.GE.2).AND.(KINC.EQ.6)) THEN
         IF ((STATEV(2).GE.0.2).AND.(STATEV(2).LT.12)) THEN
            IF ((CMNAME.EQ.'DEFECT').AND.(BN(NOEL).EQ.'CARTILAGE')) THEN
               STIFFR = 1.2
            ELSE IF ((CMNAME.EQ.'PRE_CARTILAGE').AND.
     *               (BN(NOEL).EQ.'CARTILAGE')) THEN
               STIFFR = 1.15
            ELSE
               STIFFR = 1
            ENDIF

         ELSE IF ((STATEV(2).LT.1750).AND.(STATEV(1).LT.O)) THEN
            IF (CMNAME.EQ.'SUBCHON_BONE') THEN
               STIFFR=1500

            ELSE IF (CMNAME.EQ.'PRE_SUBCHON_BONE') THEN
               STIFFR=900
            ENDIF

         ELSE IF ((STATEV(2).LT.1750).AND.(STATEV(1).GT.O)) THEN
            IF (CMNAME.EQ.'PRE_SUBCHON_BONE') THEN
               STIFFR=1500

            ELSE IF (CMNAME.EQ.'SUBCHON_BONE') THEN
               STIFFR=400

            ELSE IF (CMNAME.EQ.'CALCIF_CART') THEN
               STIFFR=400

            ENDIF

         ELSE
            STIFFR = 1
         ENDIF

      ELSE
         STIFFR = 1

      ENDIF
************************************************************************
***
***   COMPARISON BETWEEN THE INTERNAL ELEMENT ID WITH THE PART ELEMENT ID
***
***   Remove the symbol'*' for an analysis of a model with parts and assemblies
***   REM = Change the corresponding parameter in the environment file as follow:
***   cae_no_parts_input_file=OFF
***
************************************************************************

***      OPEN(UNIT=103,STATUS='UNKNOWN',
***     *   FILE='/usr/people/zm3/KNORPEL/REMODEL/DEF_NUM/TEST/internal_id.inp')
***      JRCD = 0

***      JTYP = 1
***      IF (KSTEP.GT.1) THEN
***         WRITE(103,740)KSTEP
*** 740     FORMAT('KSTEP=',T8,I4,/)

***         DO 760, M=1,726
***            CALL GETINTERNAL('CARTILAGE-DEFECT-1',LOCNUM(M),JTYP,INTNUM,JRCD)

***               WRITE(103,750)LOCNUM(M),INTNUM,CMNAME
*** 750            FORMAT('LOCNUM=',T11,I4,T16,'INTNUM=',T30,I4,T35,A)
*** 760     CONTINUE

***      ENDIF

***      CLOSE(103)
***  here final line to be removed!!
```

```
************************************************************
***
***   READING AND WRITING ELEMENT INFORMATION (III)
***   SEARCH OF THE INTERFACE REGION
***   NUMERIC VISCOSITY
***
************************************************************
      IF ((KSTEP.EQ.2).AND.(SUMME.EQ.1)) THEN
         SUMME=SUMME +1
         DO 980, I=1,698
*** CHECK:
***             WRITE(106,941)KSTEP,KINC,NOEL,EN(I),NOD1(J),NOD4(J),CMNAME
*** 941         FORMAT(I3,T5,I3,T10,I4,T15,I4,T20,I4,T26,I4,T32,A)
            DO 970, J=1,698
*** CHECK:
***                WRITE(106,951)KSTEP,J,NOEL,EN(J),NOD2(J),NOD3(J),CMNAME
*** 951            FORMAT(I3,T5,I3,T10,I4,T15,I4,T20,I4,T26,I4,T32,A,T46,E12.5)

               IF ((NOD1(I).EQ.NOD2(J)).AND.
     *            (NOD4(I).EQ.NOD3(J))) THEN
*** CHECK:
***                      WRITE(105,960)EN(I),EN(J),NOEL,CMNAME,CN(I),CN(J)
***                      WRITE(7,*) EN(I),CN(I),'Left connected for all people!!'
*** 960                  FORMAT('element',T9,I4,' is LC with',T25,I4,
***     *                         T30,I4,T36,A,T51,A,T64,A)
                  IF (CN(I).NE.CN(J)) THEN
                     IF (CN(I).EQ.'SUBCHON_BONE') THEN
***                        WRITE(7,*)NOEL,EN(J),CN(I)
***                                  WRITE(7,*)'selected elem'
                        TOT = TOT + 1
                        PLZ(TOT)=EN(J)
***                        WRITE(7,*)'TOT',TOT,PLZ(TOT)

                           DO 965, K=1, 698
                              IF ((NOD1(J).EQ.NOD2(K)).AND.
     *                           (NOD4(J).EQ.NOD3(K))) THEN
                                 SLZ(TOT)=EN(K)
***                                 WRITE(7,*)SLZ(TOT)
                              ENDIF
 965                       ENDDO
                     ENDIF

                  ENDIF
*** CHECK:
***                  ELSE
***                     WRITE(106,964)'OH.. I AM NOT CONNECTED :) !!'
*** 964                 FORMAT(/,A)

               ENDIF

 970        ENDDO

 980     ENDDO

      ENDIF

************************************************************
***
***   Strains thresholds for Tissue differentiation (from Histology)
***   Disabled when trilinear curve is defined
***   To use this block change the multiplicative factor for STATEV(2)
***   STATEV(2)= STATEV(2)*Factor. Inactive when Factor=1
************************************************************

***      WRITE(7,*)'Estoy antes de diferenciacion celular'
      IF ((KSTEP.GE.2).AND.(KINC.EQ.6)) THEN

         STATEV(9)=ABS((STATEV(3)-STATEV(13))/STATEV(13))


         IF ((NPT.EQ.NOINT).AND.(NOEL.LE.NREM)) THEN
            WRITE(7,*)'SDV9 ALOAD',STATEV(9),STATEV(3),STATEV(13),KSTEP,KINC
            WRITE(7,*)'ELEM',NOEL,STATEV(1),STATEV(2),BUT(NOEL)
            WRITE(7,*)'STIFFR',STIFFR,CMNAME,PERC(2)
            WRITE(7,*)'BN',BN(NOEL)
         ENDIF
```

```
         IF ((STATEV(9).GE.(FL)).AND.(BUT(NOEL).EQ.1)) THEN

            IF ((STATEV(3).GE.-0.3969E-4).AND.
     *          (STATEV(3).LT.0)) THEN
               STATEV(2) = STATEV(2)*1


            ELSE IF ((STATEV(3).LT.-0.3969E-4).AND.
     *               (STATEV(3).GE.-0.7023E-4)) THEN
               STATEV(2) = STATEV(2)*1


            ELSE IF ((STATEV(3).LT.-0.7023E-4).AND.
     *               (STATEV(3).GE.-0.38E-3)) THEN
               STATEV(2) = STATEV(2)*1


            ELSE IF ((STATEV(3).LT.-0.38E-3).AND.
     *               (STATEV(3).GE.-1.147E-3)) THEN

               STATEV(2) = STATEV(2)*1

            ELSE IF ((STATEV(3).LT.-1.147E-3).AND.
     *               (STATEV(3).GE.-0.1243)) THEN
               STATEV(2) = STATEV(2)*1


            ELSE IF ((STATEV(3).LT.-0.1243).AND.
     *               (STATEV(3).GE.-0.1939).AND.
     *               (CMNAME.EQ.'DEFECT')) THEN
               STATEV(2) = STATEV(2)*1

            ELSE IF ((STATEV(3).LT.-0.1939).AND.
     *               (STATEV(3).GE.-1.0).AND.(CMNAME.EQ.'DEFECT')) THEN
               STATEV(2) = STATEV(2)*1

            ENDIF

         ELSE
            BUT(NOEL)=0

         ENDIF

       ENDIF

       FIELD(1) = STATEV(2)

*****************************************************************
***
***   Elements in an interface region
***   Usage of the numerical viscosity concept
***
*****************************************************************

C In step1 Abaqus read geom and mat. propert.
C In Step2 SDV9 has a Zero value
C E modulus evolution (tissue differentiation) is started up to Step3

       IF((KSTEP.GT.2).AND.(KINC.EQ.6)) THEN
          DO L=1, TOT
             IF (NOEL.EQ.PLZ(L)) THEN
                IF ((STATEV(9).GE.(FL)).AND.(BUT(NOEL).EQ.1).AND.
     *              (STATEV(1).NE.0)) THEN
                   IF (KSTEP.LE.14) THEN
                      STATEV(2)=STATEV(2)*3
*** CHECK:
***                      WRITE(7,*)'INCREMENTING'
                   ELSE IF (KSTEP.GT.6) THEN
*** CHECK:
***                      WRITE(7,*)'SDV9=',STATEV(9),'stim',STATEV(1)
***                      WRITE(7,*)'Ele',NOEL
                      STATEV(2)=STATEV(2)*(1+FL3)
                   ENDIF

                ELSE
                   BUT(NOEL)= 0
                   IF (NPT.EQ.NOINT) THEN
***                      WRITE(7,*)'BoT.NULL','ELE',NOEL,'STEP',KSTEP
```

```
***                     WRITE(7,*)'SDV9',STATEV(9),STATEV(2)
                     ENDIF
                  ENDIF

               ENDIF
               IF (NOEL.EQ.SLZ(L)) THEN
                  IF ((STATEV(9).GE.(FL)).AND.(BUT(NOEL).EQ.1).AND.
     *                (STATEV(1).NE.0)) THEN
                     IF (KSTEP.LE.14) THEN
                        STATEV(2)=STATEV(2)*2
*** CHECK:
***                     WRITE(7,*)'ESTOY INCREMENTANDO E INTERF'
                     ELSE IF (KSTEP.GT.6) THEN
*** CHECK:
***                     WRITE(7,*)'SDV9=',STATEV(9),'stim',STATEV(1)
***                     WRITE(7,*)'Ele',NOEL
                        STATEV(2)=STATEV(2)*(1+FL2)
                     ENDIF
                  ELSE
                     BUT(NOEL)= 0
                     IF (NPT.EQ.NOINT) THEN
***                     WRITE(7,*)'BoT.NULL','ELE',NOEL,'STEP',KSTEP
***                     WRITE(7,*)'SDV9',STATEV(9),STATEV(2)
                     ENDIF
                  ENDIF
               ENDIF
            ENDDO
         ENDIF

*****************************************************************
***
***   Read in Values to State Variables
***   OBS: If the model have only one material type, then
***   active the COMP as control: the tissue is not able to jump
***   from a trilinear curve to another one.
*****************************************************************
***      IF (KSTEP.GE.1.AND.KINC.GE.1) THEN
         STATEV(5) = STATEV(13)-ABS(PERC(2))
         STATEV(6) = STATEV(13)-ABS(PERC(1))
         STATEV(7) = STATEV(13)+ABS(PERC(1))
         STATEV(8) = STATEV(13)+ABS(PERC(2))
***      ENDIF

*****************************************************************

***      IF (KSTEP.GE.1.AND.KINC.GE.1) THEN
         STIM(1) = STATEV(5)
         STIM(2) = STATEV(6)
         STIM(3) = STATEV(7)
         STIM(4) = STATEV(8)
***      ENDIF

         IF (NOEL.EQ.ELNUM.AND.NPT.EQ.NOINT) THEN

            WRITE (7,1013) STIM(1),STIM(2),STIM(3),STIM(4)
1013        FORMAT ('Tri-linear Stimuli = ',E14.8,'  ',E14.8,'  ',
     *              E14.8,'  ',E14.8)
         ENDIF

*****************************************************************
***
***   INCREMENT in which GROWTH STIMULUS is calculated
***
*****************************************************************

         IF (KSTEP.GT.2) THEN
            CALL GETVRM('EP',ARRAY,JARRAY,FLGRAY,JRCD,JMAC,JMATYP,MATLAYO,LACCFLA)
            DO 108 K1=1,3
               EP(K1) = ARRAY(K1)
               IF (NOEL.EQ.ELNUM.AND.NPT.EQ.NOINT) THEN
                  WRITE(7,*)'E MODUL',STATEV(2)
                  WRITE (7,111)K1,ARRAY(K1)
 111              FORMAT (/,'UNLOADED Conditions ....',
     *                    'PRINCIPAL STRAIN Value (',I1,') = ',E12.5)
               ENDIF
 108        CONTINUE
```

```
*********************************************************************

         FAC= EP(1)

*********************************************************************
         STATEV(3) = FAC
         B = CMNAME
***         STATEV(9)=ABS((STATEV(3)-STATEV(13))/STATEV(13))
         IF (NOEL.EQ.ELNUM.AND.NPT.EQ.NOINT) THEN
            WRITE(7,110) FAC
 110        FORMAT(/,20X,'FAC = ',E12.5)
         ENDIF
***      Normal tri-linear curve
         IF (BUT(NOEL).EQ.1) THEN
            IF (FAC.LE.STIM(1)) THEN
               STIMULUS = -ONE
            ELSE IF ((FAC.GT.STIM(1)).AND.(FAC.LT.STIM(2))) THEN
             STIMULUS = -(STIM(2)-FAC)/(STIM(2)-STIM(1))
            ELSE IF ((FAC.GE.STIM(2)).AND.(FAC.LE.STIM(3))) THEN
               STIMULUS = ZERO
            ELSE IF ((FAC.GT.STIM(3)).AND.(FAC.LT.STIM(4))) THEN
               STIMULUS = (FAC-STIM(3))/(STIM(4)-STIM(3))
            ELSE IF (FAC.GE.STIM(4)) THEN
               STIMULUS = ONE
            ELSE
               WRITE (7,1050)

 1050          FORMAT(/,2X,'Error in calculating Stimulus Value !!')
            ENDIF

         ENDIF

         IF (NOEL.EQ.ELNUM.AND.NPT.EQ.NOINT) THEN
            WRITE(7,1090)STIMULUS
 1090       FORMAT(/,4X,'STIMULUS = ',E12.5)

         ENDIF

*** STATEV(1) is the change in density at the integration point

         STATEV(1) = SIG*STIMULUS

      ENDIF

*************************************************************
***
***    CHECK EQUILIBRIUM (SELECTED STIMULUS)
***
*************************************************************
      IF ((STATEV(3).LE.STATEV(13)).AND.(CMNAME.EQ.'CARTILAGE')) THEN
         IF (STATEV(9).LT.1) THEN
            STIMULUS = ZERO
            BUT(NOEL)= 0
            STATEV(1) = STIMULUS
         ENDIF
      ENDIF
*** waiting for resorption to growth
      IF ((KSTEP.LT.6).AND.(CMNAME.EQ.'DEFECT')) THEN
         STIMULUS=ZERO
         STATEV(1) = STIMULUS
      ENDIF
*** controlling resorption at the subchondral bone
      IF ((STATEV(9).LT.0.5).AND.(CMNAME.EQ.'SUBCHON_BONE')) THEN
         IF ((NOEL.LT.NREM).AND.(BN(NOEL).EQ.'SUBCHON_BONE')) THEN
            STIMULUS = ZERO
            BUT(NOEL) = 0
            STATEV(1) = STIMULUS
         ENDIF
      ENDIF
*** end of the adaptation
*************************************************************
***
***    Intact Joint (modelled to apply load only)
***    Not remodeling
***
*************************************************************
      IF (NOEL.GE.NREM) THEN
         STIMULUS = ZERO
```

```
         BUT(NOEL) = 0
         STATEV(1) = STIMULUS
      ENDIF
************************************************************
***
***    Growth Increment, I ONLY
***
************************************************************
      IF (KSTEP.GT.1) THEN

         IF (NOEL.EQ.ELNUM.AND.NPT.EQ.NOINT) THEN
            WRITE (7,1070)
 1070       FORMAT(/,2X,'Beginning of Growth Increment')

            WRITE(7,3010) STATEV(1)
 3010       FORMAT(/,4X,'Total Stimulus for Day = ',E12.5)

         ENDIF
*********************************************************************

         IF (NOEL.EQ.ELNUM.AND.NPT.EQ.NOINT) THEN
            WRITE(7,3020)STATEV(1),STATEV(2),FIELD(1)
 3020       FORMAT(/,/,
     *   'SDV(1) = ',E12.5,' SDV(2) = ',E12.5,' FIELD(1) = ',E12.5 )
         ENDIF

         IF(KINC.EQ.6) THEN
            STATEV(2) = STATEV(2)+STIFFR*STATEV(1)
         ENDIF

         IF (STATEV(2).LE.0.2) THEN
            STATEV(2) = 0.2
            STATEV(14) = 0.2
         ENDIF
         FIELD(1) = STATEV(2)
         STATEV(15) = STATEV(4) - STATEV(2)

      ENDIF
*********************************************************************
***
*** WRITING ELEMENT INFORMATION (Ib)
***
*********************************************************************
*** Here writing element status for the defect model (102), elem_state.inp

      IF (KSTEP.GE.1) THEN
         CN(NOEL)=CMNAME
*** CHECK:
***         WRITE(102,710)KSTEP,KINC,NOEL,CMNAME,CN(NOEL)
*** 710     FORMAT(I4,T9,I4,T15,I4,T21,A,T35,A)
      ENDIF
*********************************************************************
***
**      END of the increment
***
*********************************************************************
      IF (NOEL.EQ.ELNUM.AND.NPT.EQ.NOINT) THEN
         WRITE (7,2000) FIELD(1)
 2000    FORMAT(/,'END of iteration !!!!!',
     *          /,'Final Field Variable, FIELD(1) = ',E12.5)
      ENDIF

*** REMOVE THE FOLLOWING LINES FOR A COMPLETE ANALYSIS
*********************************************************************
***
***      END of the remodeling process
***
*********************************************************************
      IF (NOEL.LT.NREM) THEN
         IF ((CMNAME.EQ.BN(NOEL)).AND.(STIMULUS.EQ.ZERO)) THEN
            BUT(NOEL)= 0
         ENDIF
      ENDIF
*********************************************************************
***
*** Reduction of Iterations (Max.=10)
***
*********************************************************************
```

```
      IF (KSTEP.GT.350) THEN
         WRITE(102,*)'ANALYSIS TERMINED BY USER'
*** 2020    FORMAT(/,A)
         CLOSE(104)
         CLOSE(139)
         CLOSE(106)
         CLOSE(105)
         CLOSE(102)

         CALL XIT

      ENDIF
************************************************************************
*** FINAL LINE TO BE REMOVED
      RETURN
      END
```

Acknowledgements

This dissertation was supervised by Professor Georg Duda of the Musculoskeletal Research Center of Berlin (MRCB) Charité. Thanks to his involvement a scholarship of DAAD in Germany became possible. I gratefully acknowledge our discussions and his guidance.

The development of this dissertation would not have been possible without a work place, computational power and cooperation in the MRCB.

This project was completely supported financially by the DAAD for which I am very grateful. I especially wish to express my thanks to my contact person at the DAAD, Frau Metje, for her advice and support.

Part of the extensive computational calculation was done at Konrad Zuse Center. I am grateful to Ing. Wolfgang Baumann for his friendly support.

Zully M. Maldonado M.

Publications

I. Related to this work:

Bone-joint behavior:

Journals

Maldonado, Z.M., Seebeck, J., Heller, M.O.W., Brandt, D., Hepp, P., Lill, H. and Duda, G.N. 2003. Straining of the intact and fractured proximal humerus under physiological-like loading. Journal of Biomechanics 36, 1865-1873.

Congresses

Maldonado, Z.M., Seebeck, J., Heller, M.O.W., Brandt, D., Hepp, P., Lill, H. and Duda, G.N. 2003. Straining of the intact and fractured proximal humerus under physiological-like loading. In ESB2002, Wroclaw. Poland.

Osteochondral healing:

Journals

Maldonado, Z, Klein P., Thompson, M., Duda, G.N., Mechanical boundary conditions in osteochondral defect healing: On the influence of the Joint Geometry and the Usage of Defects Fillings. Journal of Biomechanics. Submitted.

Duda, G.N., Maldonado, Z., Klein, P., Heller, M., Burns, J. and Bail, H. 2005. On the Influence of Mechanical Conditions in Osteochondral Defect Healing. Journal of Biomechanics 38, 843-851.

Congresses

Z. Maldonado, M. Thompson, P. Seebeck, G.N. Duda. 2004. Einfluss der lokalen Gelenkgeometrie auf den simulierten Heilungsprozess eines osteochondralen Defektes. In: 68. Jahrestagung der Deutschen Gesellschaft für Unfallchirurgie. Berlin.

Duda, G.N., Maldonado, Z., Klein, P., Heller, M., Burns, J. and Bail, H. 2004. On the Influence of Mechanical Conditions on Tissue Differentiation in Osteochondral Defect Healing. ESB2004, 's-Hertogenbosch (Den Bosch). Netherlands.

II. Other publications

Book section

Maldonado, Z., Bendayán, J., Callarotti, R., Cerrolaza, M., 1996. Finite Element Analysis of Hip Prostheses and Design of Fixation Devices for Fractures in Human Femurs. Simulation Modelling in Bioengineering. Computational Mechanics Publications. Southampton, Boston: 99-108.

Maldonado, Z., Bendayán, J., Cerrolaza, M., 2000. Análisis Comparativo Tridimensional de la Respuesta de Prótesis de Cadera Mediante Elementos Finitos. Métodos Numéricos en Ingeniería y Ciencias Aplicadas. Sociedad Venezolana de Métodos Númericos en Ingeniería. Caracas: BI-49 BI-56.

Book Chapters

Maldonado, Z., Bendayán, J., Callarotti, R., Cerrolaza, M., 1996. Análisis por Elementos Finitos de Prótesis de Cadera y Diseno de aparatos de Fijación para Fracturas de Fémur. Biongeniería Aplicada: Técnica Ingenieril para la Práctica Médica. Sociedad Venezolana de Métodos Númericos en Ingeniería. Caracas. Capítulo 3: 23-34.

Journals

Maldonado, Z, Bendayán, J., Cerrolaza, M., 2000. 3D Comparative Analysis of Hip Prostheses Response Using Finite Elements. Journal of Numerical Methods in Analysis and Design in Engineering. 16 (4), 395-420

Maldonado, Z, Bendayán, J., Cerrolaza, M., 1999. A comparative 3D FEM Stress Analysis of Geometrical Parameters Affecting the Behavior of Hip Prostheses. Journal of Medical & Biological Engineering & Computing.

Congresses

Maldonado, Z., Cerrolaza, M., 2000. 3D Comparative FEM Analysis of the Elastic Energy Density in the Interfaces Bone-Cement in Cemented Hip Prostheses. V World Congress on Computational Mechanics. Barcelona Spanien.

Maldonado, Z., Bendayan, J., Cerrolaza, M., 1999. A comparative 3D FEM Stress Analysis of Geometrical Parameters Affecting the Behavior of Hip Prostheses, EMBEC´99, (to be published as supplement to the IFMBE Journal of Medical & Biological Engineering & Computing. Vienna, Austria.

Maldonado, Z., Bendayan, J., Cerrolaza, M., 1998. Analysis by Finite Element Method of Cemented Hip Prostheses. Fourth World Congress on Computational Mechanics. Argentinean Association for Computational Mechanics (AMCA) and Spanish Association for Numerical Methods in Engineering (SEMNI). Buenos Aires, Argentina.

Maldonado, Z., Bendayan, J., Cerrolaza, M., 1998. Last Results in the Study and Analysis of a New Proposal Design of Cemented Hip Implants. International Center of Numerical Methods in Engineering and Applied Sciences. CIMENICS'98, UNEXPO.UNEG. Puerto Ordáz, Venezuela.

Maldonado, Z., Bendayan, J., Cerrolaza, M., 1997. Finite Element Analysis of Geometric Parameter Variations of Cemented Charnley Hip Prosthesis. Second Panamerican Workshop on Applied and Computational Mathematics, Gramado, Brasilien.

Maldonado, Z., Bendayan, J., Cerrolaza, M., 1997. Strain analysis of a new design of a cemented total hip prosthesis using the finite element method. IV Venezuelan Colloquium of Biotechnology. Central University of Venezuela, Simón Bolivar University, Andes University

Curriculum vitae

Name:	Zully Maritza Ritter (geb. Maldonado Mora)
Birthplace:	Cúcuta, Colombia
Date of Birth	7 June .1968
Marital Status:	married
Address	Tauroggener Straße 39 10589 Berlin
E-Mail	zully.maldonado@charite.de zm9@hotmail.com

Primary and secondary school education: Primary: Cúcuta, February 1973 to November 1977
Secondary: Cúcuta, February 1978 to November 1983
University-entrance for degree program: February 1984

Postgraduate studies:

October 2000 - present

Doctoral Thesis: Numerical Simulation of osteochondral repair. Development of a predictive tissue differentiation model for understanding the influence of mechanical conditions on osteochondral healing. Project developed at Charité. Humboldt University. Berlin. Campus Virchow Klinikum
Title to be obtained: Dr. rerum medicarum.

For this propose preliminary studies:
In Germany:
Germany language courses in the Goethe Institute of Göttingen from April to September 2000.

In the Engineering faculty at the Central University of Venezuela:
From 1998 to 1999
A 3D Boundary Element Sensitivity Formulation for Bone Remodeling.
This project ended when I obtained a DAAD scholarship

Likewise at the Engineering Faculty in the Central University of Venezuela (UCV)

From March 1995 to March 1999
Studies of Magister Scientiarum: 3D analysis, numerical simulation, and design of hip prostheses.
This thesis won the National Award "Orinoquia" for the best postgraduate applied research project 1999/2000.
Title: Magister Scientiarum in Structural Engineering. Graduation: 11 July 1999.

Undergraduate Studies

From February 1984 to December 1991
Graduate studies at the Engineering Faculty of the Francisco de Paula Santander University
Thesis: Development of a numerical model for reinforced masonry
Title: Diploma in Civil Engineering.
Graduation: 20 December 1991

Professional life as structural engineering
From 1992 to 1994. Responsible for the calculation and construction of various structural projects to be built in Cúcuta and Arauca, Colombia.

Awards and Recognitions.
- "Orinoquia" Award for the best national postgraduate applied research project 1999/2000. 16 June 2000. Caracas,. Venezuela.
- DAAD German Academic Exchange Service Scholarship to write a PhD at the Charité Humboldt University. Berlin, from April 2000 to present . (including 6 months of language courses).
- Magister Scientiarum thesis (Summa cum laude.), 7 July 1999. Caracas, Venezuela.
- Civil Engineering Degree Thesis, Maximal grade (5.0/5.0). 20 Dezember 1991. Cúcuta. Colombia.

Languages: Spanish (native language), German, English.
Hobbies: Literature, chess, astronomy, reading about theoretical physics, travel .

EIDESSTATTLICHE ERKLÄRUNG

Hiermit erkläre ich an Eides Statt, dass die vorliegende Dissertationsschrift von mir selbst und ohne Hilfe Dritter verfasst wurde. Die Arbeit enthält in allen ihren Teilen keine Kopien anderer Arbeiten. Die benutzten Hilfsmittel sowie die Literatur sind vollständigen angegeben.

Berlin, 05.10.2005

Zully M. Maldonado M.